

DOE F 4600.2

(5/09)

(All Other Editions are Obsolete)

**ATTACHMENT 3
U.S. Department of Energy
FEDERAL ASSISTANCE REPORTING CHECKLIST
AND INSTRUCTIONS**

1. Identification Number: DE-FE0002056		2. Program/Project Title: Modeling CO2 Sequestration in Saline Aquifer and Depleted Oil Reservoir to Evaluate Regional CO2 Sequestration Potential of Ozark Plateau Aquifer System, South-Central Kansas																						
3. Recipient: University of Kansas Center for Research																								
4. Reporting Requirements:	Frequency	No. of Copies	Addresses																					
	A. MANAGEMENT REPORTING <input checked="" type="checkbox"/> Progress Report <input checked="" type="checkbox"/> Special Status Report B. SCIENTIFIC/TECHNICAL REPORTING * (Reports/Products must be submitted with appropriate DOE F 241. The 241 forms are available at https://www.osti.gov/elink) <table border="0"> <thead> <tr> <th align="left"><u>Report/Product</u></th> <th align="left"><u>Form</u></th> <th></th> <th></th> </tr> </thead> <tbody> <tr> <td><input checked="" type="checkbox"/> Final Scientific/Technical Report</td> <td>DOE F 241.3</td> <td>Q</td> <td rowspan="2">Electronic Version to NETL></td> </tr> <tr> <td><input checked="" type="checkbox"/> Conference papers/proceedings/etc.*</td> <td>DOE F 241.3</td> <td>A</td> </tr> <tr> <td><input type="checkbox"/> Software/Manual</td> <td>DOE F 241.4</td> <td>FG</td> <td rowspan="2">Electronic Version to E-link></td> </tr> <tr> <td><input checked="" type="checkbox"/> Other (see special instructions)</td> <td></td> <td>A</td> </tr> <tr> <td>Topical</td> <td>DOE F 241.3</td> <td></td> <td></td> </tr> </tbody> </table> * Scientific/technical conferences only C. FINANCIAL REPORTING <input checked="" type="checkbox"/> SF-425, Federal Financial Report D. CLOSEOUT REPORTING <input type="checkbox"/> Patent Certification <input type="checkbox"/> Property Certificate <input type="checkbox"/> Other E. OTHER REPORTING <input checked="" type="checkbox"/> Annual Indirect Cost Proposal <input checked="" type="checkbox"/> Annual Inventory Report of Federally Owned Property, if any <input type="checkbox"/> Other F. AMERICAN RECOVERY AND REINVESTMENT ACT REPORTING <input type="checkbox"/> Reporting and Registration Requirements			<u>Report/Product</u>	<u>Form</u>			<input checked="" type="checkbox"/> Final Scientific/Technical Report	DOE F 241.3	Q	Electronic Version to NETL>	<input checked="" type="checkbox"/> Conference papers/proceedings/etc.*	DOE F 241.3	A	<input type="checkbox"/> Software/Manual	DOE F 241.4	FG	Electronic Version to E-link>	<input checked="" type="checkbox"/> Other (see special instructions)		A	Topical	DOE F 241.3	
<u>Report/Product</u>	<u>Form</u>																							
<input checked="" type="checkbox"/> Final Scientific/Technical Report	DOE F 241.3	Q	Electronic Version to NETL>																					
<input checked="" type="checkbox"/> Conference papers/proceedings/etc.*	DOE F 241.3	A																						
<input type="checkbox"/> Software/Manual	DOE F 241.4	FG	Electronic Version to E-link>																					
<input checked="" type="checkbox"/> Other (see special instructions)		A																						
Topical	DOE F 241.3																							
FREQUENCY CODES AND DUE DATES: A - As required; see attached text for applicability. FG - Final; within ninety (90) calendar days after the project period ends. FC - Final - End of Effort. Q - Quarterly; within thirty (30) calendar days after end of the calendar quarter or portion thereof. S - Semiannually; within thirty (30) calendar days after end of project year and project half-year. YF - Yearly; 90 calendar days after the end of project year. YP - Yearly Property - due 15 days after period ending 9/30.																								

QUARTERY PROGRESS REPORT

Award Number: DE-FE0002056

**Recipient: University of Kansas Center for Research &
Kansas Geological Survey
1930 Constant Avenue
Lawrence, KS 66047**

**“Modeling CO₂ Sequestration in Saline Aquifer and Depleted Oil Reservoir
to Evaluate Regional CO₂ Sequestration Potential of Ozark Plateau Aquifer System,
South-Central Kansas”**

**Project Director/Principal Investigator: W. Lynn Watney
Principal Investigator: Jason Rush**

Eleventh Quarter Progress Report

Date of Report: July 31, 2012

Period Covered by the Report: April 1, 2012 through June 30, 2012

**Contributors to this Report: Robin Barker, Ken Cooper, Saugata Datta, John Doveton,
Mina Fazelalavi, David Fowle, Martin Dubois, Paul Gerlach, Tom Hansen, Dennis Hedke,
Eugene Holubnayak, Reza Maleki, Larry Nicholson, Jennifer Roberts, Jason Rush, Aimee
Scheffer, Ayrat Sirazhiev, Ray Sorenson, Georgios Tsoflias, John Victorine, Lynn Watney,
John Youle, Dana Wreath**

EXECUTIVE SUMMARY

The project “Modeling CO₂ Sequestration in Saline Aquifer and Depleted Oil Reservoir to Evaluate Regional CO₂ Sequestration Potential of Ozark Plateau Aquifer System, South-Central Kansas” is focused on the Paleozoic-age Ozark Plateau Aquifer System (OPAS) in southern Kansas. OPAS is comprised of the thick and deeply buried Arbuckle Group saline aquifer and the overlying Mississippian carbonates that contain large oil and gas reservoirs. The study is collaboration between the KGS, Geology Departments at Kansas State University and The University of Kansas, BEREXCO, INC., Bittersweet Energy, Inc. Hedke-Saenger Geoscience, Ltd., Improved Hydrocarbon Recovery (IHR), Anadarko, Cimarex, Merit Energy, GloriOil, and Cisco.

The project has three areas of focus, 1) a field-scale study at Wellington Field, Sumner County, Kansas, 2) 25,000 square mile regional study of a 33-county area in southern Kansas, and 3) selection and modeling of a depleting oil field in the Chester/Morrow sandstone play in southwest Kansas to evaluate feasibility for CO₂-EOR and sequestration capacity in the underlying Arbuckle saline aquifer. Activities at Wellington Field are carried out through BEREXCO, a subcontractor on the project who is assisting in acquiring seismic, geologic, and engineering data for analysis. Evaluation of Wellington Field will assess miscible CO₂-EOR potential in the Mississippian tripolitic chert reservoir and CO₂ sequestration potential in the underlying Arbuckle Group saline aquifer. Activities in the regional study are carried out through Bittersweet Energy. They are characterizing the Arbuckle Group (saline) aquifer in southern Kansas to estimate regional CO₂ sequestration capacity. Supplemental funding has expanded the project area to all of southwest Kansas referred to as the Western Annex. IHR is managing the Chester/Morrow play for CO₂-EOR in the western Annex while Bittersweet will use new core and log data from basement test and over 200 mi² of donated 3D seismic. IHR is managing the industrial partnership including Anadarko Petroleum Corporation, Cimarex Energy Company, Cisco Energy LLC, Glori Oil Ltd., and Merit Energy Company. Project is also supported by Sunflower Electric Power Corporation.

PROJECT STATUS

Subtasks completed to date include:

Task Name	Planned Start Date	Actual Start Date	Planned Finish Date	Actual Finish Date	% Complete
1.0 Project Management & Planning	12/8/2009	12/08/09	12/7/2012		55%
2.0 Characterize the OPAS (Ozark Plateau Aquifer System)	1/1/2010	01/01/10	6/30/2012		50%
3.0 Initial geomodel of Mississippian Chat & Arbuckle Group - Wellington field	1/1/2010	01/01/10	9/30/2010	09/30/10	100%
4.0 Preparation, Drilling, Data Collection, and Analysis - Well #1	9/15/2010	12/15/10	3/31/2011	08/30/11	100%
5.0 Preparation, Drilling, Data Collection and Analysis - Well #2	1/1/2011	02/20/11	6/30/2011	08/30/11	100%
6.0 Update Geomodels	5/1/2011	05/01/11	9/30/2011	*	95%
7.0 Evaluate CO2 Sequestration Potential in Arbuckle Group Saline Aquifer	8/1/2011	08/01/11	12/31/2011	++	85%
8.0 Evaluate CO2 Sequestration Potential in Depleted Wellington field	10/15/2011	10/15/11	3/31/2012	+++	85%
9.0 Characterize leakage pathways - risk assessment area	1/1/2010	01/01/10	6/30/2012	+	85%
10.0 Risk Assessment related to CO2-EOR and CO2 Sequestration in saline aquifer	6/1/2012	06/01/12	9/30/2012	**	70%
11.0 Produced water and wellbore management plans - Risk assessment area	1/1/2012	01/01/12	10/31/2012		80%
12.0 Regional CO2 sequestration potential in OPAS	8/1/2012		12/7/2012		50%
13.0 Regional source sink relationship	1/1/2010	1/1/2010	12/7/2012		50%
14.0 Technology Transfer	1/1/2010	01/01/10	12/7/2012		

Milestones – name, planned completion date, actual completion date, validation

KGS Milestone 2.2: Complete Well#2 at Wellington - Drill, DST, log, case, perforate, test zones	6/30/2011	08/30/11	Completed, email summary
KGS Milestone 2.3: Update Wellington geomodels - Arbuckle & Mississippian	9/30/2011		85% complete****
KGS Milestone 2.4: Evaluate CO2 Sequestration Potential of Arbuckle Group Saline Aquifer - Wellington field	12/31/2011		85% complete+
KGS Milestone 3.1: CO2 sequestration & EOR potential - Wellington field	3/31/2012		85% complete++
KGS Milestone 3.2: Characterize leakage pathways - Risk assessment area	6/30/2012		85% complete+++
KGS Milestone 3.3: Risk assessment related to CO2-EOR and CO2-sequestration	9/30/2012		70% complete++++
KGS Milestone 3.4: Regional CO2 Sequestration Potential in OPAS - 17 Counties	12/7/2012		50% complete

Key

* Geologic data acquired. Seismic data acquired and analysis in progress. Newly discovered production/injection data being assimilated.
**Workover rig moved into location 7-8-11
*** New geomodels for Arbuckle and Mississippian will use depth and shear wave seismic undergoing final interpretation
****Seismic inversion has been completed and porosity model with initial discrete fracture network has been obtained for the 3D volume in Wellington Field. Model validation and refinement continues with integration of well test, geochemistry, and core and log petrophysical information. Plan is to finish this task by 9/1/2012.
+ Seismic inversion and structural modeling will soon lead to completion of the geomodel. Plan is to finish this task by 9/1/2012
++ See Milestone 2.4. Plan is to finish the task by 10/1/2012.
+++ Fault, fracture, and structural drape are being validated with seismic that was donated, locating abrupt stratigraphic changes, and surface lineaments and gravity-magnetic anomalies. Presence of evaporite karst is also being noted. Planned completion date is now September 2012.
++++ Planned completion date is first quarter BP3, September 2012. This should be met.

Subtasks in progress:

Task 2. -- Characterize the OPAS (Ozark Plateau Aquifer System) by integration of well, 3D seismic, gravity and magnetics, and remote sensing information to further evaluate faults, caprocks, and establish distribution of flow units in the Arbuckle saline formation.

Task 6. -- Update geomodels of Arbuckle and Mississippian at Wellington Field. –1) integrating well tests, core analyses, 3D seismic, and log interpretation to obtain revise geomodel of Mississippian oil reservoir, caprock interval, and Arbuckle saline formation; 2) conduct final water sampling at Wellington KGS #1-32 to confirm distinct zonal variation in brine composition.

Task 16. -- Review and integrate regional (112 mi²) 3D seismic with well data and interpret structure and stratigraphic variability from basement to surface.

Task 17. -- Prepare to collect new 2D share and 3D multicomponent seismic data and drill test borehole #3 in Stevens County, Kansas.

Task 18. -- 1) finalize Pleasant Prairie south oil field geomodel and revise simulation for CO₂-EOR; B) revise geomodel for Eubank oil field and prepare for simulation.

Project Status: Subtasks completed within current quarter

Subtasks completed within current quarter: Subtask 4.11. Geochemical analysis of water samples from drilling in Wellington Field (KU's Arbuckle study) and Subtask 4.12. Microbiological studies on produced water from Wellington Field. 4.13. Correlate log & core (Wellington) - extend to OPAS.

ONGOING AND COMPLETED ACTIVITIES - REGIONAL STUDY INCLUDING SOUTHWEST KANSAS)

Regional Studies

Task 2. Characterize the OPAS.

Task 12. Regional CO Sequestration Potential in OPAS.

Task 15. Extend Regional Study of Ozark Plateau Aquifer System (OPAS) to the Western Border of Kansas – “Western Annex”

Task 16. Collect and Analyze Existing Data for Developing Regional Geomodel for Arbuckle Group Saline Aquifer in Western Annex

New Java software tools to facilitate analysis of well data

New Java software tools/applications were released during the quarter including –

1. DST web site to the GEMINI Tools Web page
<http://www.kgs.ku.edu/Gemini/Tools/Tools.html>.
2. The web site is at <http://www.kgs.ku.edu/software/DST/> with the HELP Files at <http://www.kgs.ku.edu/software/DST/HELP/>.

The DST application is in English units only with hooks to allow metric units to be added later. This program has a digitizer to capture the shut in pressure-temperature-time data. CSV input feature was not included since format has yet to be determined, i.e. only shut in pressure-temperature-time data or all DST data like the Trilobite CSV files that created the Trilobite Database Tables.

The DST data is also saved to the Log ASCII Standard (LAS) version 3.0 file to allow the DST program to be read as an existing LAS 3.0 file of a well with all other accompanying data. Running the DST program with the original LAS data will allow the DST data to be added to the original file.

Each DST test has its own data section in the LAS 3.0 file including General Information, Mud & Cushion and Gas Rates Data in the Parameters Section and the Pressure Summary Table, Recovery Table, Gas Rates Table and the Shut In Pressure-Temperature-Time Data in the Data Section of the LAS 3.0 File. Data Descriptor Flag is used to let the program know what type of data it is and to sort it to the correct variables. It is clear enough to let the user distinguish the data type at a glance in the LAS 3.0 file, the beauty of working with ascii format!

Figure 1. illustrating DST

**Characterization work focused on support of Class VI application
for small scale injection project at Wellington**

Work on regional characterization continues, but current focus is to provide information to complete the application for the Class VI CO2 Injection as specified in the DOE contract (DE-FE0006821) funding the small scale field test CO2 injection in the Arbuckle saline formation at Wellington Field.

Key parts of the Class VI application are dependent on the characterization in this project.

- **USDW**

Regional and local review and characterization of the freshwater has been completed. It will be demonstrated in the Class VI application that considerable seals exist above the primary (lower Mississippian argillaceous dolosiltstone, Chattanooga Shale), and secondary caprock (Cherokee shale) by multiple thick shales and finally 200 ft thick evaporite near the surface below the USDW (**Figures 2, 3, 4, 5, 6**).

Geochemical and isotopic studies of brines in the Arbuckle and Mississippian show no linkage to the USDW. Mississippian and Arbuckle brines also do not appear to be hydraulically connected in this area even though they are considered to be part of the same regional hydrogeologic aquifer system (**Figures 7 and 8**).

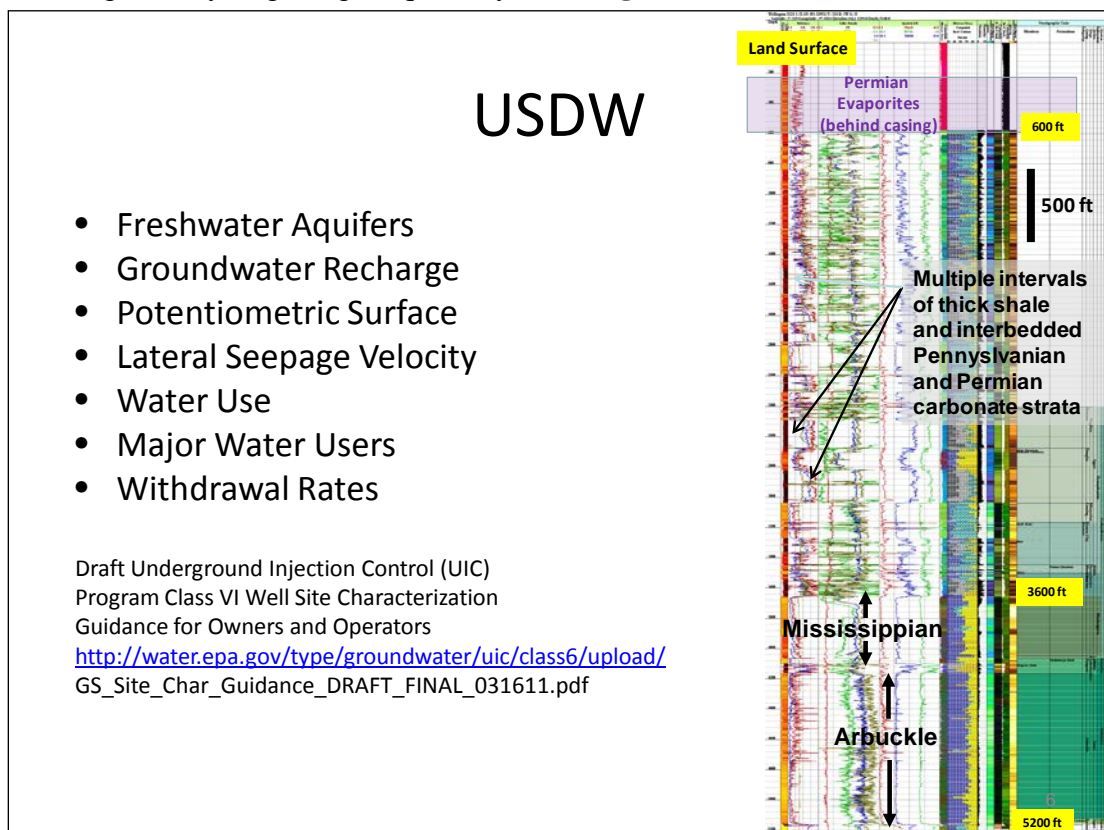


Figure 2. Stratigraphic column showing the stratigraphic succession in KGS #1-32 highlighting the CO2 injection intervals (Mississippian and Arbuckle), overlying

thick shales, near surface evaporites, and the land surface. USDW is very thin alluvium, coluvium, and Permian Ninnescah Shale.

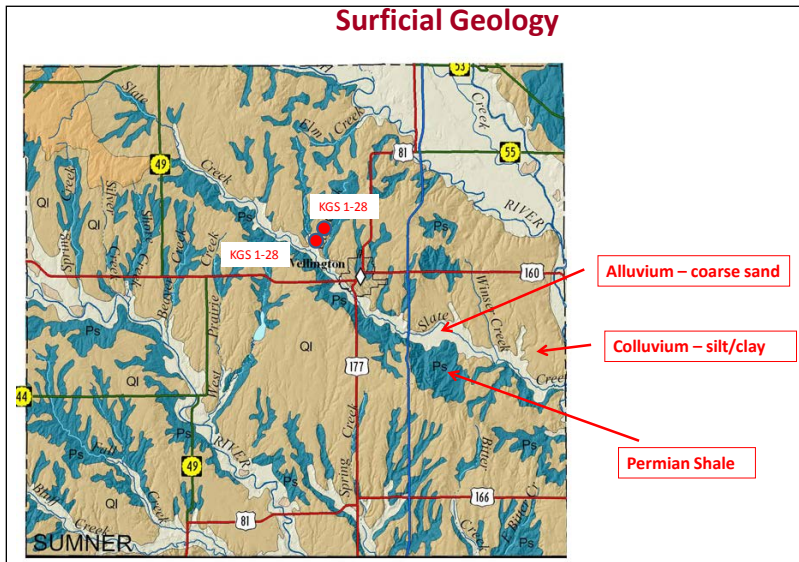


Figure 3. Surficial geologic map of Sumner County showing wells and surface USDW deposits – alluvium, coluvium, and Permian shales (Ninnescah Shale).

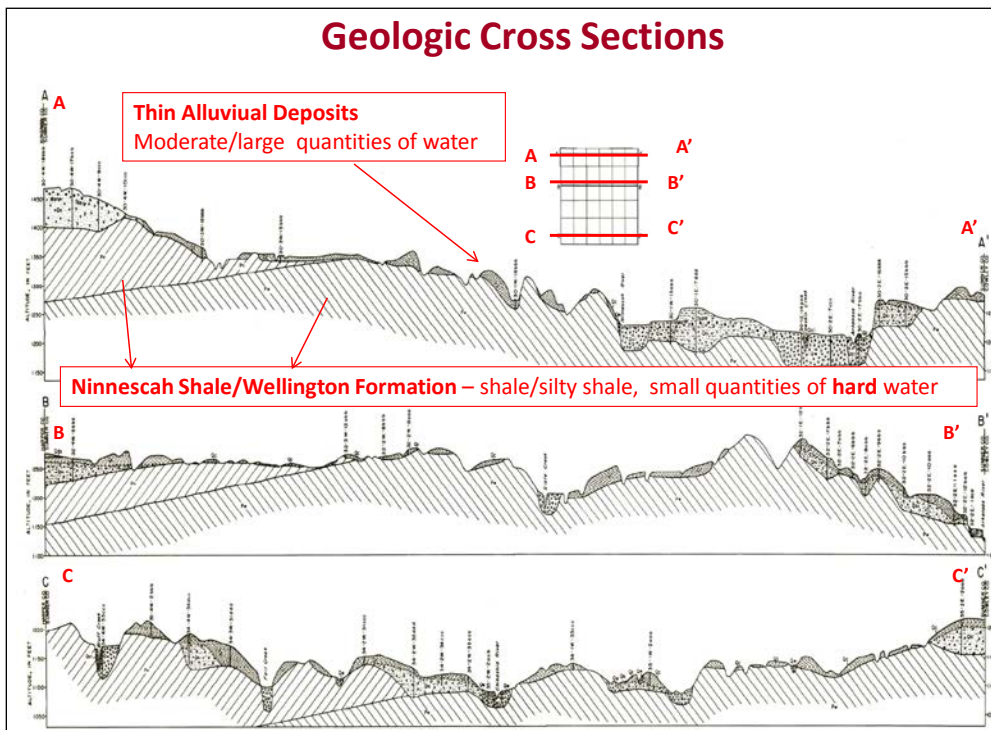


Figure 4. Cross sections through the shallow USDW deposits in Sumner County.

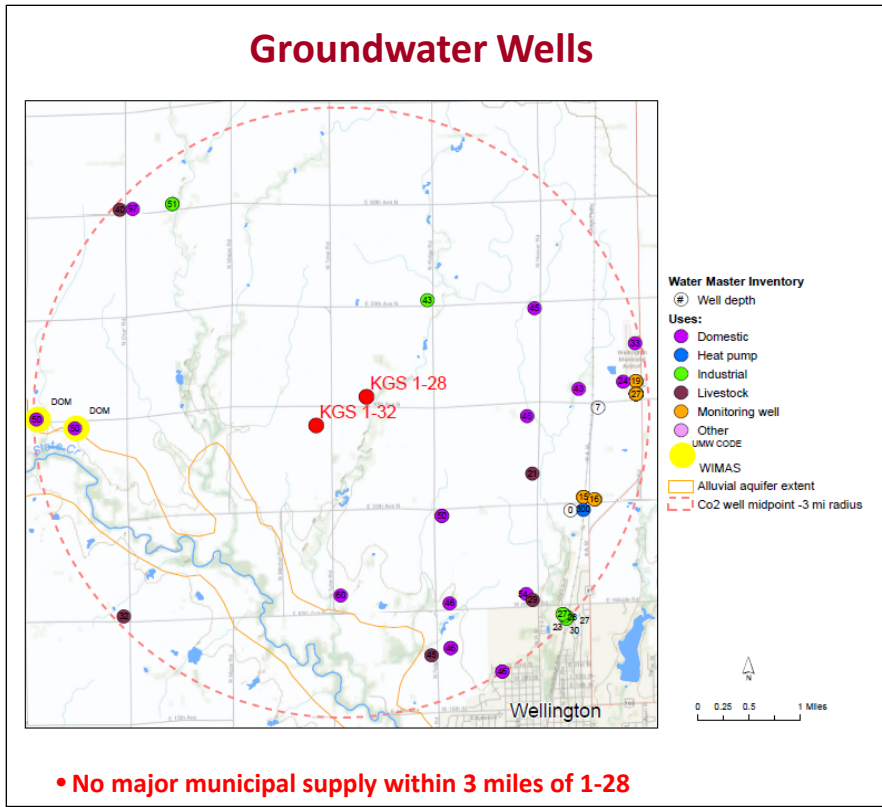


Figure 5. Groundwater wells in a three-mile radius around the CO₂ small scale injection site.

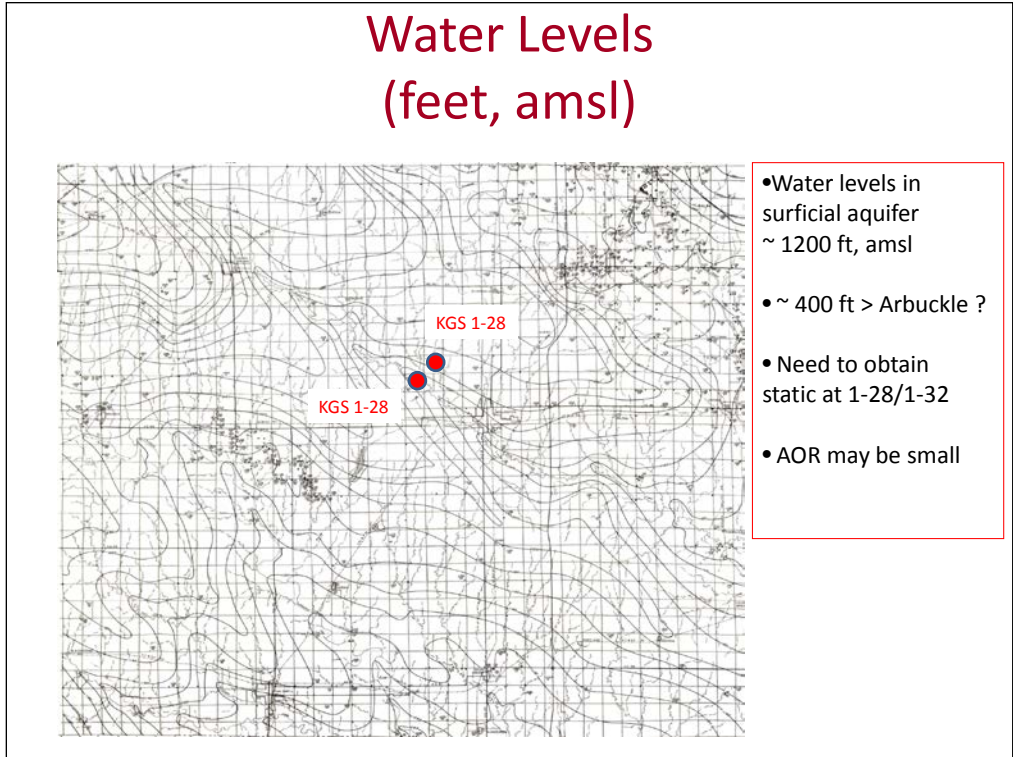


Figure 6. Water level map of Sumner County and location of two wells drilled in DE-FE0002056.

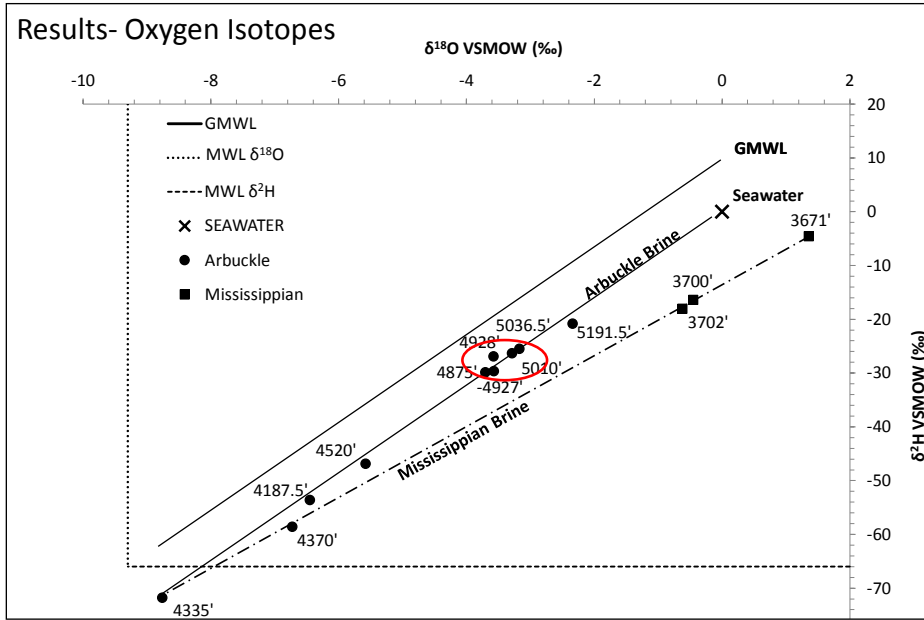
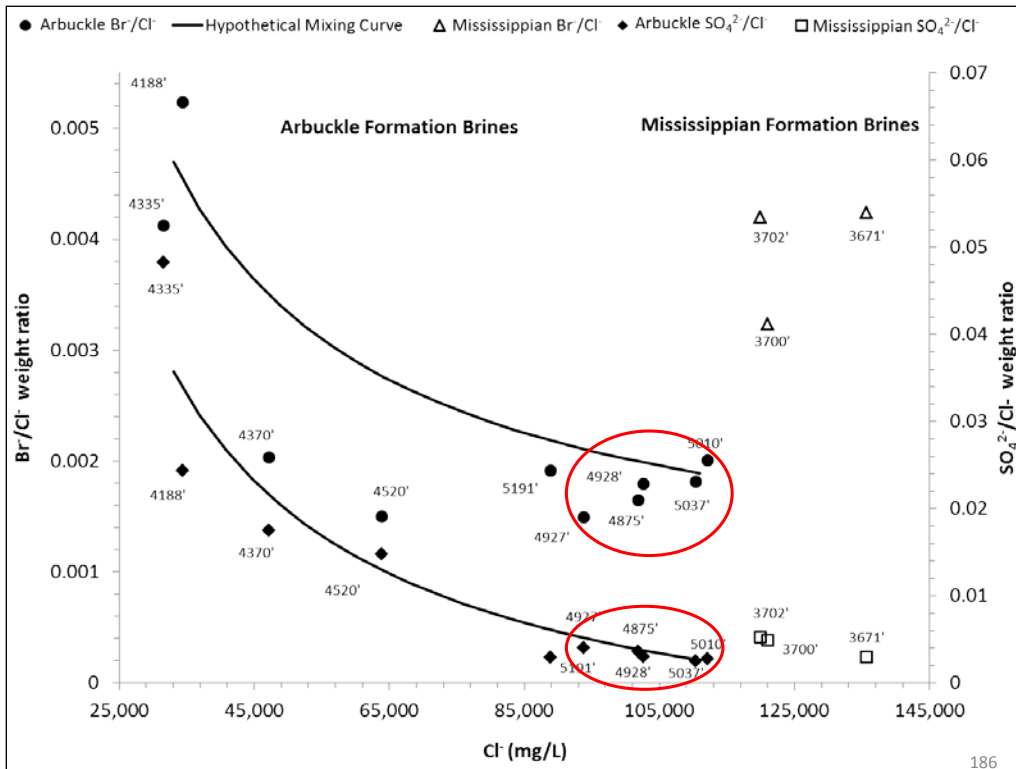


Figure 7. The upper Arbuckle is isotopically depleted from other brines and meteoric water. Lower Arbuckle brines all cluster together suggesting a high rate of mixing. Values of upper brines differ substantially from those of the lower brines.



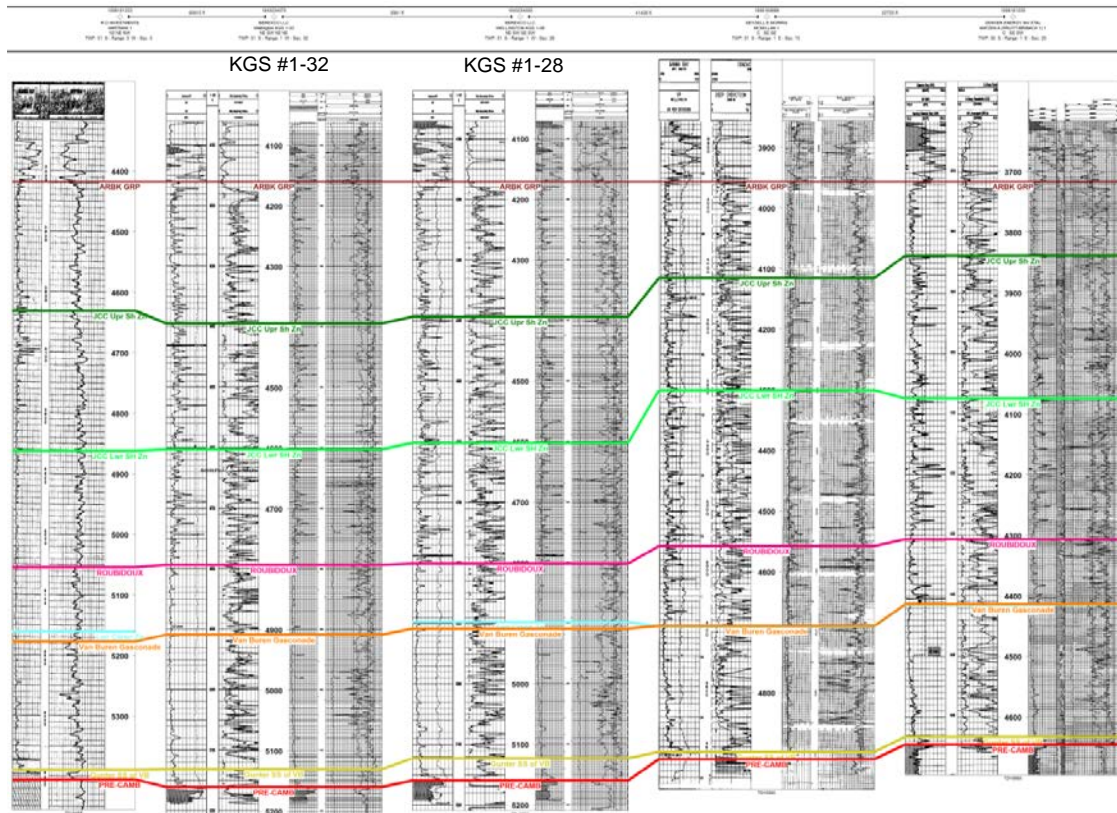


Figure 10. Subregional cross section in the region of new well #1-32 and #1-28 datumed on top of the Arbuckle showing major subdivisions of the Arbuckle saline formation.

The location, orientation, and properties of known or suspected faults and fractures that may transect the confining zone(s) in the AoR [§146.82(a)(3)(ii)].

This topic continues to be reviewed with the new seismic processing and will be incorporated into Petrel as a discrete fracture network.

Data on the depth, areal extent, and thickness of the injection and confining zone(s) [§146.82(a)(3)(iii)].

Maps and cross sections of the 1) Arbuckle injection interval – Gasconade to Gunter, 2) baffle/storage interval in upper Arbuckle, 3) Chattanooga Shale, and 4) lower Mississippian “Pierson” to base of Simpson Group will be refined in new Petrel model using latest depth-migrated seismic data.

Information on lithology and facies changes [§146.82(a)(3)(iii)].

Lithology and facies work done to date are based on core, samples, and well logs. New seismic will be inverted and will be used to obtain refined 3D distribution of these rock properties in addition to porosity using Petrel geocellular modeling.

Information on the seismic history of the area, including the presence and depth of seismic sources [§146.82(a)(3)(v)].

Seismic occurrence map prepared by US Geological Survey will be used to convey historical earthquakes and to assess risk of future earthquakes. Area has no record of earthquakes that have occurred near the site, nor are the risks for seismic activity elevated at the site.

Geologic and topographic maps and cross-sections illustrating regional geology, hydrogeology, and the geologic structure of the local area [§146.82(a)(3)(vi)].

This data is readily available.

Maps and stratigraphic cross-sections indicating the general vertical and lateral limits of all USDWs, water wells, and springs within the AoR, their positions relative to the injection zone(s), and the direction of water movement (where known) [§146.82(a)(5)].

Regional inventory of over 3700 drill stem tests from the Arbuckle have established a reliable static shut-in pressure that has been converted to equivalent freshwater head (**Figure 11**).

Baseline geochemical data on subsurface formations, including all USDWs in the area of review [§146.82(a)(6)].

This information has been identified and will be summarized in the Class VI application.

Arbuckle Saline Aquifer Connected to Outcrop

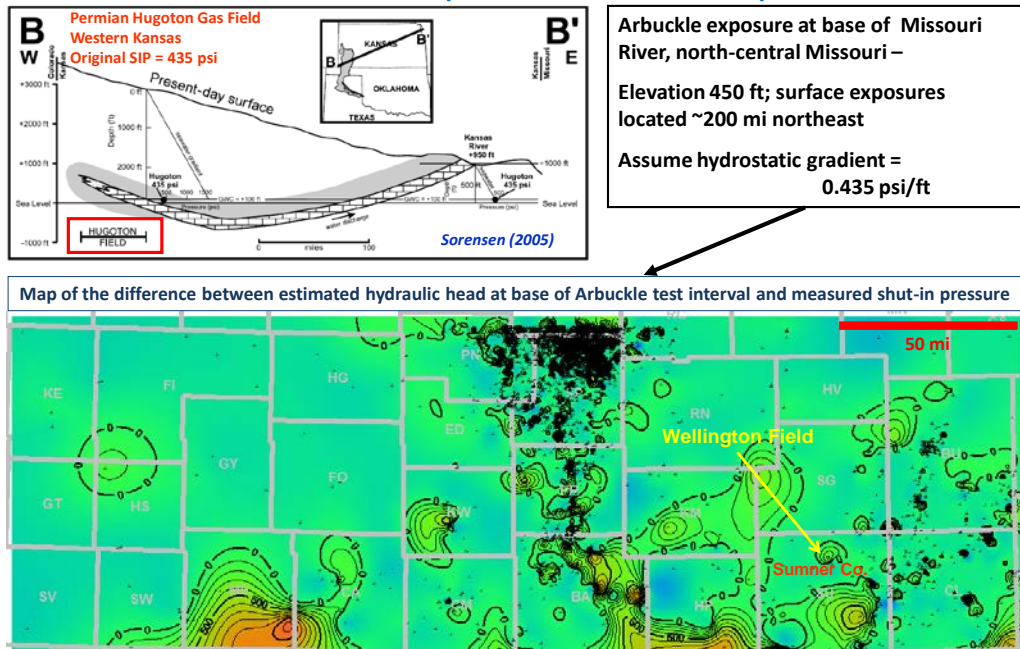


Figure 11. Arbuckle shut-in pressures are a reflection of the saline formation being hydraulically connected to the surface exposures of the unit in Missouri ~150 miles east of the injection site.

Regional Geology –

Regional geologic mapping is well underway in DE-FE0002056 for the Arbuckle based on stratigraphic tops correlated from hundreds of key wells. Reference wireline logs that penetrate deeply into the Arbuckle with good suites of wireline logs provide lithology, porosity, and eventually will be used to estimate permeability (**Figure 12**). The regional extent of the mapping extends over 25,000 mi² includes regions of the Arbuckle in southern Kansas where CO₂ would be in a supercritical state in the saline formation.

The regional mapping is also being used to identify significant fracture and fault systems in relationship to degree of flexure and evaluation of any accompanying stratigraphic changes (**Figure 13**).

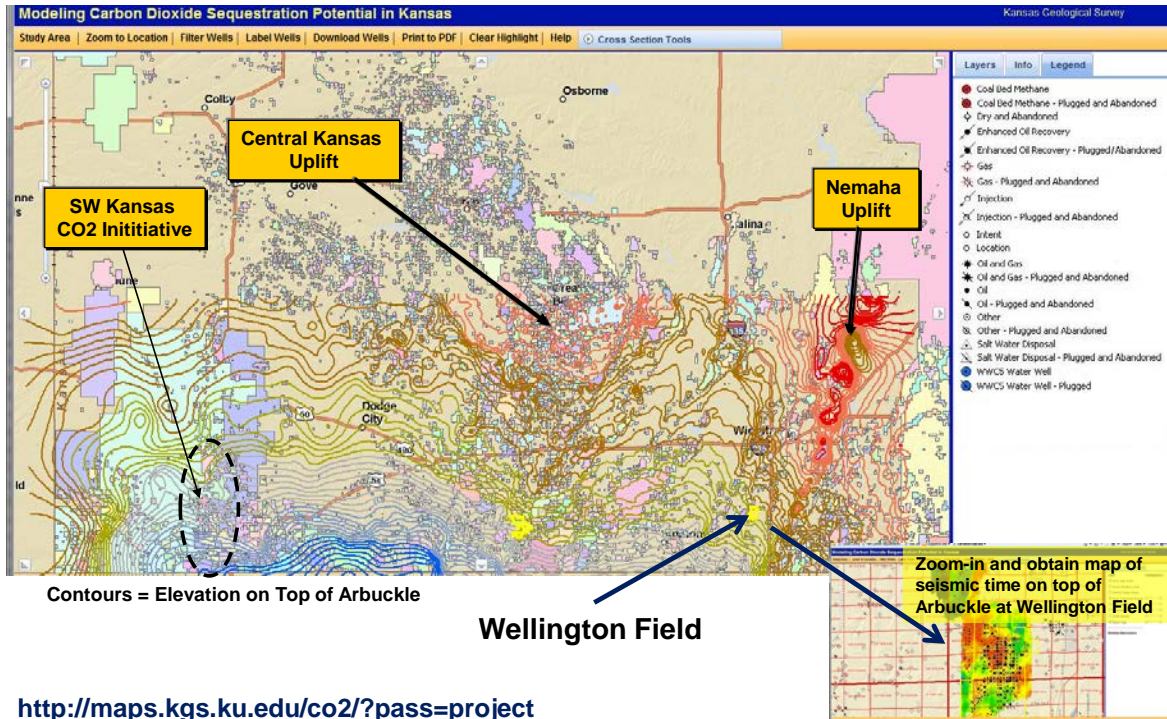


Figure 12. Regional mapping has been accomplished to provide regional context the Wellington small scale test injection and background needed for the Class VI CO₂ injection application.

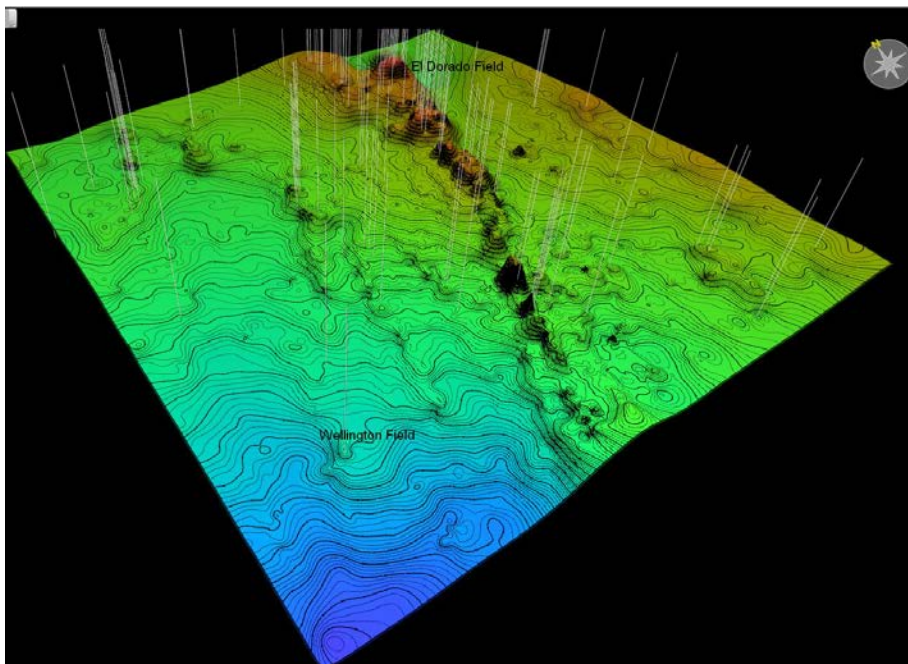


Figure 13. Three dimensional perspective of the top of the Arbuckle in south-central Kansas.

Task 18. -- 1) Finalize Pleasant Prairie South oil field geomodel and revise simulation for CO2-EOR; B) revise geomodel for Eubank oil field and prepare for simulation.

Geomodel and simulation of the Pleasant Prairie South oil field has been completed. The report draft is included in **Appendix A** at the end of the quarterly report.

Pleasant Prairie South reservoir characterization, modeling and simulation

Martin K. Dubois¹, Eugene T. Williams², Dennis E. Hedke³, Peter R. Senior⁴, and John C. Youle⁵

ONGOING & COMPLETED ACTIVITIES - WELLINGTON FIELD

Subtask 6.5 Update geomodel for Arbuckle and Mississippian

Capillary pressure data in the Mississippian is limited and belated analyses will be done by Weatherford. Logtech software was used to determine if the nuclear magnetic resonance could be used to estimate capillary pressure curves for the Mississippian oil reservoir. The NMR tool provides a measure of pore size and equations have been developed to use these properties of the pores to estimate pore throat size and related capillarity. A summary of the preliminary work on this method is described below. This could similarly be applied to the Arbuckle to extend measurements of capillary trapping based on analyses of core samples.

Capillary Pressure curve from NMR in Mississippian formation by Mina Fazelalavi

Introduction

Initial water saturation (S_w) is determined from deep resistivity logs where porosity is available. Old wells in Mississippian formation of Wellington field do not have good porosity logs and often they do not have a deep resistivity log. New wells are drilled after the reservoir had been invaded by water and obtained saturations from log data may not represent initial condition of the reservoir in these wells. For reservoir simulation, initial S_w of the reservoir is crucial. Initial saturation can also be obtained from capillary pressure curves and depth of FWL. Depth of FWC is estimated to be below -2480 ft and it can be assumed at -2480 ft. FWL in measure depth in well 1-28 and 1-32 are 3750 and 3752ft respectively. Capillary pressure curve for each depth can be derived from T2 distribution of NMR log of Well 28 and 32. Mississippian formation can be divided into several zones based on T2 distribution data and an average P_c curve can be calculated for each zone. Average capillary pressure curves derived from NMR logs can be extended to other wells with the same rock type to derive initial water saturation of the reservoir. Based on NMR Mississippian formation was divided into several zones and five average P_c curves were derived for these zones.

NMR Analysis for Pc

Well 1-28 and 1-32 had NMR log. Therefore, NMR logs from these two wells were analyzed by Techlog to derive capillary pressure curves, initial water saturation and irreducible water saturation at a certain capillary pressure. To generate capillary pressure curves, a module called Capillary pressure from T2 distribution was run. **Table 1** and **2** show the parameters used to calculate capillary pressure curves, irreducible water saturation and NMR water saturation (initial water saturation) in well 1-28 and 1-32 respectively.

Figure 14 and 15 are the layouts for well 1-32 and 1-28 respectively. These layouts show T2 distribution and NMR analysis results. Capillary pressure curves are labeled as PC_Lab_NMR on the layouts. SW_NMR is equivalent to initial water saturation and SW_IRR is irreducible water saturation at capillary pressure of 7 bars.

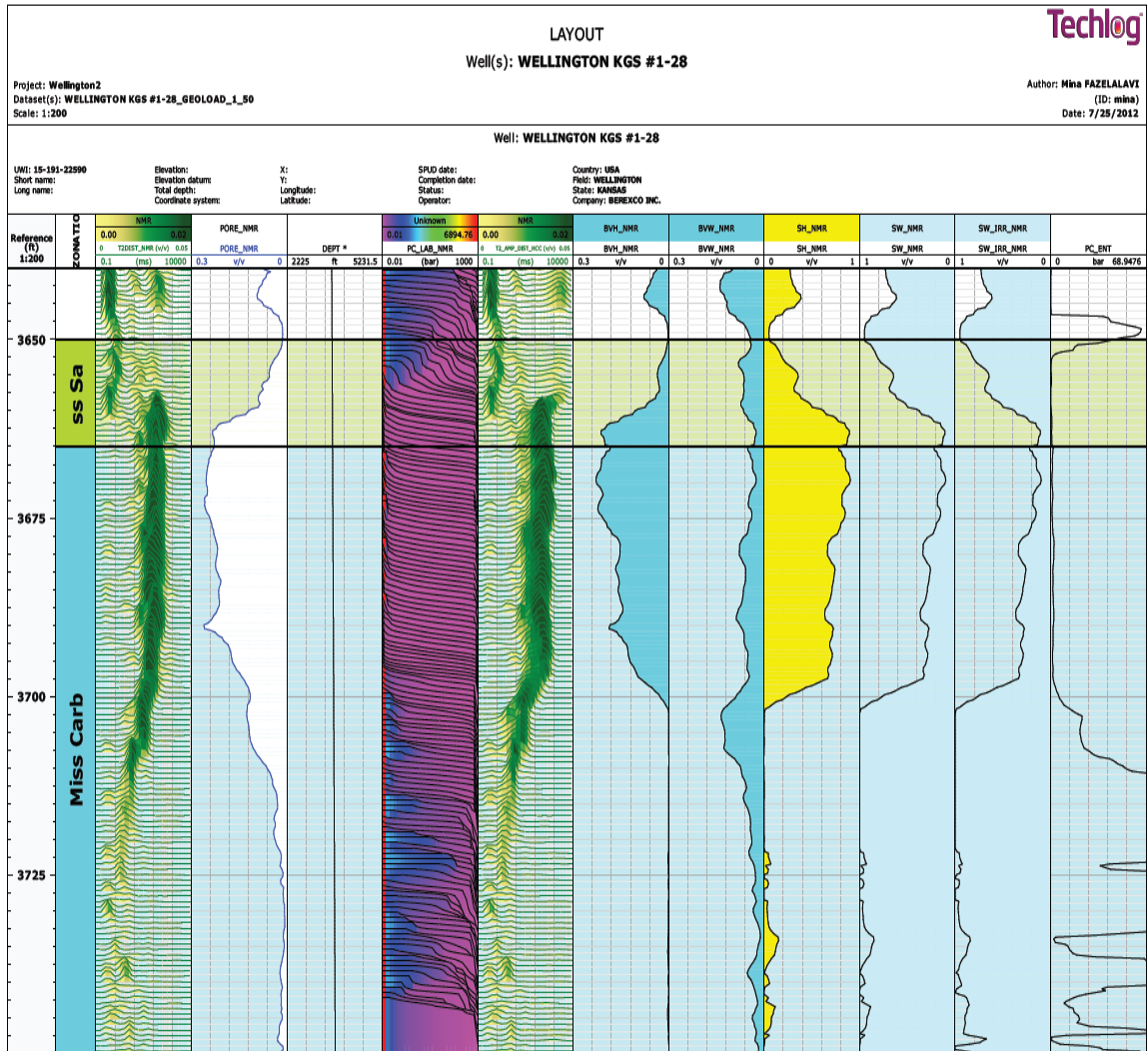


Figure 15: Capillary pressure and irreducible water saturation layout in well 1-28.

Capillary Pressure Zones

Different intervals in Mississippian have different T2 distributions. The formation can be divided into three zones based of T2 distribution. Depth and description of these zones are given in the following table for wells 28 and 32. Zone 1 is a cherty zone having small to big pore sizes. Zone 2 is a porous zone mainly with big pore sizes and zone 3 is a tight zone with smaller pore size.

Well 1-28

Zones	Interval, ft	Interval, ss	Pore size	Lithology
1	3649-3658	-2379 to -2388	Medium to Big	chert
2	3659-3701	-2389 to -2431	Big	Carbonate with some sand
3	3702-3750	-2432 to -2480	small	Carbonate with some sand

Well 1-32

Zones	Interval, ft	Interval, ss	Pore size	Lithology
1	3658-3668	-2386 to -2396	Medium to Big	chert
2	3669-3704	-2397 to -2432	Big	Carbonate with some sand
3	3705-3751	-2433 to -2479	small	Carbonate with some sand

For each zone, capillary pressures and corresponding water saturations at each depth were exported from Techlog to Excel with a sampling rate of 0.25ft. Average Pc was calculated for each water saturation. The average Pc for Zones 1 to 3 of well 28 are plotted versus Sw in Fig 1 to 3 respectively and average Pc of well 32 for these zones are given in **Figures 16 to 17**.

	1	2
Group		
Well	WELLINGTON KGS #1-32	WELLINGTON KGS #1-32
Dataset	HES INSITE_1_51LQC_2	HES INSITE_1_51LQC_2
Zone	Mississippian sand	Mississippian
Top	3658	3668
Bottom	3668	4100
FWL	3752	3752.001
FWL Unit	ft	ft
Hydrocarbon Density (g/cm3)	0.83	0.83
Water Density (g/cm3)	1.11	1.11
IFT_RES (dyne/cm)	20	20
Hydrocarbon Correction	yes	yes
Kappa (psi.s)	4	8
Kappa Flex Point (ms)	20	80
Kappa Low (psi.s)	10	10
PC Irreducible	7	7
PC Irreducible Unit	bar	bar
Spectrum from Water	no	no

Table 1: Parameters used for Capillary pressure module in well 1-32.

Method settings			
Capillary pressure from T2			
save and display			
Inputs	Zonation	Parameters	
	1	2	3
Group			
Well	WELLINGTON KGS #1-28	WELLINGTON KGS #1-28	WELLINGTON KGS #1-28
Dataset	GEOLOAD_1_50	GEOLOAD_1_50	GEOLOAD_1_50
Zone	Shale zone	Miss Sand	Miss Carb
Top	3600	3645	3663
Bottom	3645	3663	4058
FWL	3750	3750	3750
FWL Unit	ft	ft	ft
Hydrocarbon Density (g/cm3)	0.83	0.83	0.83
Water Density (g/cm3)	1.11	1.11	1.11
IFT_RES (dyne/cm)	20	20	20
Hydrocarbon Correction	yes	yes	yes
Kappa (psi.s)	4	4	8
Kappa Flex Point (ms)	20	20	80
Kappa Low (psi.s)	10	10	10
PC Irreducible	0.1	0.1	0.1
PC Irreducible Unit	bar	bar	bar
Spectrum from Water	no	no	no

Table 2: Parameter used for capillary pressure module in well 1-28.

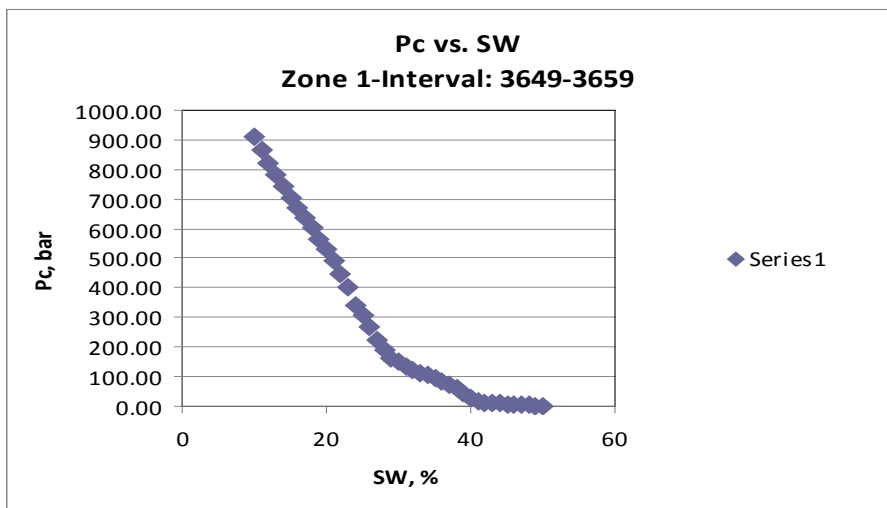


Figure 16: Capillary pressure vs. water saturation for zone 1 in well 1-28.

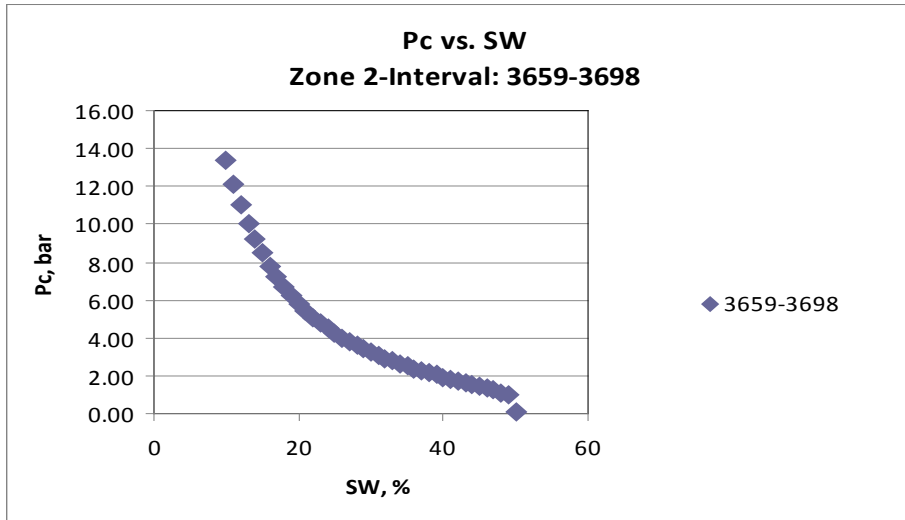


Figure 17: Capillary pressure vs. water saturation for zone 2 in well 1-28.

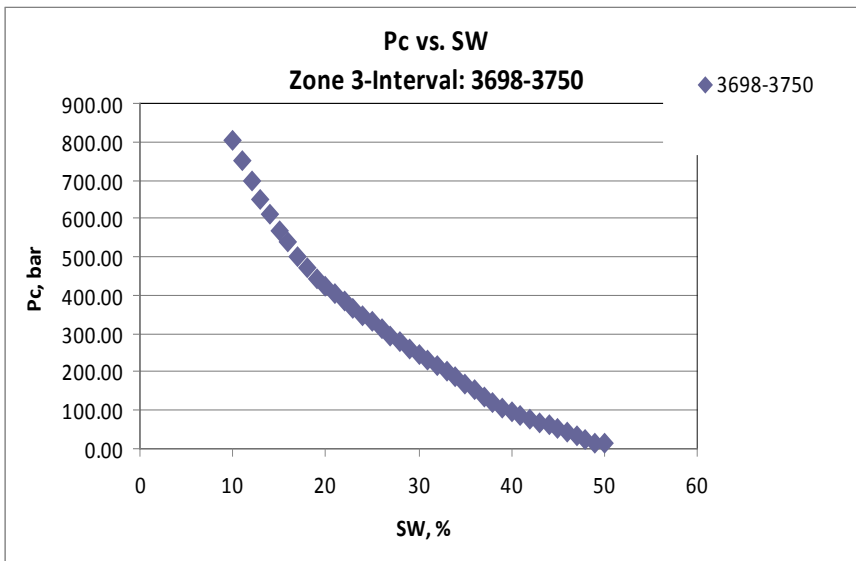


Figure 18: Capillary pressure vs. water saturation for zone 3 in well 1-28.

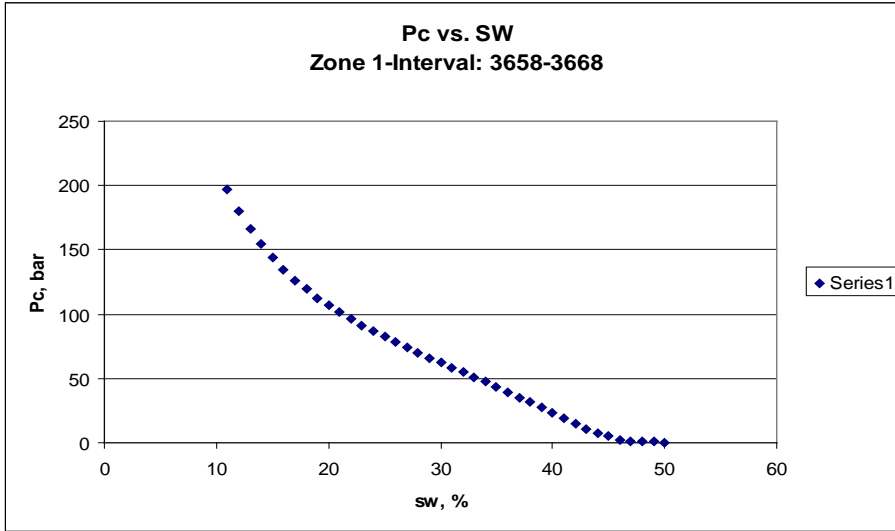


Figure 19: Capillary pressure vs. water saturation for zone 1 in well 1-32.

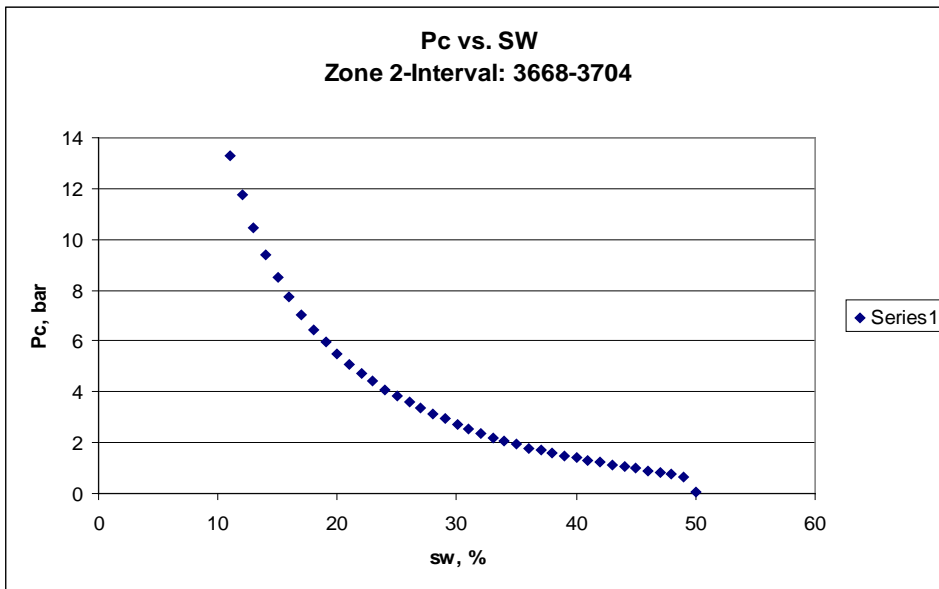


Figure 20: Capillary pressure vs. water saturation for zone 2 in well 1-32.

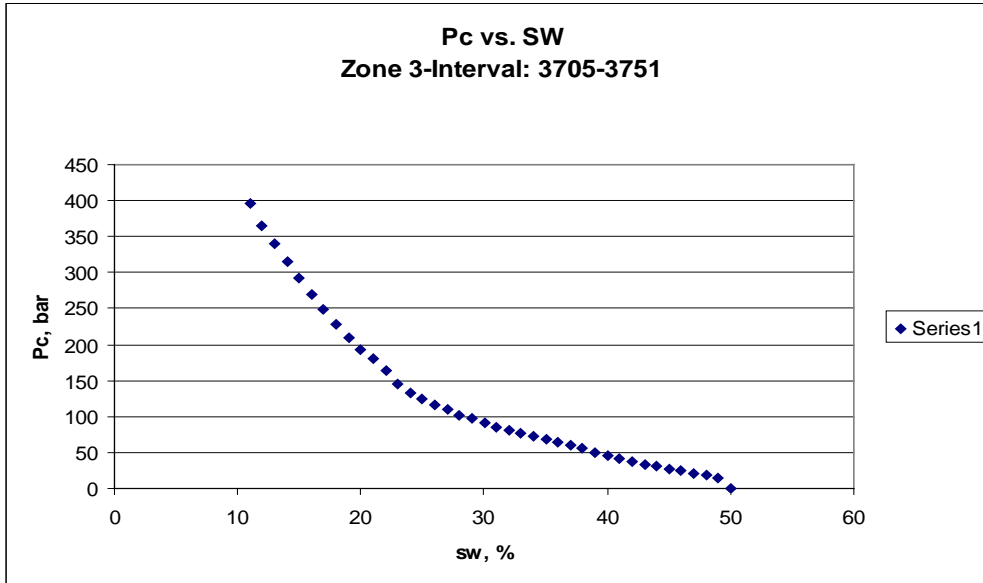


Figure 21: Capillary pressure vs. water saturation for zone 3 in well 1-32.

Free water level is assumed to be at -2480 and crest of Mississippian reservoir is about 130 ft above FWL. Based on oil and water density of the reservoir (0.83 and 1.11g/cc), PC is about 1.1 bar at the crest of the formation. However the average Pc curves do not have sufficient points below 1.1bar to obtain a Pc curve applicable to Mississippian. There is also a discrepancy between these Pc curves and calculated Sw by NMR over the formation interval. NMR Sw in the formation seems to be accurate and these Sw data was used for definition of Pc by another approach.

Another Approach

Second approach was used to get the average initial water saturation of the reservoir for each zone. For second approach, height above free water level was graphed against NMR sw that is equivalent to initial water saturation. Zone 2 was divided into 2 zones in this approach. Capillary pressure curves, with assumed shapes, were drawn through data points for each zone so that capillary pressure becomes zero at water saturation of one. For Zone 2, two Pc curves obtained; one for the interval 3659 to 3678 and a second curve for interval 3678 to 3700. These Pc curves are shown in **Figure 23**. For Zone 1, an average Pc curve as given in **Figure 22** was obtained. Zone 3 is very dense and with low permeability and water saturation is 90 % or more. This zone has Pc curve similar to **Figure 24**. Graphs are shown in **Figures 22, 23 and 24**. Equations for each graph was derived from initial water saturation versus height above free water level and average initial water saturation were calculated for each zone. Equations for each zone in well 1-28 are in the following table:

Zone	Interval	Equations
1	3649-3658	$y = 1.1088x - 0.0996$

2	3659-3678	$y = 1.018x - 0.424$
2	3678-3701	$y = 1.5818x - 0.3965$
3	3702-3750	$y = 5E-05x^2 - 0.0039x + 0.989$

The average initial water saturation of each zone was compared with NMR water saturation. Graphs are shown in Figure 10, 11 and 12.

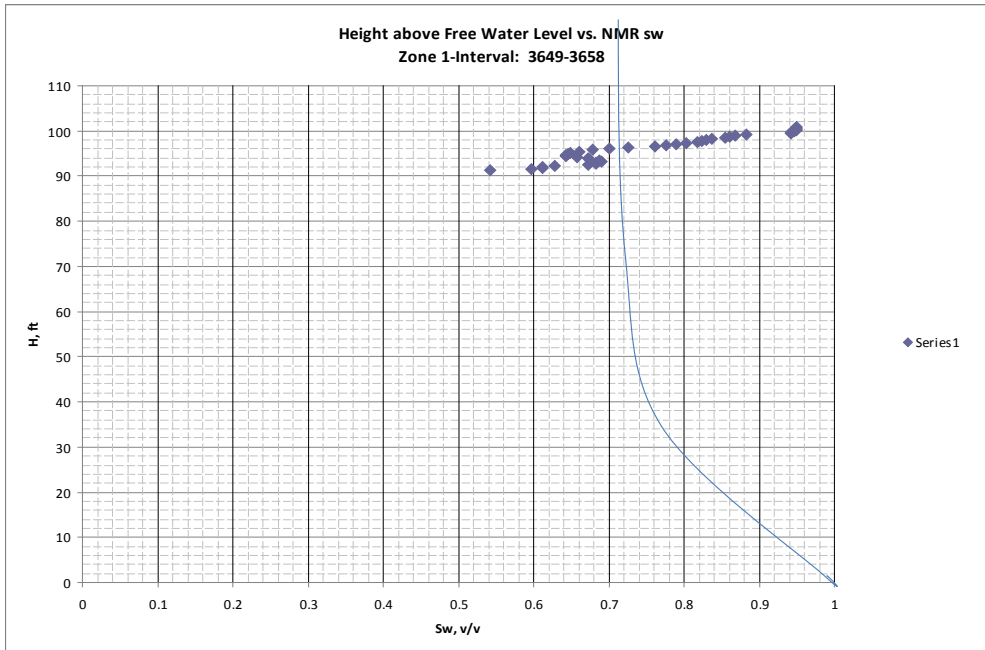


Figure 22: Height above free water level vs. initial water saturation for zone 1 in well 1-28.

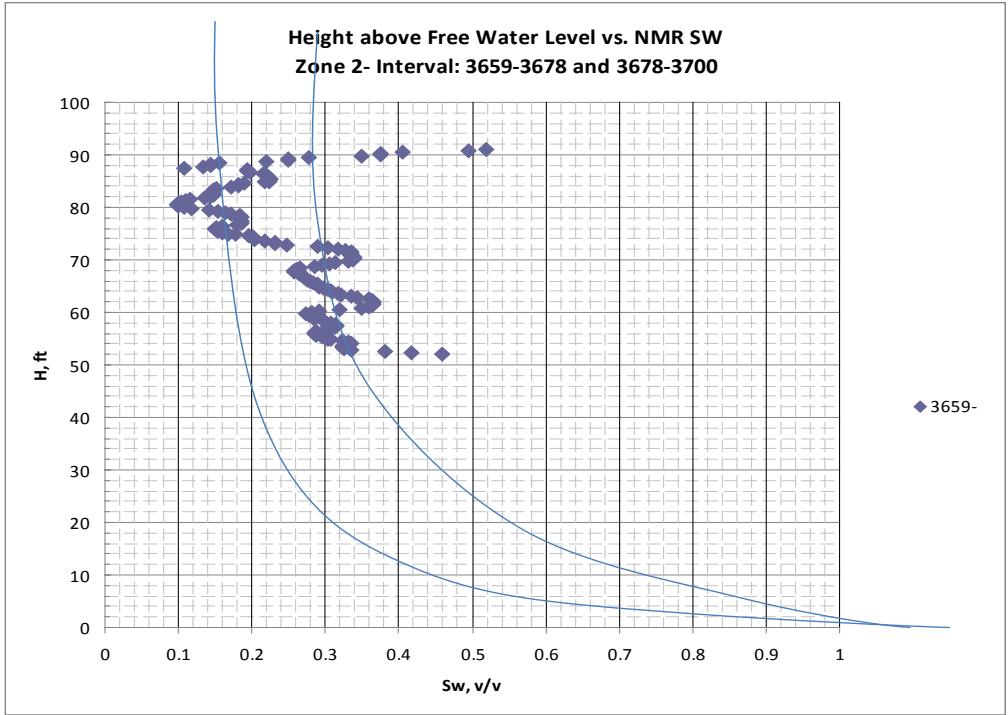


Figure 23: Height above free water level vs. initial water saturation for zone 2 in well 1-28.

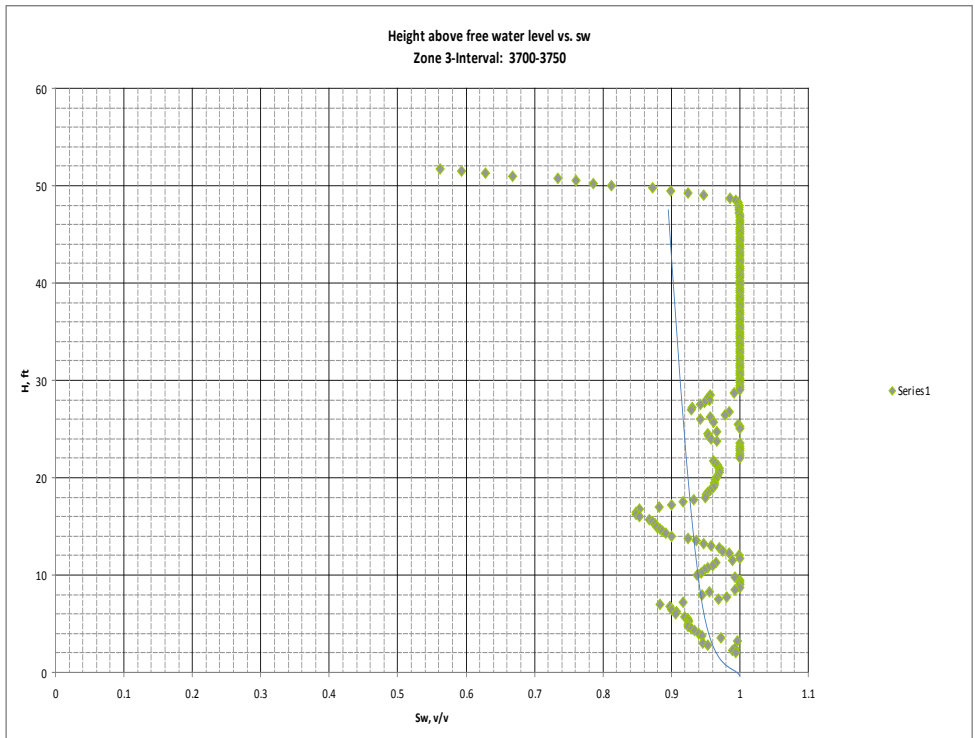


Figure 24: Height above free water level vs. initial water saturation for zone 3 in well 1-28.

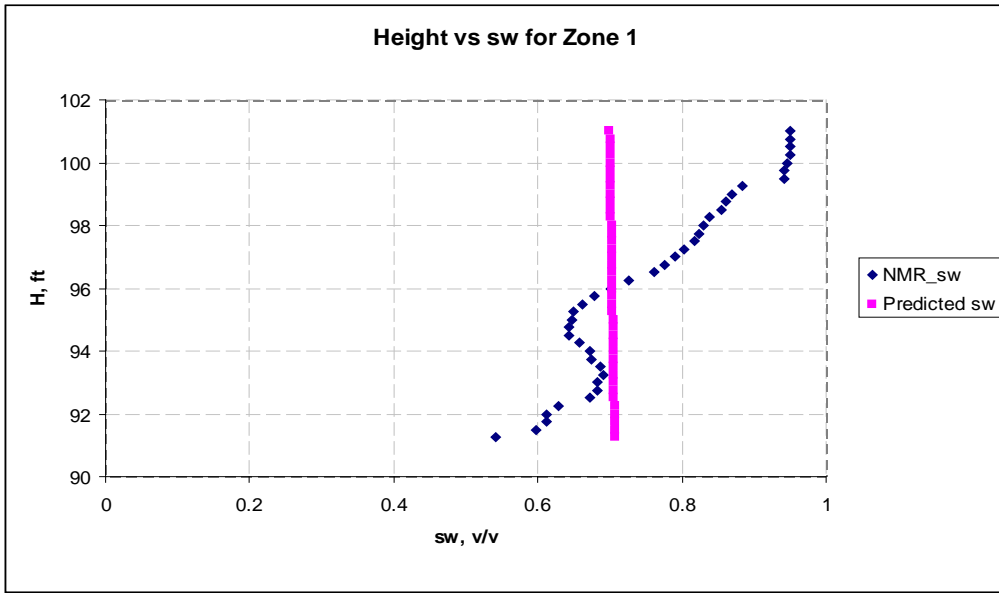


Figure 25: Height vs. sw for zone 1 in well 1-28, comparing the calculated average water saturation with the initial water saturation from NMR.

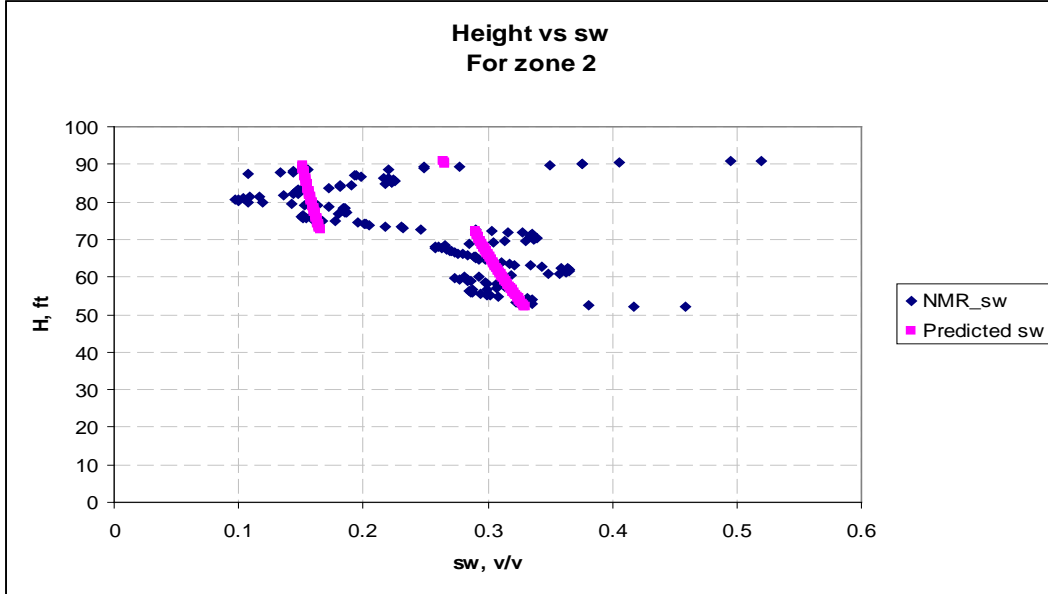


Figure 26: Height vs. sw for zone 2 in well 1-28, comparing the calculated average water saturation with the initial water saturation from NMR.

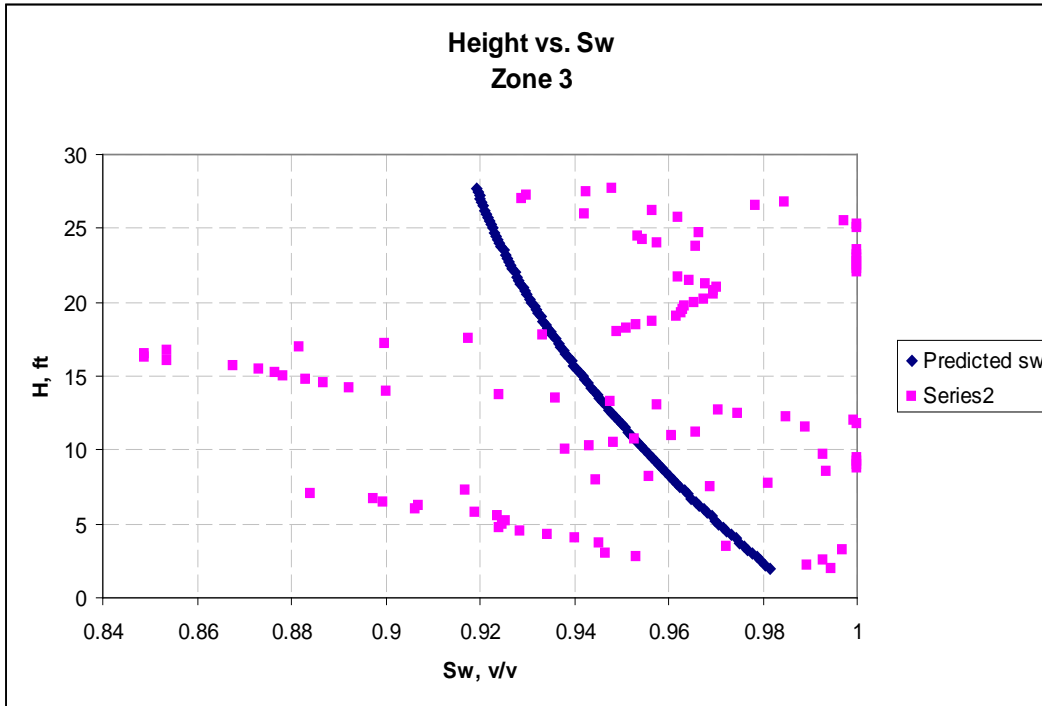


Figure 27: Height vs. sw for zone 3 in well 1-28, comparing the calculated average water saturation with the initial water saturation from NMR.

Conclusion

Four Pc curves for Zones 1 to 3 of Mississippian formation were obtained based on analysis results of NMR logs. These curves can be used to define initial water saturation in other wells. Initial water saturation in wells 28 and 32 are also determined from NMR logs. It is intended to find similar zones in other well which have good porosity data from logs and apply the mentioned Pc curves to respective zone to find initial water saturation in other wells.

**Initial Oil-Water Contact in Mississippian Formation Wellington Field
by Mina Fazelalavi**

As discussed below, results of log interpretations (water saturation), DST data and production history of the field were studies for oil-water contact determination. OWC could not be determined from any of these methods however, the deepest depth that has produced hundred percent oil was found from production history of the wells. One of the wells had produced oil without water from -2480 ft. Therefore there had been oil in this reservoir down to -2480 feet SS. It is concluded that initial oil water contact in Mississippian formation had been below -2480 ft.

- 1) Resistivity logs of wells in Wellington field in Mississippian formation were studied. Also water saturations from logs were reviewed, but these data were inconclusive. Apparently there is a change in water saturation in newer wells due to either invasion by water flood or formation water. Older wells with older completion date didn't have any resistivity logs therefore, BVW-HAFWL function could not be applied to find free water level and OWC.
- 2) All available DST data for Wellington field in Mississippian formation were studied. DST data from new wells were not useful due to water invasion of the field. Therefore, all DST data from older wells with older spud dates in the field study area was tabulated and analyzed for oil-water contact determination. All DST data were in the oil zone therefore, OWC could not be determined from DST data. However, the deepest depth of oil zone could be determined from DST data. DST in well #00492 shows mud and slightly oil from 2460 -2503 feet which is not conclusive. Also DST in well # 19024 shows some oil with some water from 2401-2405 feet which may not be correct. DST data in well # 43782 with spud day of 11/1/1935 shows oil and gas from -2394 feet SS to -2431 feet SS. DST data are tabulated in Table 1.
- 3) There were no RFT or MDT available for this field. In the absence of RFT and MDT, Final shut in pressure from DST can be used for OWC determination if plotted against depth. However, several pressure points in both oil and water zone in the same well are needed in order to have a separate pressure gradient for oil and water. No well had shut in pressure curves both in oil and water zone. Also DST data of the new wells, as an instance 1-32, could not be used due to water invasion. Therefore, this method did not work.
- 4) Production history of Wellington field was the only useful data for OWC estimation.

It seems from the production history that the field production started in 1929 without any significant water production prior to 1943. Production history shows that waterflood started in ~1950. Production data in well #10299 with completion date of May-12-1947 shows 200 bbl of oil produced in 1947 with no water production in 2 years. The total depth of this well is at -2481 and from casing shoe at -2442 to -2481 is the open hole producing interval in this well. This shows the OWC is below this depth however, the exact depth can not be determined. Also well #10285 with completion day of Nov-28-1936 shows 15 bbl of oil produced in 1937 with no water production at -2471 feet SS. Production data is tabulated in Table 2.

Conclusion

There is oil down to -2480 feet from production history of the wells and depth of initial OWC is deeper than -2481 ft. Section 18 and 19 in Trezell field might be connected to Mississippian reservoir and they may have a common OWC because the deepest counter line between these culminations (**Figure 28**) is shallower than -2481 ft. Also, one of the wells in section 19 has produced 100 bbl of S1 oil with mud from -2479 feet (Table 1, DST data).

Table 1: DST data

API	Section	Spud Day	Elevati on	Elevati on	DST interval, SS	DST interval, MD	Fluid recovered
15-191- 43782	28-31- 1W	11/1/193 5	1267.0 0	KB	-2394-2409 -2413-2417 -2413-2423	3661-76 3680-84 3680-3690	O & G odor GSO & G 15 BO/13 hrs, 3000 A: 166 BOPD
15-191- 10103	33-31- 1W	Sep/17/1 935	1260	DF	-2390-2396 -2401-2403 -2406-2413 -2413-2426	3650-56 3661-63 3666-73 3673-86	increase in gas 200 ft of oil in hole 2500ft of oil in hole 125 bbl natural
15-191- 10082	32-31- 1W	5/22/193 6	1264	DF	-2391 -2394 -2401-2405	3655 3658 3665-69	show of Gas Show of oil Increase of oil
15-191- 43782	28-31- 1W	11/1/193 5	1267	KB	-2394-2409 -2413-2417 -2417-2423 -2423-2431	3661-76 3680-84 3684-90 3690-98	Smell of gas Increase in gas Oil filled in hole Swabbed 15 bbls oil in 13 hrs
15-191- 19024	33-31- 1W	Apr-21- 1936	1265	KB	-2401-2405 -2422-2427 -2401-2427	3666-70 3687-92 3666-92	oil and some water water exhausted 200 bbls oil
15-191- 00492	8-32- 1W	6/12/194 6	1258	DF	-2460-2503	3718-61	90ft M & SSO
15-191- 00537	19-31- 1W	3/4/1959	1253.0 0	KB	-2470-2479	3723-32	100 SL OCM

Table 2: Production data

We ll	Location	Completi on Date	Total depth, MD	Total depth, SS	Top of Mississippi an	Elev ation	Elev Referen ce	First day of Production	oi l	wa ter	Open/clo se hole
10 29	T32SR1 W, Sec 8	May-12- 1947	3689	-2481	3649	1208	DF	1947	2 0 0	0	open
10 28	T32SR1 W, Sec 5	Nov-28- 1936	3689	-2471	3655	1218	DF	1937	1 5	0	open

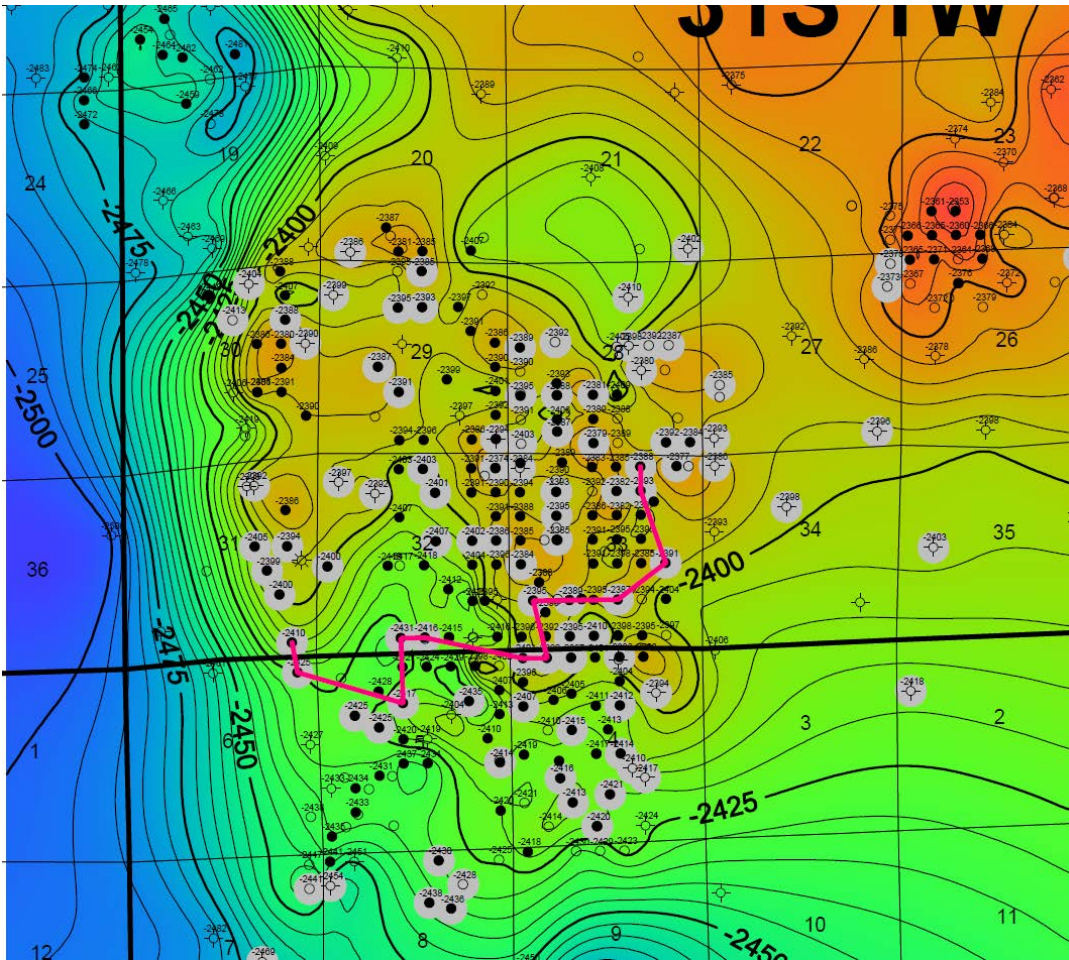


Figure 28: Contour map of Mississippian formation in Wellington field

Geomodeling and Reservoir Simulation in Wellington Field for use in the application for Class VI injection at Wellington Field supported under DE-FE0006821

Injection zone – The characterization of the lower Arbuckle, Gasconade Dolomite to Gunter Sandstone Member has determined that this interval has sufficient permeability and net porous thickness of strata in the interval to accommodate the 40,000 tons of CO₂ to be injected during the small scale test (**Figure 29**). The assessment is based on analysis of core, wireline logs, interference test, and continuity of impedance/porosity mapping from 3D seismic and new coupled flow and geomechanical dynamic modeling. Similarly, the excellent response of the waterflood in the Mississippian oil reservoir strongly suggests that the 30,000 ton CO₂ injection will have a favorable response.

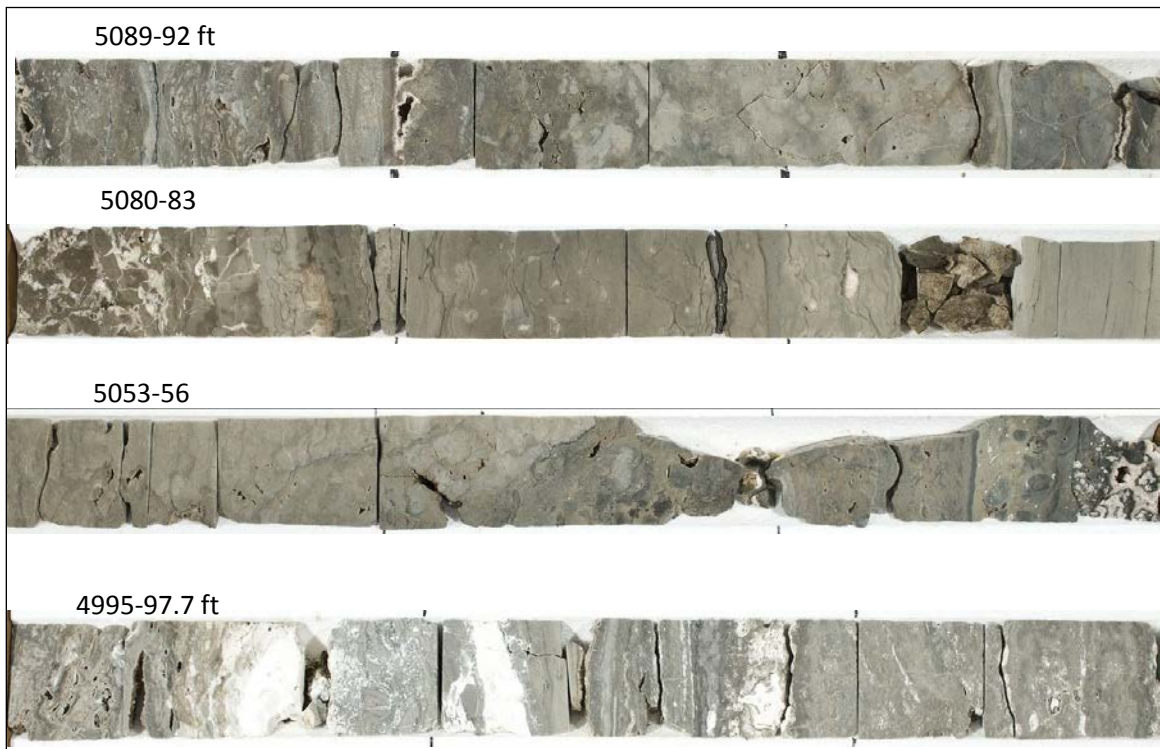


Figure 29. Representative samples from the injection zone in KGS #1-32 core.

Baffle and trapping of CO₂ in the Arbuckle saline formation – The comprehensive set of measurements from wells #1-32 and #1-28 and inversion and impedance analysis of the 3D seismic indicate that the middle ~300 ft interval of the Arbuckle (lower Jefferson City Cotter down to near the top of the Roubidoux Formation) is predominantly tight, slightly argillaceous dolomite with thin alternating shales and permeable intervals (**Figure 30**). Moreover, major and minor element, cation and anion geochemical and isotopic (carbon and deuterium) analyses of formation brines using multiple limited interval drill stem tests and perforation of casing and swabbing indicate that brines in the upper and lower Arbuckle are not in communication on the scale of geologic time. This isolation of the hydrostratigraphic units is at least the case for the local area studied. Core, wireline logs, seismic, and geochemistry together corroborate the extensive continuity of the tight mid Arbuckle interval. The result should be at least baffling of the CO₂ that is injected beneath and flow of CO₂ into thinner permeable intervals leading to CO₂ trapping in the finer pores and mixing and solution of the CO₂ into the brine making it heavier and further decreasing the buoyant, free phase CO₂.

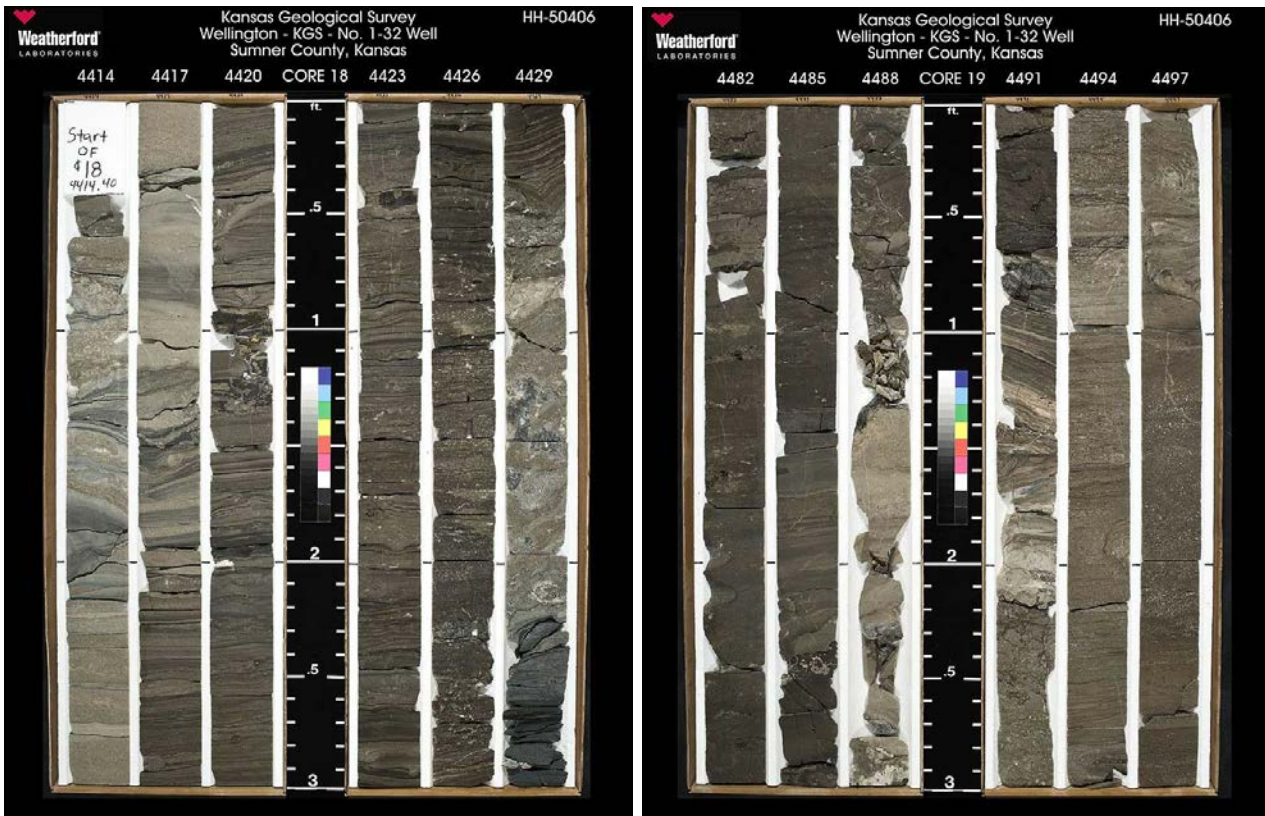


Figure 30. Mid Arbuckle barrier/baffle interval lower Jefferson City-Cotter. Note shale at 4431 ft an abundant darker laminated micritic dolostone that dominates the baffle/barrier in the mid Arbuckle.

Primary caprock interval – A very important elements besides injectivity and storage in the saline aquifer where the CO₂ injection will take place is the integrity of the primary caprock. The caprock interval that is being intensely studied includes the 1) ~120 ft thick, Middle and Lower Mississippian-age tight, dark argillaceous dolosiltite that is tentatively correlated to the Pierson Formation and 2) the black, clay-rich Upper Devonian Chattanooga Shale (**Figure 31**). The underlying Simpson Group shales and sandstones rest on the Arbuckle and appear to be locally sealing since oil is locally trapped in the sandstones on this structural dome in Wellington Field, albeit off to the edge of the structure and not near the injection site.

An abundance of data is being synthesized from existing study for use in the application for injection including 1) core analysis consisting of mechanical tests, CO₂ “soak” tests of plug samples to examine reaction via geochemical and CT scans of plugs, capillary pressure, and helical CT scans of whole core; 2) and wireline logs including dipole sonic, density, microimaging, and NMR; and 3) 3D seismic imaging to correlate to well

calibration data and map properties for use in building a refined geomodel. The latter activity, specifically, the geomechanical dynamic modeling is only now beginning due to recent receipt of final mechanical measurements from the lab during the quarter.

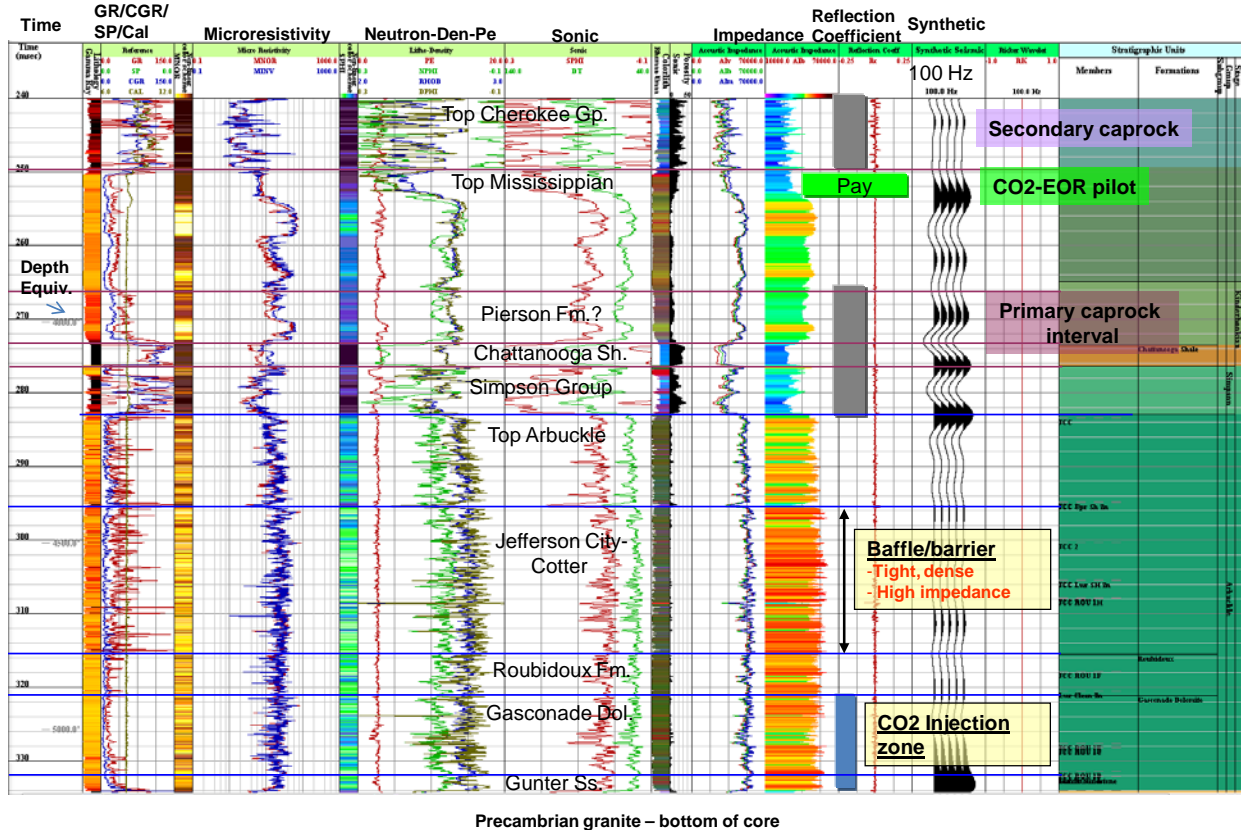


Figure 31. Synthetic seismogram, impedance, and triple combo log suite KGS #1-28 (CO₂ injection well in Arbuckle at Wellington Field). Vertical scale is in 2-way seismic travel time with tick marks and depth noted alongside this scale. The illustration identifies the Arbuckle injection zone, baffle/barrier in mid Arbuckle, primary caprock interval (Pierson, Chattanooga, and where predominately shale, the Simpson Group), pay and CO₂-EOR test interval in the Mississippian, and the secondary caprock of the Arbuckle and primary caprock of the Mississippian injection.

The primary caprock as noted above continues to be studied at a micro to macro field-wide level. The interval has generally lower seismic impedance and can be distinguished from surrounding strata (Figure 4). The relatively thick (120 ft) silty lower Mississippian that is tentatively correlated to the Pierson Formation is mappable with seismic, an activity that is still being refined, and is distinctively dark and tight argillaceous dolomite siltstone. The higher organic content (one sample is 1% TOC) is enough to give the rock a dark gray-brown to black color (Figure 32). Measurements of permeability from two

samples of this interval were carried out in the NETL lab in Pittsburgh during fall 2011 and results indicated pico- and nano-darcy permeability.

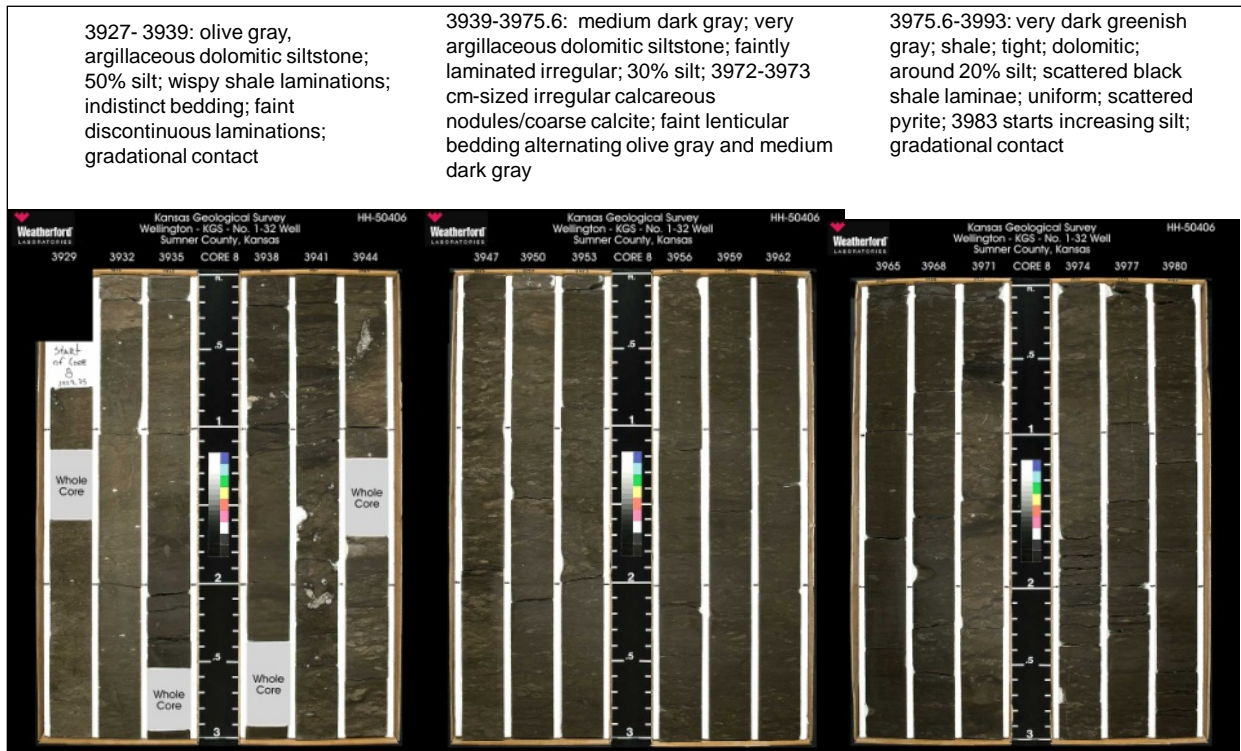
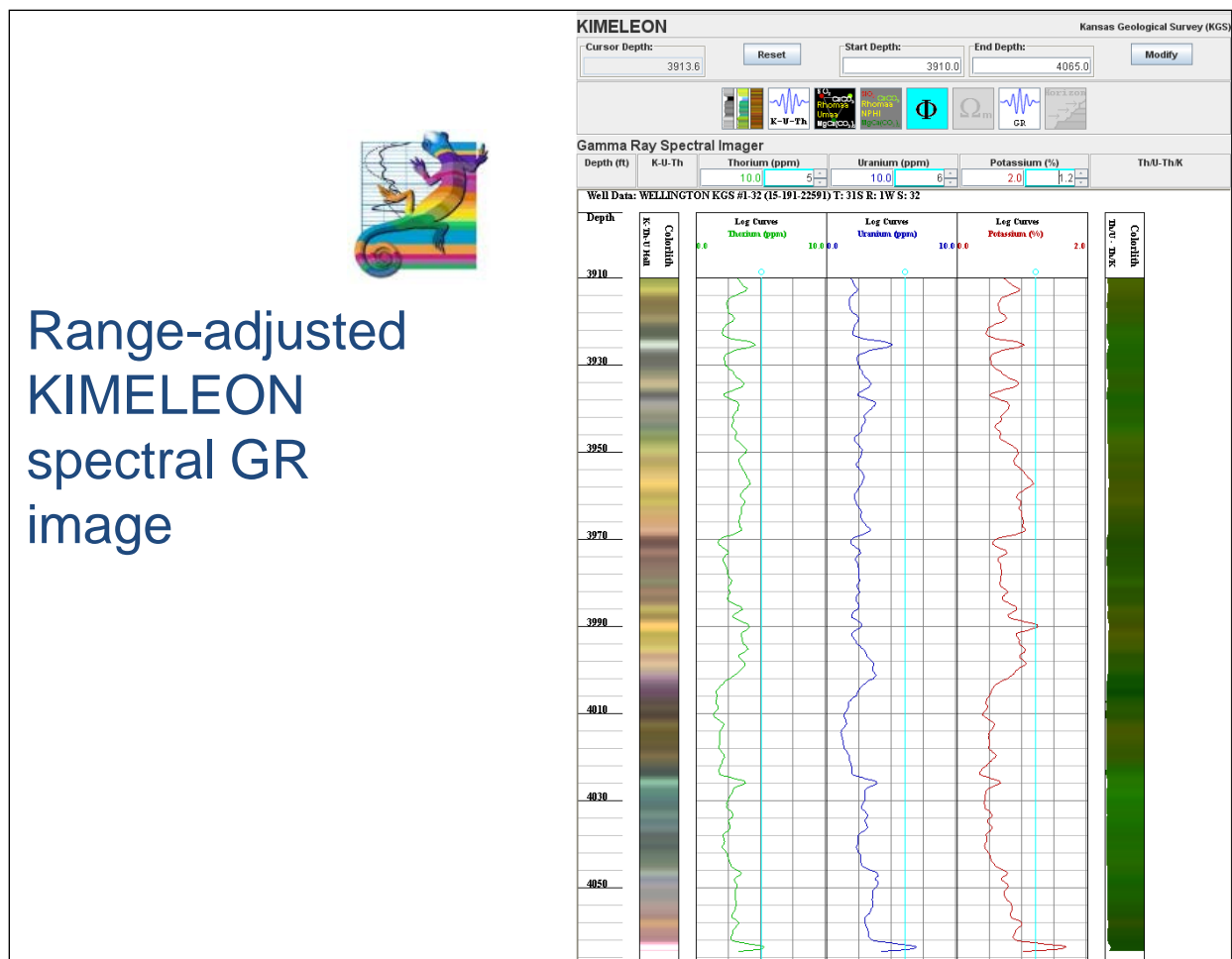


Figure 32. Representative samples from the lower Mississippian Pierson Formation that overlies the Chattanooga Shale is being evaluated as part of the primary caprock overlying the Arbuckle.

The complexity of the stratigraphic succession of the dark fined-grained interval of the Pierson Formation is illustrated by the spectral gamma ray spectral imaging tool, Java freeware app developed at the KGS with DOE support of the characterization project , DE-FE0002056, <http://www.kgs.ku.edu/stratigraphic/ KIMELEON/> (Figure 33). The more organic rich intervals generally ties very closely to the higher uranium interval, the middle track in Figure 6. The organic matter may be an important contributor to both the integrity of the caprock providing an additional means to trap CO₂ that may move along fractures within the interval.



Range-adjusted KIMELEON spectral GR image

Figure 33. Gamma ray spectral imager of the portion of the lower Mississippian Pierson Formation that appears to be able to serve as part of the primary caprock. A complex succession of strata are denoted via potassium, uranium, and thorium distribution.

The caprock is further examined using the nuclear magnetic resonance (NMR) imaging tool (**Figure 34**). The tool is a mature technology, but not often used to help define pore size distribution, water/hydrocarbon saturation, and estimate permeability. It was run in both wells drilled under DE-FE0002056, KGS #1-32 and #1-28. It has been compared with porosity and permeability from core analysis and used to compare Kh from drill stem tests and step-rate test. Together with the sonic, density, and resistivity logs, it provides a means to substantially increase the understanding of both porous and permeable rocks and distinguish them from low porosity and low permeability rocks. Such is the case for the interval considered as the primary caprock for the Arbuckle.

Magnetic resonance imaging analysis

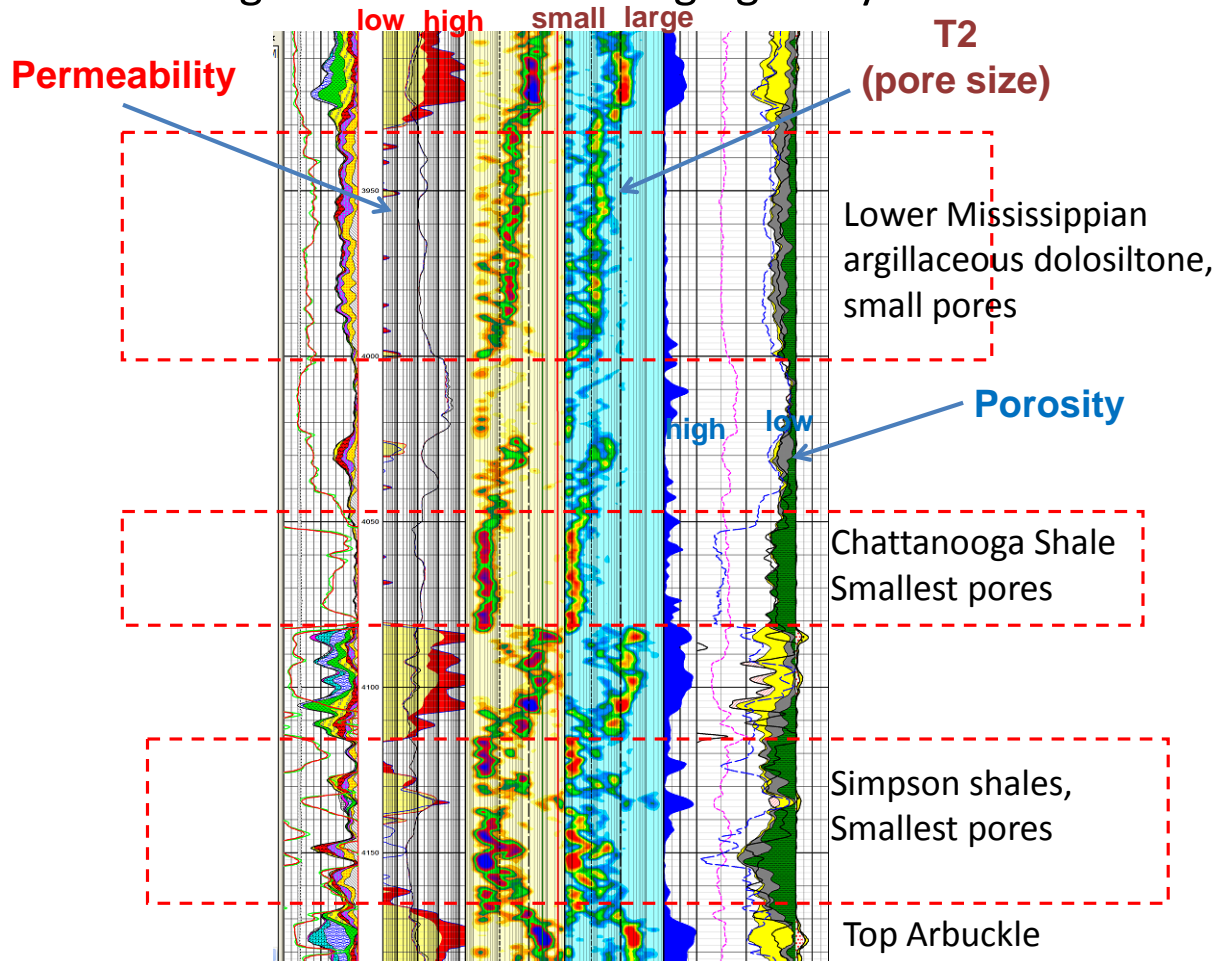


Figure 34. Magnetic resonance imaging profile in well KGS #1-28 from the interval being considered as the primary caprock for the Arbuckle CO₂ injection at Wellington Field. The NMR is very useful in allowing continuous comparison of properties of the matrix pore system that comprises this interval.

Fracture and fault characterization is being completed for the application for Class VI injection. The 1600 ft of core taken from KGS #1-32 was described over the course of a week by Lorenz and Cooper. **Figure 35, 36, and 37** summarize the fracture distribution as visually described from the interval extending from the Cherokee shale, the secondary caprock above the Mississippian, to below the CO₂ injection zone near the base of the Arbuckle. The fracture summary show that both the primary (particularly the lower Mississippian Pierson Formation) and secondary caprock have low fracture density and lack the horizontal high porosity enhanced fractures (HZ HPZ) seen in the Arbuckle. Fracture heights are also less than 1 ft in the caprocks compared to several feet common to the mid Arbuckle baffle/barrier and the lower injection zone of the Arbuckle. Finally, remnant porosity varies but tends to be higher in the mid Arbuckle baffle/barrier as the brine geochemistry and microbial population suggests that the interval is more isolated

and less cement due to smaller pore volumes of brine passing through might be a logical conclusion.

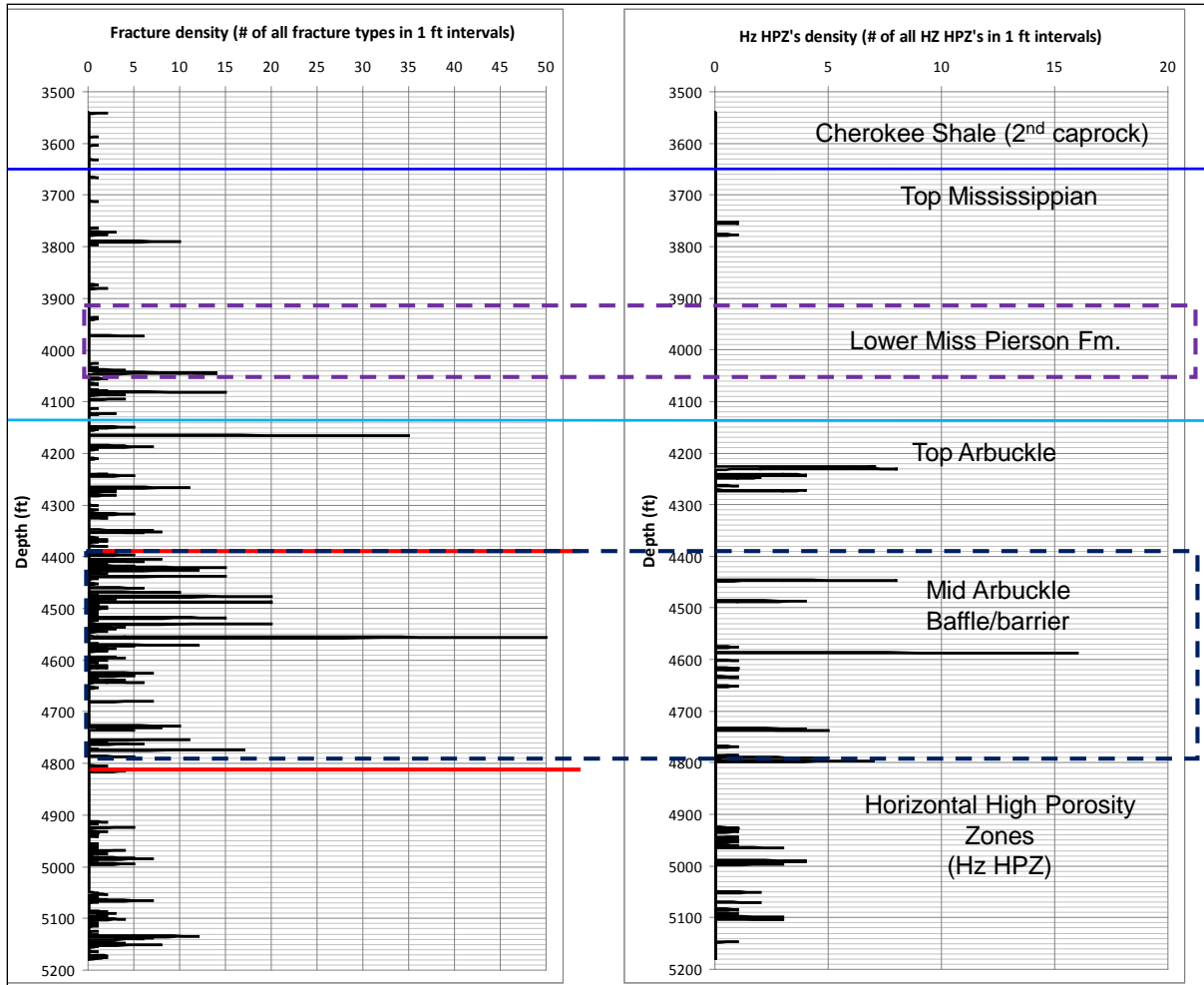


Figure 35. Fracture characterization of KGS #1-32 core by Lorenz and Cooper showing fracture density (# fractures in 1 ft intervals) (left) and frequency of horizontal high porosity zones (Hz HPZ) (right).

Additional fracture characterization has been made with the microresistivity imaging tool, the spectral (oriented dipole) sonic, and 3D seismic. The spectral sonic establishes the fracture intensity, the imaging logs similar map the fracture and recognizing open, partial, closed. The seismic is being used to recognize discrete fracture networks that are resolvable with the seismic.

A final version of the 3D seismic data will be depth migrated and used to map faults, fractures, and apparent porosity. The seismic time-impedance presented as an arbitrary section through Wellington Field that includes available velocity control is shown in Figure 11. The injection zone and upper Arbuckle have lower impedance than the middle

Arbuckle baffle/barrier, and the lower Mississippian and Cherokee shale have lower impedance indicative of their shaly nature. The higher low impedance interval above the Cherokee is the upper Pennsylvanian shale that dominates the southern portion of the Kansas and is clearly a thick rather uniform interval of strata that can serve to prevent CO₂ from moving upward toward the USDW. This entire interval up to the level of the Heebner Shale (**Figure 38**) is deep enough for CO₂ to be in a supercritical state.

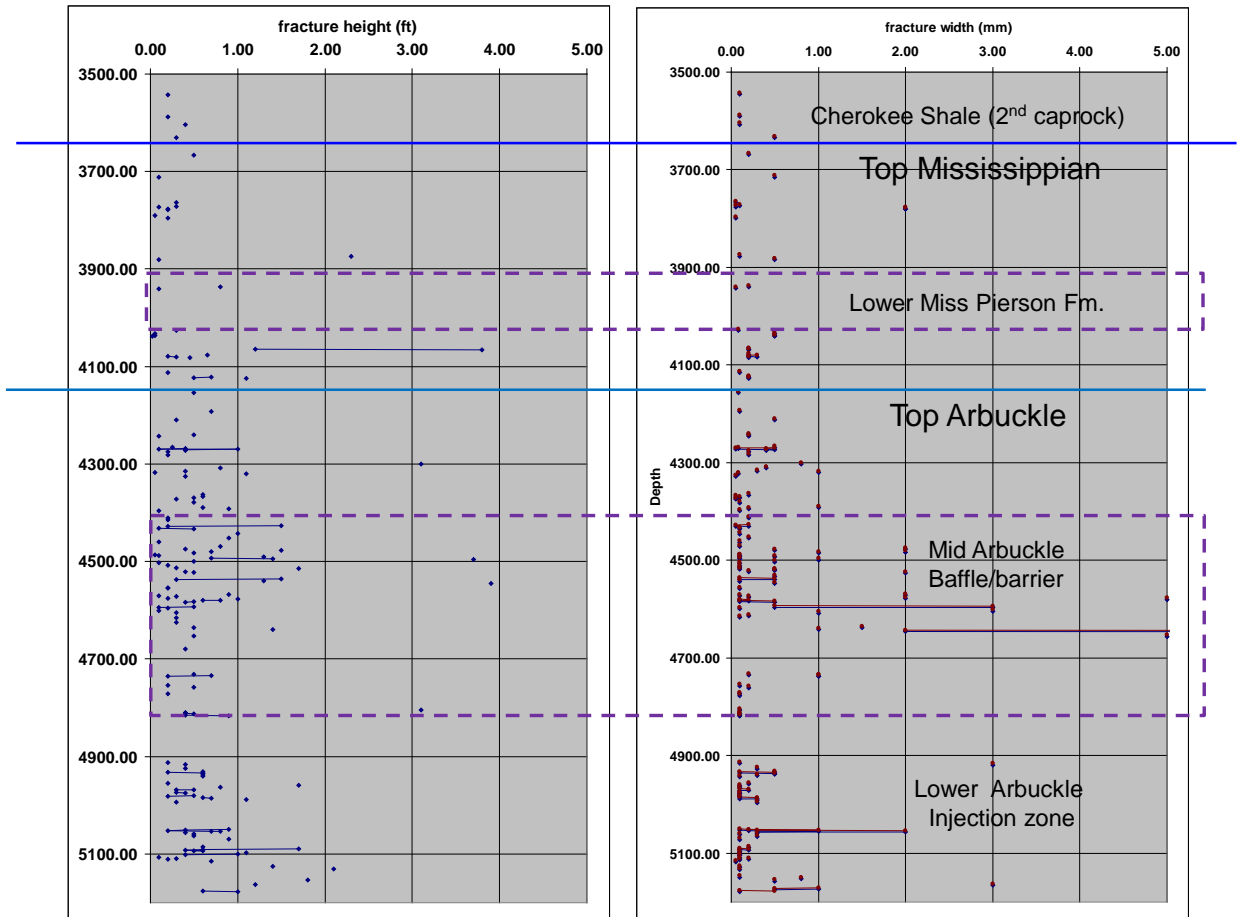


Figure 36. Fracture height (left) and fracture width (right).

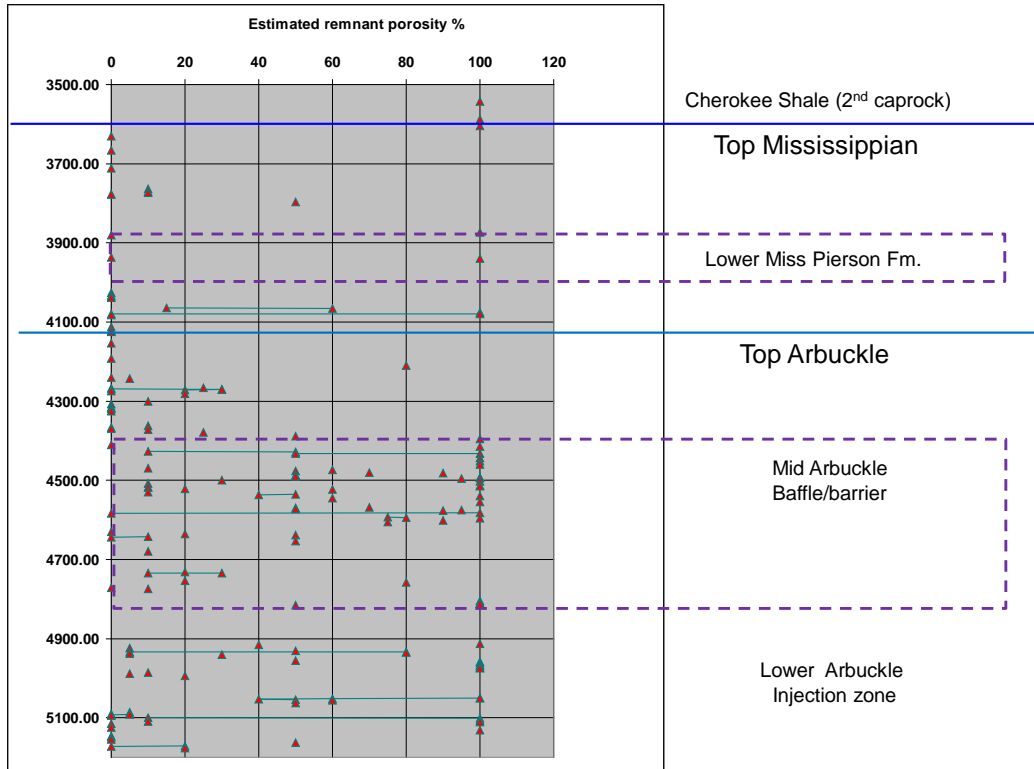


Figure 37. Estimated remnant porosity (%) from the fractures described by Lorenz and Cooper for the core taken from KGS #1-32.

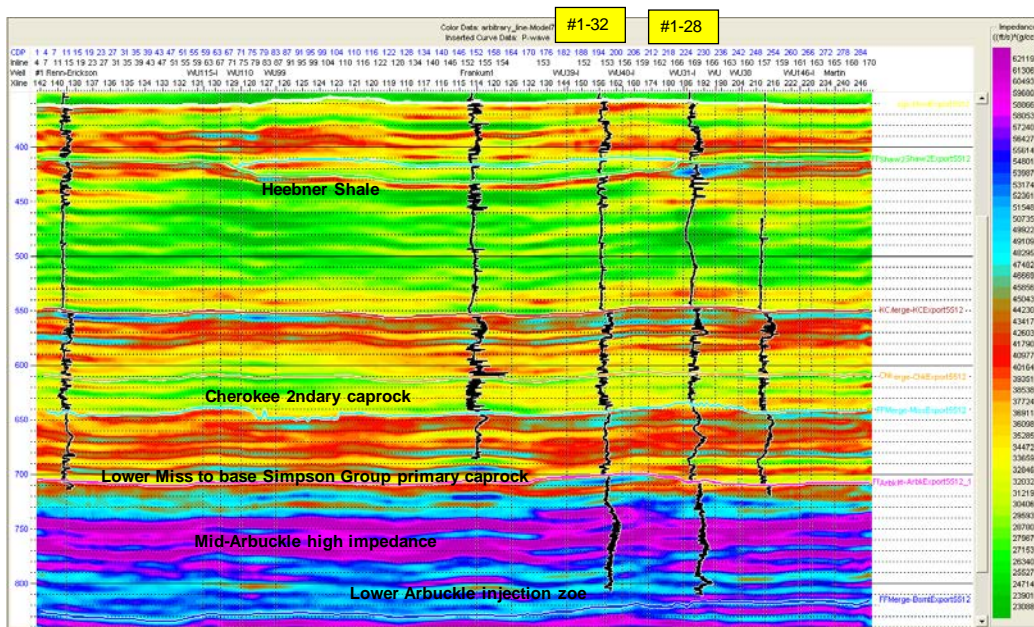


Figure 38. Arbitrary seismic section in time from 3D volume showing seismic impedance profile in Wellington Field including new wells drilled through the Arbuckle (KGS #1-32 and KGS #1-28). Porosity in the injection interval as inferred impedance, the mid Arbuckle baffle, and the caprocks are rather continuous.

The static geomodel used in the Class VI application will include a combination of the information obtained from the wireline logs, core analyses, and seismic data. Once a final version of the seismic interpretation is made the results will be imported into Petrel geocellular model for additional processing and visualization. The updated Petrel geomodel will be imported into CMG to conduct the dynamic model.

The iteration of dynamic model to be used for the Class VI injection permit is based on both the geomechanical and physical properties that have been obtained from the characterization project, DE-FE0002056. The models will dictate 1) the area of review; 2) the location, size, and composition of the CO₂ plume over time; 3) design the injection profile so that conformable sweep is obtained in multiple flow units, plume is observable in the observation well, but injection is designed to limit longer lateral migration; 4) the extent of the free phase CO₂ both vertically and laterally as the plume interacts with the flow units baffles, barriers, and fracture systems; 5) the pressure field and the stresses imposed on the caprock to understand and avoid parting existing fractures or create new fractures. The dynamic model and its updated versions during injection will predict the degradation of the plume and its location so that the project can be brought to closure.

An initial coupled geomechanical and flow model is currently being tested and refined, integration appropriate data that has been analyzed, but short of having a refined Petrel model that includes the latest seismic interpretation. Thus this model is isotropic with no compartments or larger scale fractures. The mature model will have included shallower caprock and seals to demonstrate that the CO₂ injection will not affect the USDW.

Goals of modeling –

- To evaluate different injection scenarios for selection of optimal operation procedures
- To understand a pressure response of Arbuckle reservoir as a result of CO₂ injection
- To project the reservoir injectivity and transmissibility properties
- To estimate a degree of CO₂ solubility in the in-situ brine
- To correlate reservoir and cap-rock properties with existing data analyses and other modeling results

Model Parameters --

- 40,000 metric tons of CO₂ injection into lower Arbuckle zone where middle Arbuckle is considered as impermeable barrier
- Closed boundaries
- Dual porosity/permeability (**Table 1, Figure 39**)

- 3D “Layered Cake” (50x50x46 cells) model with homogeneous properties within each layer representing geologic formations:
 - Chattanooga Shale (low porosity no perm)
 - Upper Arbuckle (high porosity and perm)
 - Lower Arbuckle (lower porosity and perm)
 - Arbuckle injection zone (high porosity and perm)
- CO2 solubility in water is considered
- 3 cases of permeability estimations were considered (P10; P50; & P90) (Table 1, Figure 12).

Case Name	Perm – Matrix, Top Arbuckle, md	Perm – Fractures, Top Arbuckle, md	Perm – Matrix, Mid. Arbuckle, md	Perm – Fractures, Mid. Arbuckle, md	Perm – Matrix, Inj. Arbuckle, md	Perm – Fractures, Inj. Arbuckle, md	Fracture spacing, m	CO ₂ Injected, MT
High Permeability	1000	1500	1e-7	1e-7	<u>600</u>	<u>1500</u>	3	40
Mid. Permeability	500	1000	1e-7	1e-7	<u>300</u>	<u>1000</u>	3	40
Low Permeability	200	500	1e-7	1e-7	<u>100</u>	<u>500</u>	3	40

Table 1. Permeability applied in the dual-porosity model.

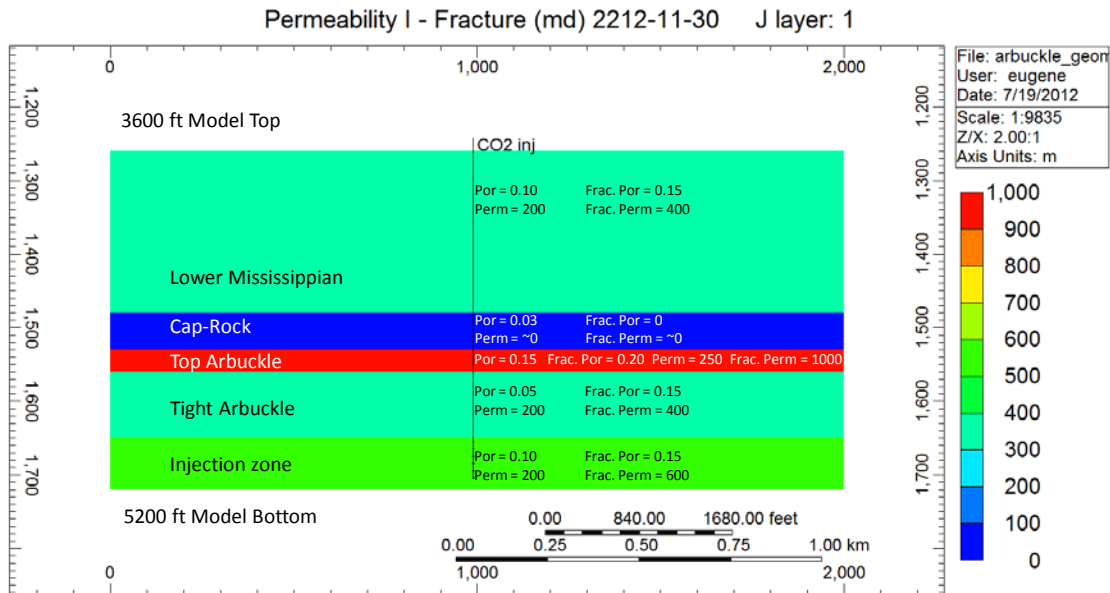


Figure 39. Model parameter permeability shown for stratigraphic divisions used in this initial coupled geomechanical-flow simulation.

Rock Type	Poisson's Ratio	Young's Modulus *10 ⁶ , kPa	Cohesion, kPa	Fracture spacing, m	Rock Compressibility, 1/kPa
Cap-rock - Matrix	0.25	4.997	689285	3	5.8e-7
Cap-rock - Fractures	0.25	4.997	689285	3	5.8e-6
Arbuckle - Matrix	0.30	9.720	689285	3	5.8e-7
Arbuckle - Fractures	0.30	9.720	689285	3	5.8e-6

Table 2. Geomechanical model parameters used in initial coupled simulation. Properties obtained from mechanical measurements to core from KGS #1-32.

The modeled injection was also carried out using three injection scenarios.

The modeled injection scenarios --

- 9 months, 70 kt CO₂ injection
 - Projected amount of CO₂ at projected rate
- 3 months, 100 kt CO₂ injection
 - Rapid pressure increase to brake a cap-rock
- 1 months, 70 kt CO₂ injection
 - Projected amount of CO₂ in shorter time period, or “economically safe”

The results are very encouraging (**Figures 40 and 41**). The pressure exerted on the caprock is minimal and the plume undergoes degradation in the lower Arbuckle, as currently modeled. The pressure/stress regimen from the injected CO₂ was not sufficient to compromise the cap-rock integrity in this modeling configuration. Additional configurations will be examined including fracture & fault scenarios once the new Petrel model is available.

Interim results –

- The pressure response to 40 kt CO₂ injection is minimal for all three estimated permeability cases (~400 kPa or ~60 psi max) even if closed boundaries model is utilized
- It is suggested to investigate a higher injection rate and higher volume of injected CO₂ scenarios
- Additional attention and analysis are required for permeability estimations
- It is projected that most of the injected CO₂ will be dissolved in water

- It insures CO2 containment and reduces its mobility
- Geochemical investigations will be critical, especially if additional/commercial scale injection is projected.

kgs-28 CO2 co2 water solub 2 no perm 2 tight.irf

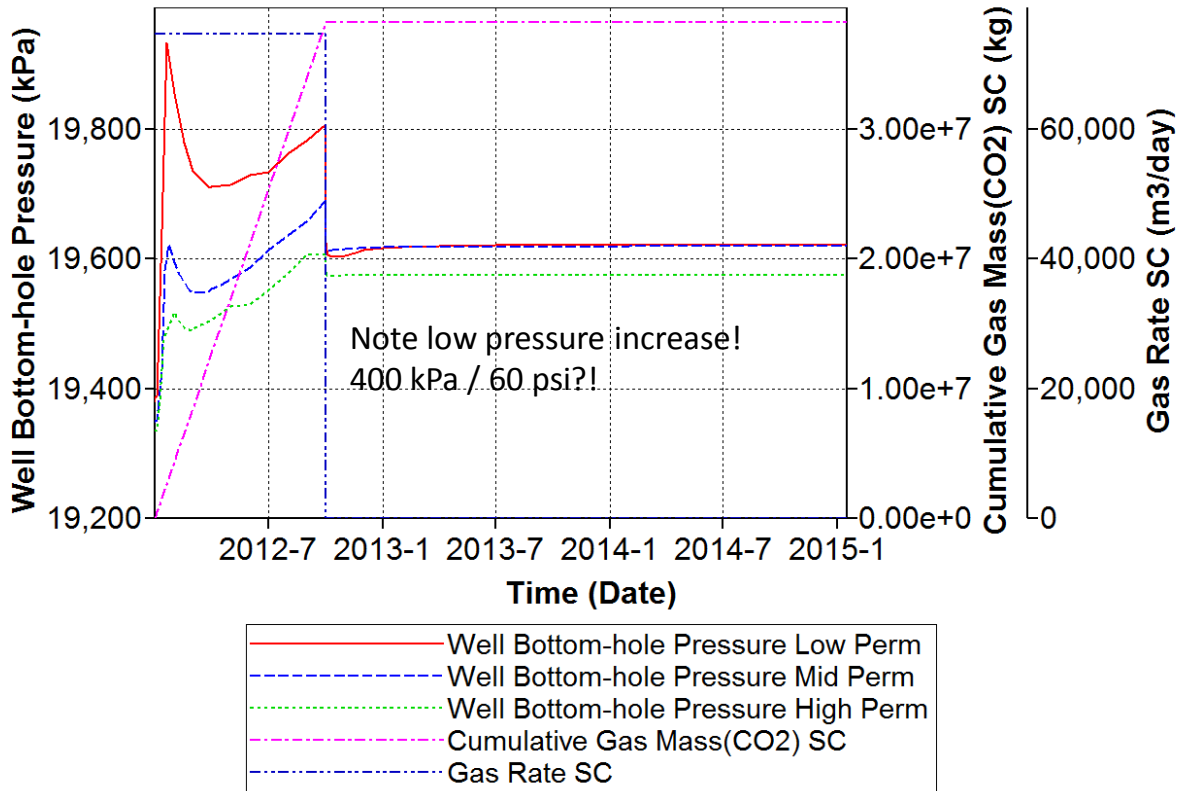


Figure 40. Pressure response comparison for 3-cases = 40 Kt CO2, pressure, cumulative gas, and gas rate plot. Small pressure increase noted in the current model.

9 Months Injection Scenario – High Permeability Case – 40 kt CO₂ Fracture Flow

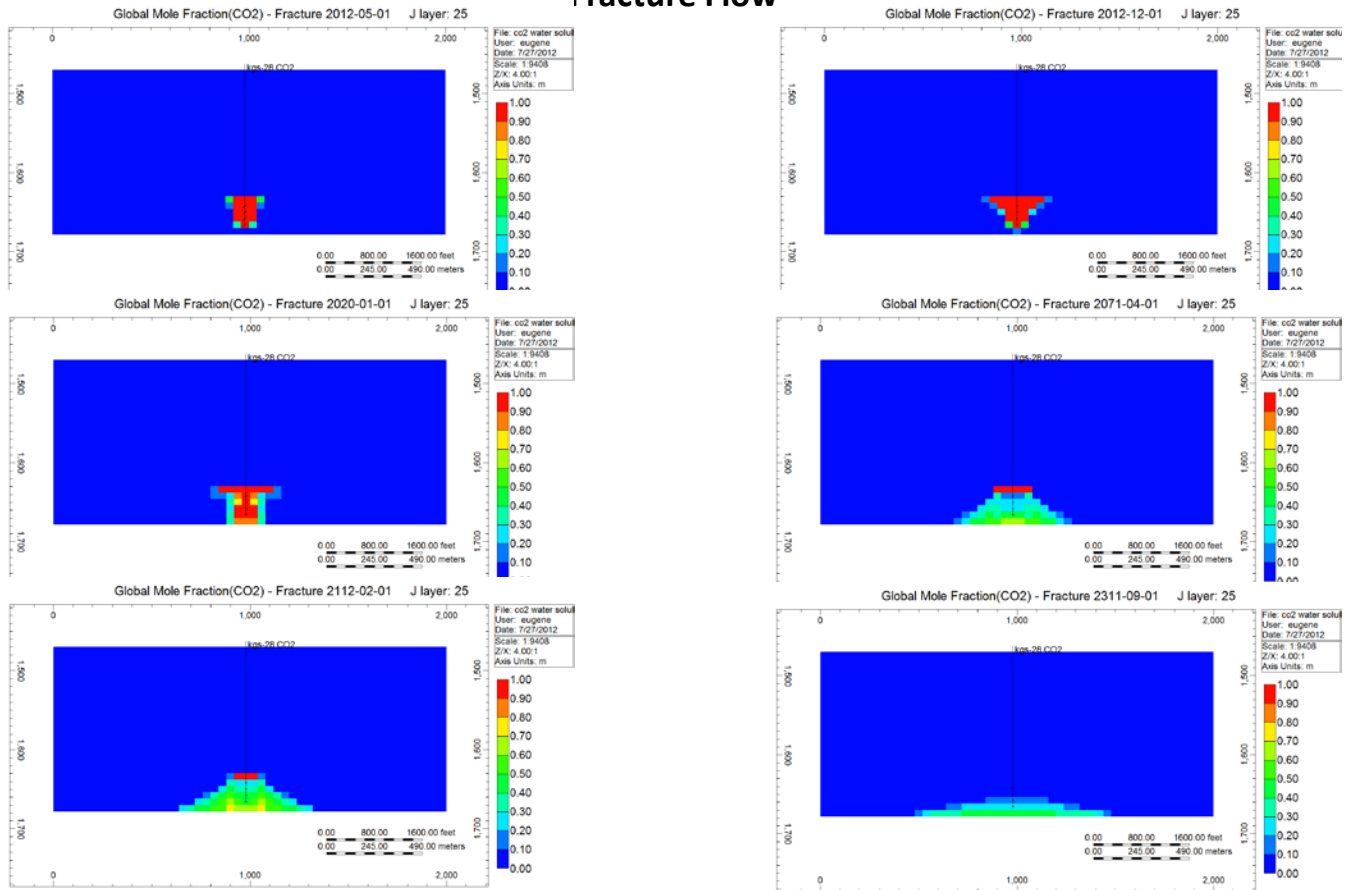


Figure 41. Nine month injection scenario – high permeability case – 40 kt CO₂ with fracture flow. CO₂ plume develops in the lower Arbuckle below and top of the plume is defined by the base of the tight mid Arbuckle. See model parameters in Figure 12.

PRESENTATIONS

April 2-3, 2012 – Invited presentation to Kansas Interdisciplinary Carbonates Industrial Associates Meeting, Lawrence, KS

April 4-6, 2012 – Invited presentation to PTTC-CO₂ Capture and EOR conference in Golden Colorado.

April 23, 2012 – Invited presentation to AAPG Annual Meeting, Long Beach, CA

KEY FINDINGS

1. Significant progress made in compiling information and characterizing site for use in the application for Class VI CO₂ injection permit in the Arbuckle under DOE contract DE-FE0006821. .
2. Incorporated depth-migrated seismic into initial Petrel geocellular model, but obtaining reprocessed seismic volume for use in revising the Petrel model for eventual use in simulation modeling for the Class VI permit application.
3. Completed geochemical and isotopic analyses of the brines samples in KGS #1-28 and #1-32. Results indicate that the Upper and Lower Arbuckle are hydraulically isolated by a mid Arbuckle barrier. This tight ~300 ft thick interval is also recognized on well logs, core, and 3D impedance mapping. While potentially reducing the injection interval to the ~300 ft thick lower Arbuckle, the mid Arbuckle will likely serve as an interval to “pancake” the CO₂ plume into thin layers of higher porosity and higher permeability intervals mixed with tight rock. Multiple layers perhaps accesses by localized fractures will facilitate mixing of CO₂ and brine, promote capillary entrapment of the CO₂, and limit or eliminate free phase CO₂ from accumulated beneath the primary caprock. The net effect could be to notably increase CO₂ storage.
4. Initial geomechanical modeling of the caprock interval is very positive. The 120 ft-thick lower Mississippian-age dark argillaceous siltstones are tight and have relatively minor evidence of fracturing based on a fully cored, logged, and seismically imaged and analyzed interval.
5. Two preliminary coupled dynamic models of the small scale CO₂ injection in the Arbuckle have been completed. Between solubility trapping and capillary effects the 40,000 tons will be likely be rapidly trapped in the lower Arbuckle where the CO₂ is injected. Further analysis will continue. Pressures are such that CO₂ escape from a worst case scenario of open wells in the AOR will likely not cause a leak of CO₂ to the surface due to relatively low pressure beyond the injection well. However, more modeling is needed to firmly conclude this.
6. The geomechanical component in the simulation run under CMG software is based on a complete suite of mechanical tests from core analysis. Initial results indicate mechanical integrity in this rock system will not be compromised by the 40,000 ton injection into the lower Arbuckle over 9 month timeframe.
7. Reprocessing of the 3D seismic will be used to discretely map fractures and faults. Yet, current geomechanical modeling indicates that reactivation of these structures is unlikely. An updated geomodel from Petrel based on a new seismic volume will used as input into final simulations including sensitivity analyses, as required by EPA for use in the Class VI application. These will be the results to establish the Area of Review.

PLANS

Key points about new seismic and drilling in Stevens County to evaluate CO2 sequestration in DOE contract DE-FE0002056 --

1. A new well, the Berexco Cutter KGS #1, 2440' FNL-1320' FEL Section 1-T31S-R35W, in the northeast corner of Stevens County, Kansas will commence drilling on July 29th. This location will be the second and final calibration site in a 3-year program to evaluate carbon sequestration potential in southern Kansas under a NETL-DOE funding to the KGS (DE-FE0002056) started in 2010.
2. This western Kansas well will be drilled in Cutter Field, operated by Berexco, LLC, Wichita, KS. The drilling selection process involved bids tendered by several of the companies who operate oil fields that are being characterized and modeled as part of the Southwest Kansas CO2 Initiative Consortium managed by Improved Hydrocarbon Recovery. Companies include Berexco, Cimarex, Elm II, GloriOil, Merit, and Anadarko who operate oil fields in this area including Pleasant Prairie South, North Eubanks, Shuck, and Cutter. These industry partners donated seismic, well, and production data to make this evaluation possible and participate in needed cost share. The concentration of these fields among others in this area could provide the basis for implementing commercial scale CO2 sequestration should evaluation be successful.
3. The drilling is being preceded by acquisition of nearly 9 square miles of 3D multi-component seismic imaging by Paragon Geophysical and designed by Hedke-Saenger Geoscience Ltd., both from Wichita, KS. Seismic data will be used to map the rock properties around the new well. Existing data was also used to site the well on a structural high that would aid CO2 plume management.
4. The Cutter KGS #1 and new seismic data will be combined with over 120 square miles of seismic data donated by industry partners to the project to augment and enhance the interpretations from the local scale and regional subsurface well based mapping.
5. The well is scheduled for 55 days of drilling by Berexco's drilling company Beredco, Inc., during which time approximately 1200 ft of core will be acquired between the Pennsylvanian Morrowan-age strata and the Precambrian basement, estimated to be located at 7550 ft beneath the surface.
6. Coring by Devilbiss, core analysis by Weatherford Labs, extensive wireline logging by Halliburton, and analysis of fluids and rock by Geology departments at Kansas State University and The University of Kansas will provide critical geologic, geochemical, and engineering data that will be used to evaluate recovery of incremental oil using CO2 from the field's sandstone reservoir, quantify the storage capacity of the underlying deep Arbuckle saline formation, and investigate properties of caprocks to contain and manage commercial quantities of CO2.
7. The analysis of the Cutter Field well parallels a study of Wellington Field in Sumner County in south-central Kansas started in 2010 where 3D seismic imaging and two new wells are being used to evaluate CO2 storage capacity at that site. Wellington Field has also been selected by NETL-DOE (DE-FE0006821) for a small scale injection to

evaluate the efficacy of CO₂ storage capacity in the Mississippian oil field and the underlying Arbuckle saline formation. The characterization project is slated to be completed in late 2013 and the small scale injection at Wellington in 2015.

8. Wellington and Cutter field data will be integrated with subsurface mapping by Bittersweet Energy subcontractor over the 25,000 square miles between and beyond these two fields in southern Kansas. Regional mapping of rock properties is being used to develop new CO₂ storage capacity estimates and establish a geologic framework that will aid potential future site selection for CO₂ storage projects.

SPENDING PLAN

	COST PLAN STATUS											
	Year 1 Starts: 12/8/09	Ends: 2/7/11	12/8/09-12/31/09		Ends: 4/7/11	BP 2 Starts 2/8/11		Ends: 8/7/12	10/1/11 - 12/31/11		1/1/12 - 3/31/12	4/1/12 - 6/30/12
Baseline Reporting Quarter	Q1	Q2	Q3	Q4	Q5	Q6	Q7	Q8	Q9	Q10	Q11	
Baseline Cost Plan (from SF-424A)	12/8/09-12/31/09	1/1/10-3/31/10	4/1/10-6/30/10	7/1/10-9/30/10	10/1 - 12/31/10	1/1/11 - 3/31/11	4/1/11 - 6/30/11	7/1/11-9/30/11	10/1/11 - 12/31/11	1/1/12 - 3/31/12	4/1/12 - 6/30/12	
	Q1	Q2	Q3	Q4	Q5	Q6	Q7	Q8	Q9	Q10	Q11	
Federal Share	\$1,007,622.75	\$1,007,622.75	\$1,007,622.75	\$1,007,622.75	\$0.00	\$0.00	\$0.00	\$1,169,543.00	\$1,169,543.00	\$1,169,543.00	\$1,169,543.00	
Non-Federal Share	\$277,260.75	\$277,260.75	\$277,260.75	\$277,260.75	\$0.00	\$0.00	\$0.00	\$303,182.75	\$303,182.75	\$303,182.75	\$303,182.75	
Total Planned (Federal and Non-Federal)	\$1,284,883.50	\$1,284,883.50	\$1,284,883.50	\$1,284,883.50	\$0.00	\$0.00	\$0.00	\$1,472,725.75	\$1,472,725.75	\$1,472,725.75	\$1,472,725.75	
Cumulative Baseline Cost	\$1,284,883.50	\$2,569,767.00	\$3,854,650.50	\$5,139,534.00	\$5,139,534.00	\$5,139,534.00	\$5,139,534.00	\$6,612,259.75	\$8,084,985.50	\$9,557,711.25	\$11,030,437.00	
Actual Incurred Costs												
Federal Share	\$4,019.93	\$84,603.97	\$494,428.37	\$111,405.52	\$238,675.97	\$1,902,936.55	\$625,653.17	\$275,754.50	\$523,196.12	\$453,026.11	\$239,049.31	
Non-Federal Share	\$0.00	\$43,980.04	\$40,584.78	\$13,195.88	\$526,210.30	\$35,887.31	\$414,511.02	\$20,247.24	\$16,687.00	\$61,683.20	\$38,958.38	
Total Incurred Costs-Quarterly (Federal and Non-Federal)	\$4,019.93	\$84,603.97	\$535,013.15	\$124,601.40	\$764,886.27	\$1,938,823.86	\$1,040,364.19	\$296,001.74	\$539,883.12	\$514,709.31	\$278,007.69	
Cumulative Incurred Costs	\$4,019.93	\$68,623.90	\$623,637.05	\$748,238.45	\$1,513,124.72	\$3,451,948.58	\$4,492,312.77	\$4,788,314.51	\$5,328,197.63	\$5,842,906.94	\$6,120,914.63	
Variance												
Federal Share	\$1,003,602.82	\$923,018.78	\$513,194.38	\$896,217.23	-\$238,675.97	-\$1,902,936.55	-\$625,653.17	\$893,798.50	\$646,346.88	\$716,516.89	\$930,493.69	
Non-Federal Share	\$277,260.75	\$233,280.71	\$236,675.97	\$264,064.87	-\$526,210.30	-\$35,887.31	-\$414,511.02	\$282,935.51	\$286,495.75	\$241,499.55	\$264,224.37	
Total Variance-Quarterly (Federal and Non-Federal)	\$1,280,863.57	\$1,156,299.49	\$749,870.35	\$1,160,282.10	-\$764,886.27	-\$1,938,823.86	-\$1,040,364.19	\$1,176,724.01	\$932,842.63	\$958,016.44	\$1,194,718.06	
Cumulative Variance	\$1,280,863.57	\$2,437,163.06	\$3,187,033.41	\$4,347,315.51	\$3,582,429.24	\$1,643,605.38	\$603,241.19	\$1,779,965.20	\$2,712,807.83	\$3,670,824.27	\$4,865,542.33	

APPENDIX A.

Pleasant Prairie South reservoir characterization, modeling and simulation

Martin K. Dubois, Eugene T. Williams, Dennis E. Hedke, Peter R. Senior, John C. Youle

1. Introduction (Martin K. Dubois)

The Pleasant Prairie South study is part Kansas Geological Survey (KGS) University of Kansas project, *Modeling CO₂ Sequestration in Saline Aquifer and Depleted Oil Reservoir to Evaluate Regional CO₂ Sequestration Potential of Ozark Plateau Aquifer System, South Central Kansas*, a U.S. Department of Energy funded program (DE-FE0002056). This report covers the reservoir characterization, modeling and dynamic simulation of the first of four fields being evaluated for concurrent CO₂ sequestration and enhanced oil recovery in depleted petroleum reservoirs. The study area is informally referred to as the Western Annex to a more regional investigation covering southern Kansas (Fig. 1.1).

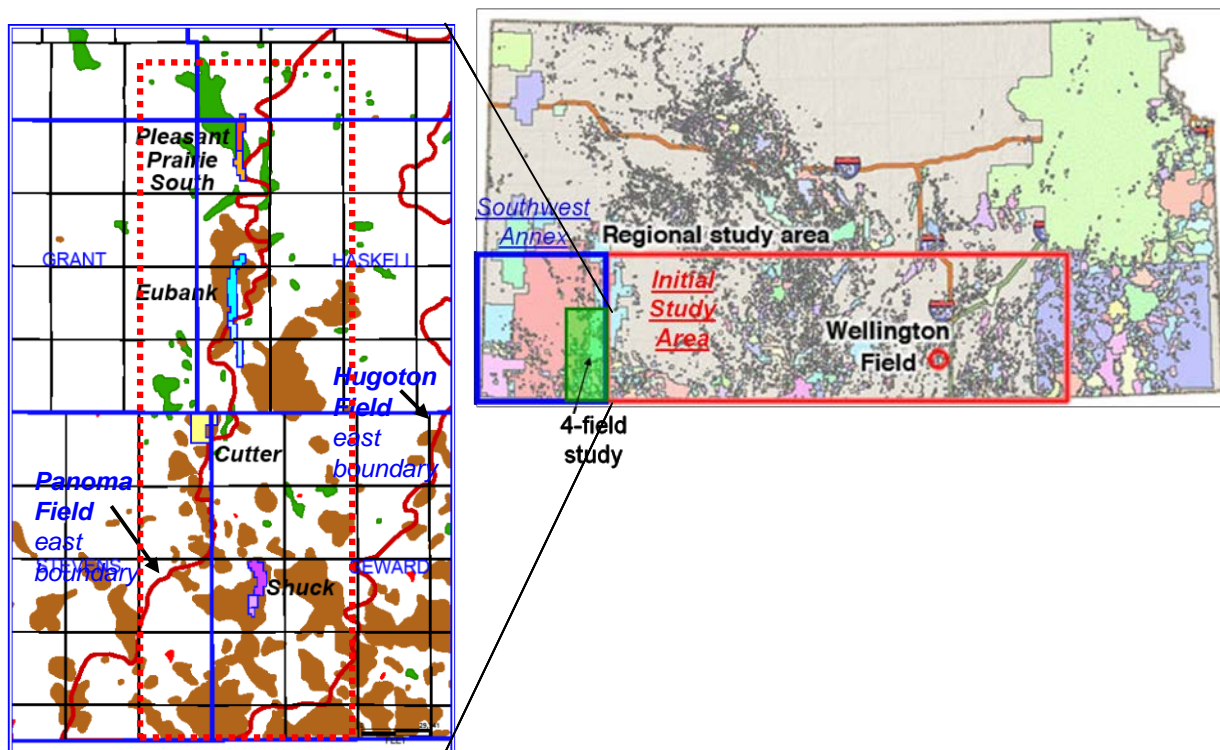


Fig. 1.1 Western Annex and geographical relationship to the larger regional study (right), and location of four fields being studied (left). Oil fields are in green, oil and gas are brown, and the outline of the giant Hugoton and Panoma fields are outlined in red.. Pleasant Prairie South is the subject of this report.

1.1 Objective

The primary purpose of the four-field study is to 1) determine the technical feasibility to inject and sequester CO₂ into a set of depleted oil reservoirs and concurrently recover oil, and 2) quantify the volumes of CO₂ sequestered and oil recovered during the process. To accomplish these goals the tasks were to characterize the geology, build a detailed static reservoir model, and to use dynamic models, both black oil and compositional simulators, to match field history and predict the results of CO₂ injection.

1.2 Operators, technical team and KGS project relationship

A consortium of six oil operating companies, five of which own and operate the four fields, and was formed and is managed by the KGS. Each of the four fields are prolific, albeit small, having produced over 20 million barrels of oil, by primary and secondary waterflood methods (approximately 50% from each). The fields were good waterfloods and may be good candidates for CO₂ EOR if combined. Their relatively small size and, in some cases, split ownership, make it difficult to economically justify the compression and pipeline infrastructure as individual projects. Combined they may be a viable target for CO₂ EOR concurrent with sequestration. The consortium has pooled their seismic, engineering, core, operations and technical well data for a comprehensive, integrated, depositional system-scale study. Improved Hydrocarbon Recovery, LLC (IHR) has been subcontracted by the KGS to manage the consortium transfer of data and the technical study. IHR manages its subcontracts to a team of geologists and an engineer that work closely with KGS staff and KGS subcontractors on the multi-discipline study.

1.3 Workflow

The reservoir characterization, and modeling of the Pleasant Prairie South pool is the integration of many disciplines culminating in dynamic reservoir simulation to project possible outcomes of CO₂ injection (Fig. 1.2). The static geomodel for the Pleasant Prairie South Chester reservoir was constructed in Petrel™ using a standard workflow illustrated in Figure 1.3. A simplified version of the steps to build the model are: 1) identify lithofacies and sequence stratigraphy in core, 2) relate core petrophysical properties to lithofacies, 3) identify lithofacies in wells without core based on wireline log curve responses, 4) build fine-grid structural (wireframe) model using depth-converted seismic surface and well formation tops, 5) populate model with lithofacies using sequential indicator simulation (SIS), 6) populate model with porosity using sequential gaussian simulation (SGS), 7) calculate permeability at each cell using lithofacies-based porosity-permeability transform equations, and 8) calculate Sw using Leverett J-Function with Blueback™ plugin. The model was then upscaled in the Z direction to a coarser-layered cellular model and exported for dynamic modeling. Field and well-scale histories were matched in a

black oil simulator and CO2 sequestration and enhanced oil recovery were forecast in a compositional simulator.

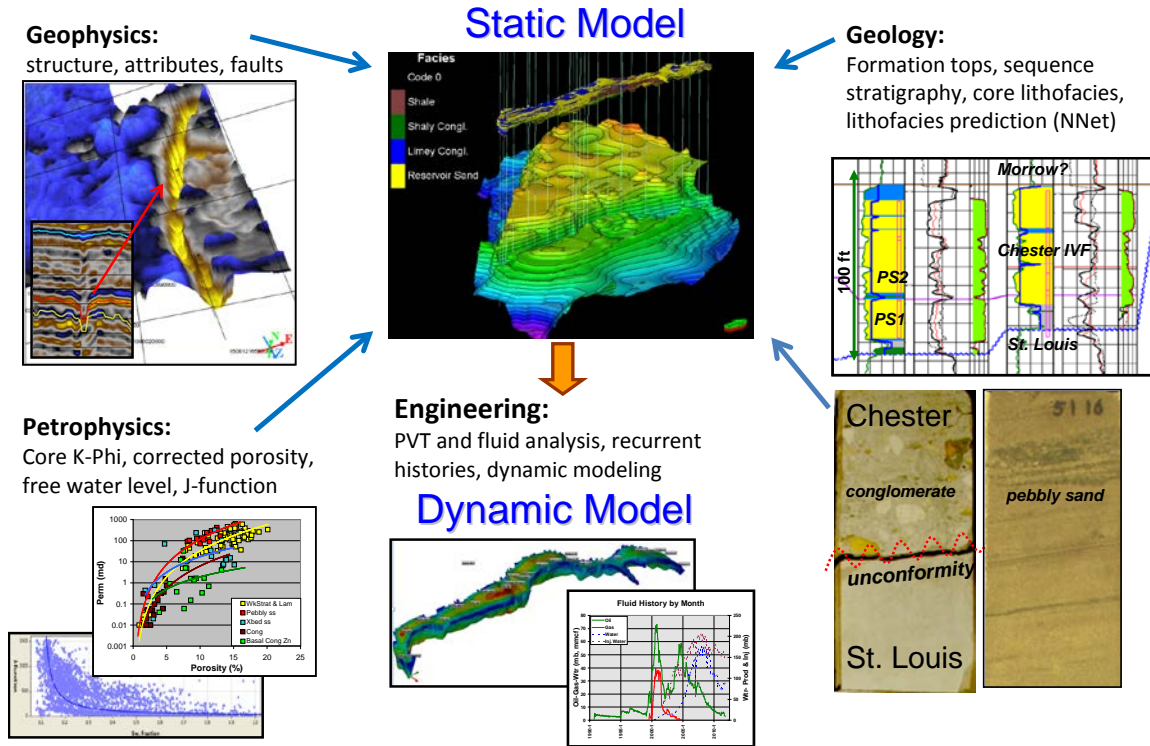


Fig. 1.2 The Pleasant Prairie study is the integration of multiple disciplines

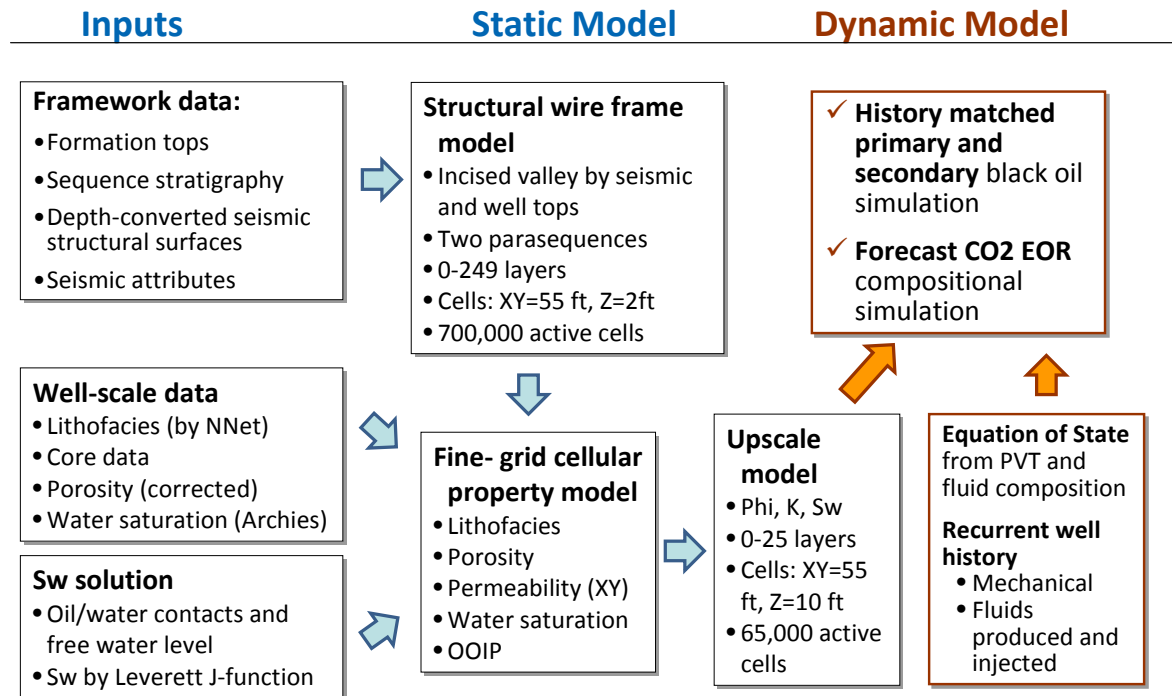


Fig. 1.3 Simplified workflow for the technical work showing the main inputs and construction of the static model and inputs and simulation in the dynamic model phase.

2. Pleasant Prairie South Pool history (Martin K. Dubois)

2.1 Discovery and development

The oil pool commonly known as Pleasant Prairie South produces from the Chester Sandstone is not officially recognized as a separate pool by the State of Kansas. Rather, it is a part of the larger Pleasant Prairie Field covering all or parts of 32 sections (Figure 2.1). Pleasant Prairie has produced 33.9 mmbo since its discovery in 1954, primarily from the Mississippi St. Louis (depth 5200 ft), while the Pleasant Prairie South has produced 4.5 mmbo of the Pleasant Prairie total from the younger Mississippian Chester sandstone (depth 5100 ft).

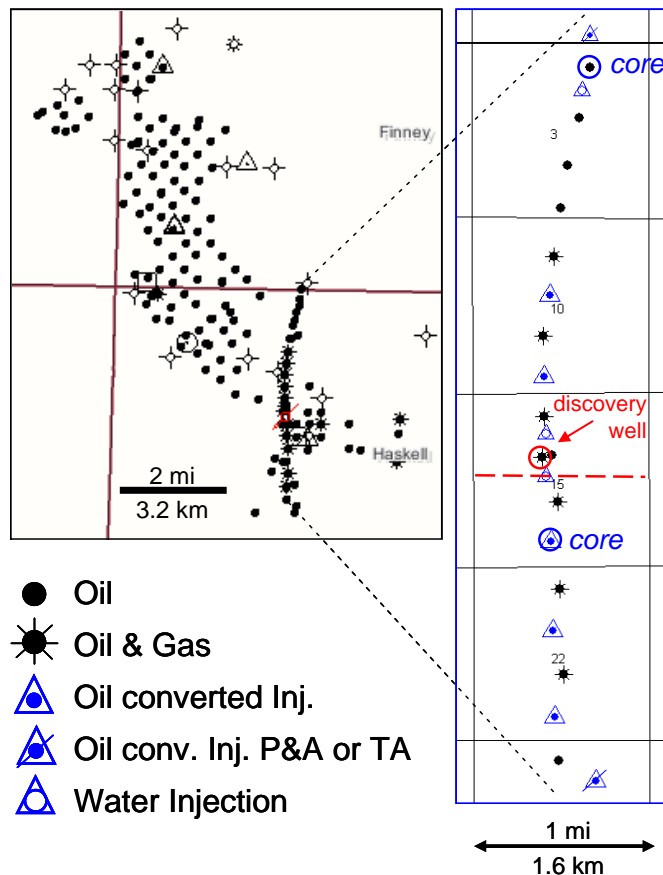


Fig. 2.1 Pleasant Prairie Field (left) and pool commonly known as Pleasant Prairie South (right). Map on left is from Kansas Geological Survey Field Viewer (<http://geoportal.kgs.ku.edu/kgs/oilgas/imageviewer/map.cfm>) and includes all wells in Pleasant Prairie. Map on right includes only the 23 wells in the Pleasant Prairie South pool. Well status legend is for the map on the right. Cores in this study are from wells with the “core” notation. The red dashed line is an ownership boundary dividing the model into regions referred to as the North and South regions throughout the report.

The first well to produce from the Chester in the Pleasant Prairie South was drilled in 1990. It was not until late 1994 that another well was drilled in the incised valley a half mile to the north. By the time the second well was put on line the discovery well had produced over 160 mbo. A third well was drilled a mile north of the discovery in 1996. Development of the Chester sandstone reservoir expanded after 3D seismic data was acquired with six wells added in 1999, another six in 2000, and two in 2001 to fully develop the pool. Five additional wells drilled from 2003 through 2006 for injection purposes or as infill wells. Well are spaced approximately 1320 ft (quarter-mile) throughout most of the pool. An exception is in Sec. 15 where two injection wells were drilled between producers, which are approximately 1320 ft apart, and an additional oil producer drilled a short distance from the discovery well. Table 2.1 provides a summary of the history of the Pleasant Prairie South pool.

Producing zone	Mississippian Chester
Discovered	1990
Main development	1999 - 2000
Waterflood initiated	2001
Cumulative Oil	4.5 mmbo
Cumulative Gas	0.7 BCF
Cum. water injected	18.0 mmbo
Cum. water produced	12.4 mmbo
Waterflood oil recovery	Appx. 50% of cumulative
Oil wells total	19*
Current oil wells	13
Current water injectors	8
Plugged or TA water injectors	9

*6 oil wells were converted to injectors

Table 2.1 Pleasant Prairie South pool history summary table. Abbreviations: mmbo - million barrels oil; BCF - billion cubic feet.

2.2 Completion techniques

Wells were drilled through the Chester and more than 100 ft into older Mississippian and then 5-1/2 inch casing set through to TD and cemented. In most wells all porous sandstone was perforated with 1-2 shots per foot from top to bottom of the reservoir sandstone. There was no gas cap to avoid. Treatments vary widely, with about half the wells completed with an acid job only (3000 gallons was common), or natural (without any treatment reported). At least seven wells were hydraulically fractured with sand volumes ranging from 30,000 to 96,000 pounds, with the exception that one well was a fluid fraced without sand. Most fracture treatments were performed by the operator of the northern part of the field, but the three wells drilled as water injectors were not facture treated. Based on well performance, completion technique did not appear to have been significant impact on ultimate recoveries, but may have influenced rates early in the life of the wells.

2.3 Production and waterflood history

Fluid histories through December 2011 (Fig. 2.2) is based on monthly data from the two companies operating the pool and the Kansas Geological Survey online data base. (One operator's data set is through December 2011, while the other, covering the south half of the pool is through May, 1999. For the south half of the field, production data from May 1999 through December 2011 is from the Kansas Geological Survey.

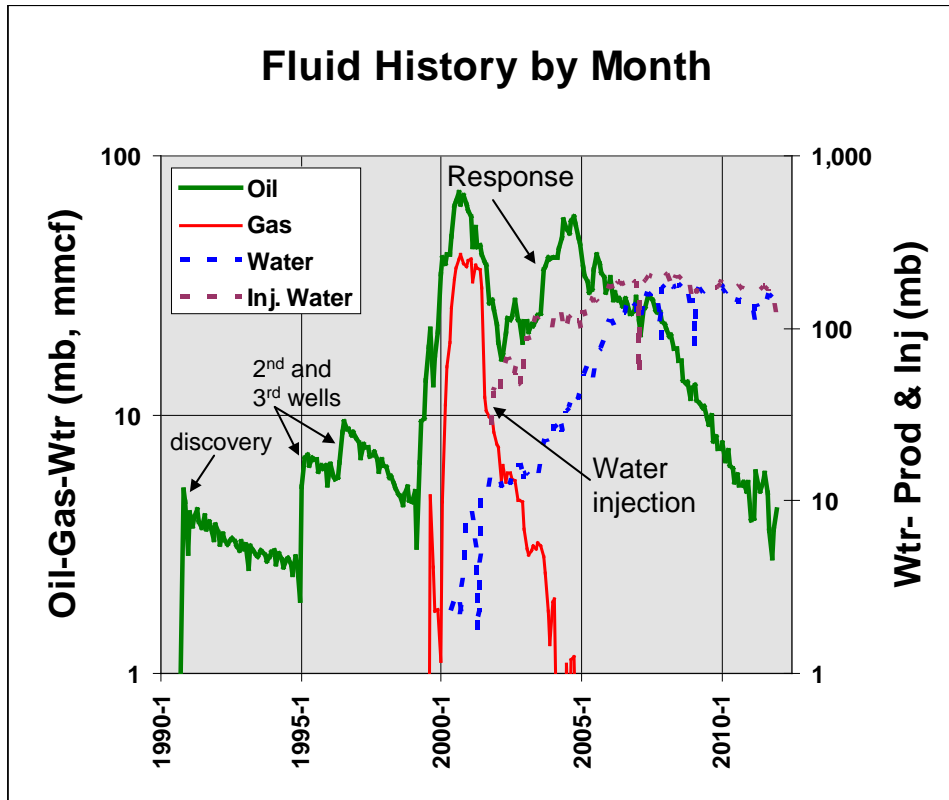


Fig. 2.2 Fluid production and injection history.

Development well drilling history from 1990 through 2000 is reflected in the fluid production and injection history (Fig. 2.2). Increases in production as the first three wells were drilled is indicated by distinct increases in oil production. The flurry of activity, twelve wells in 1999 and 2000, resulted in production rates as high as 70,000 barrels of oil per month followed by a steep decline in 2002. The "flashy" production, high initial rates and rapid decline is typical of gas-solution-drive reservoir systems, the reservoir drive in Pleasant Prairie South. Water production

was minimal in primary production, and not even reported until 2000. No gas production is reported until late 1999.

The southern part of the pool was unitized for waterflooding but the northern portion was not. Water was first injected into four injection wells, converted from oil wells to injectors in the southern portion of the field in October 2001, ramping up to approximately 2000 barrels of water per day (bwpd) a year later. Some of the overall production decline in late 2001 and into 2002 could be due to the lag between the change in wells from oil producers to injectors and the oil production response in adjacent wells. Water injection was initiated in the northern portion of the pool in two wells (converted oil producers) in December 2002. In the years 2004 through 2006 three water injectors were drilled, one of them placed at the boundary between operators, and another oil well was converted to injector. With all injectors in place 7,000 bwpd was injected into eight wells.

The reservoir system being flooded appears to be a closed system because the volume of water injected is very close to the volume of fluid produced (oil, water, and gas) (Table 2.1). The trapping mechanism is structural and stratigraphic. Stratigraphic in the sense that the reservoirs is bounded by the incised valley. Structural in the sense that the south end is bounded by a down-to-the-south fault that defines the southwest limits of the Pleasant prairie Mississippi field and the north end is defined by structural dip, possibly faulted to the north.

A rigorous assessment of what portion of production could be considered secondary recovery (waterflood) versus what would have been produced by primary methods has not been conducted. This would be rather tenuous because the waterflood was initiated relatively soon after peak by primary production methods, before a decline could be well established. We estimate that approximately half the production can be attributed to the waterflood.

3. General geologic setting (John C. Youle and Martin K. Dubois)

3.1 Regional geologic setting

Pleasant Prairie South pool is located in very northwestern Haskell County Kansas, near the center of the Hugoton Embayment (Fig. 3.1). The Hugoton Embayment is the shallow subsurface extension of the Anadarko basin into Kansas. The Anadarko reaches its maximum depth about 200 miles SE of the field, in southwestern Oklahoma (Rascoe and Adler, 1983; Merriam, 1963; Maher and Collins, 1949).

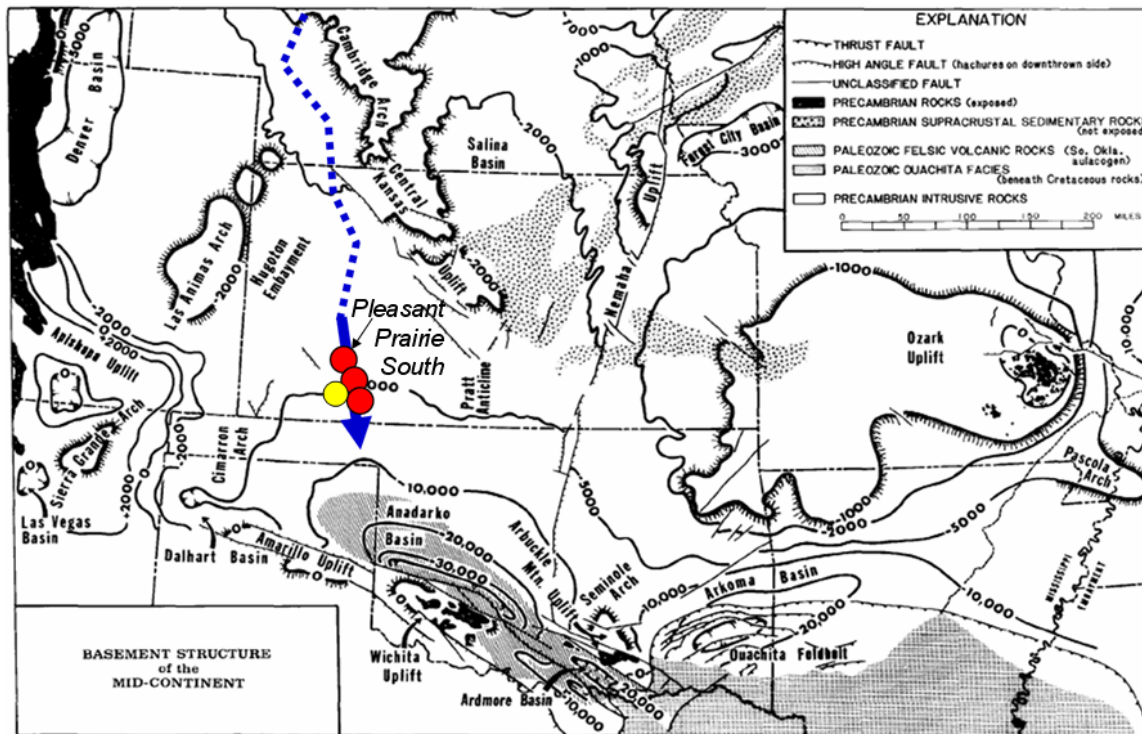


Fig. 3.1 Present day basement configuration map (Rascoe and Adler, 1983) showing location of fields in overall study. Chester incised valley fields are indicated by red dots, north to south Pleasant Prairie South, Eubank, and Shuck. Yellow dot indicates a Morrow sandstone field, the Cutter. Solid blue line shows Chester valley axis where preserved beneath Pennsylvanian rocks, dotted blue line shows postulated original valley course subsequently removed by Ouachita (Pre-Pennsylvanian) erosion.

The sedimentary section in the Hugoton embayment has been affected by multiple tectonic events many of which reactivated pre-existing Pre-Cambrian basement faults and fault blocks.

Most faults and fault blocks in the area trend NW-SE, although N-S to NE-SW oriented structures are also present. Additional structures formed in the area as a result of karsting and solution collapse in Ordovician aged Arbuckle carbonates, and dissolution and collapse of salts and anhydrites in lower-middle Meramecian (Mississippian) rocks. Current maximum principle stress axis in southwestern Kansas is oriented about N70E (Laubach et al. 2004, Watney, 2008).

Subsurface seismic in the region show movement along faults during post-Ordovician to pre-Mississippian time (Taconic and Acadian Orogenies), lower and middle Mississippian time, late Permian time, and again during the late Cretaceous to middle Tertiary time (Laramide Orogeny). However, the rock column in southwestern Kansas owes most of its character to events that transpired during the Ouachita Orogeny of latest Mississippian and early Pennsylvanian time. It was during the Ouachita Orogeny that the Anadarko basin reached its greatest depths, and areas surrounding the Hugoton embayment were uplifted and severely eroded. Because southwestern Kansas has always been an area where basement rocks have existed at relatively shallow depths, tectonic and climatic events have been recorded with great fidelity in the rock record and are read as multiple unconformities and abrupt facies changes.

3.2 Pleasant Prairie South in context of larger Chester incised valley system

The subtle beginning stages of the Ouachita orogeny can be discerned from the stratigraphy of the upper Mississippian in the Pleasant Prairie South pool area (Fig. 3.2). Although seas began their cyclic withdraw to the south during Meramecian time, it wasn't until late Meramecian time that eolian deposits in the Ste. Genevieve limestone became widespread in the area (Abegg, 1992; Handford et al, 1991). As Meramecian seas withdrew from Kansas they were chased by linked alluvial/fluvial systems at least as far south as northern Oklahoma. The largest of the rivers that formed during this regression was located near the center of the Hugoton embayment and eroded a valley over 200' deep in places that can be traced for over 100 miles from Finney county Kansas into Oklahoma (Severy, 1975) (Figure 3.3). Fifty miles north of the Oklahoma border, the Pleasant Prairie South pool produces from rocks deposited within this deeply incised valley.

System	Series	Stratigraphic Unit
Pennsylvanian	Virgillian	Admire Wabaunsee Shawnee Douglas
	Missourian	Lansing- Kansas City Gp.
	Desmoinesian	Marmaton Gp. Cherokee Gp.
	Atokan	Atoka Gp.
	Morrowan	Morrow Gp.
Mississippian	Chesterian	 Chester Gp.
		 Ste. Genevieve
	Meramecian	St. Louis
		Salem
		Warsaw
	Osagian	Osage
	Kinderhookian	Gilmore City/Hannibal

Fig. 3.2 Generalized stratigraphic column (Montgomery and Morrison, 1999).

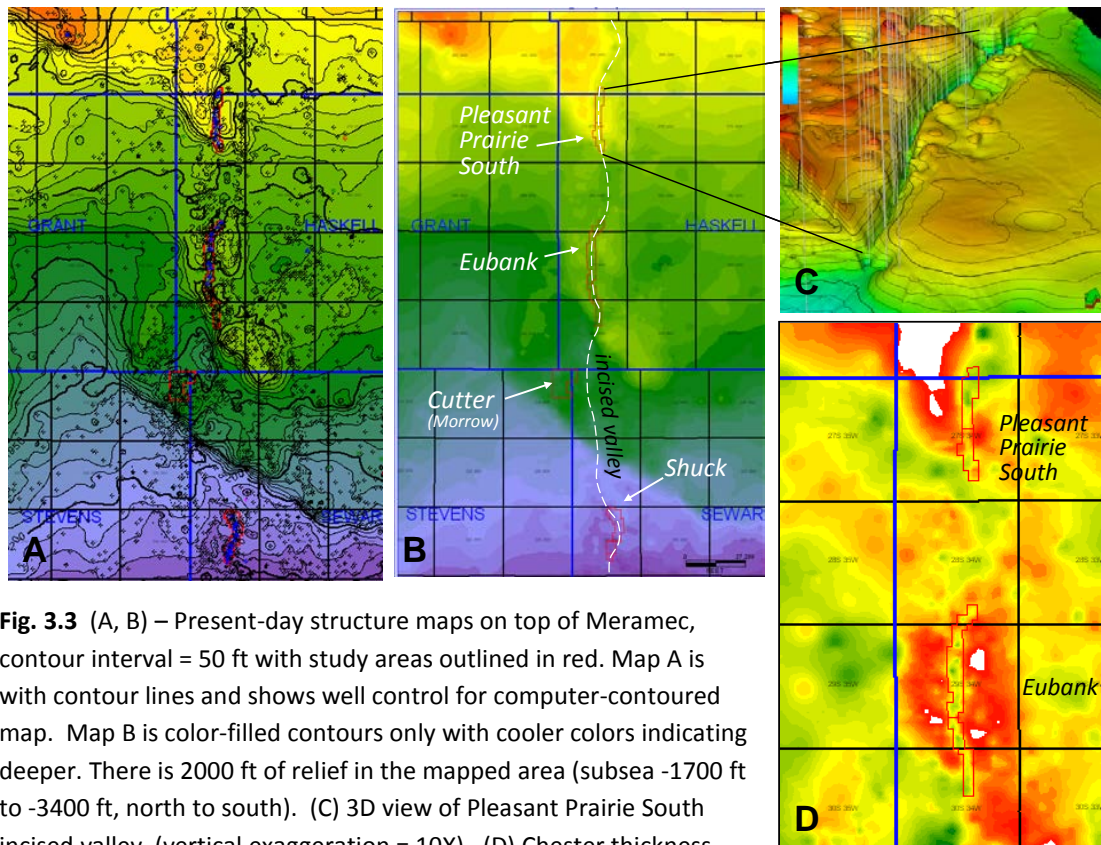


Fig. 3.3 (A, B) – Present-day structure maps on top of Meramec, contour interval = 50 ft with study areas outlined in red. Map A is with contour lines and shows well control for computer-contoured map. Map B is color-filled contours only with cooler colors indicating deeper. There is 2000 ft of relief in the mapped area (subsea -1700 ft to -3400 ft, north to south). (C) 3D view of Pleasant Prairie South incised valley (vertical exaggeration = 10X). (D) Chester thickness map around Pleasant Prairie South and Eubank fields. Grids are Township lines, six miles apart. Cooler colors are thickest.

Mississippian seas re-entered Kansas during Chesterian time (Severy, 1975) through a series of pulses or cycles, with each younger pulse advancing the shoreline farther north than the previous one. Chester rocks in Kansas reach their maximum thickness of nearly 500' near the Oklahoma border in southern Seward county, and thin north and northeastward by onlap and erosional truncation to a zero line in Finney and western Gray counties. The pulsing advance of the Chesterian seas filled pre-existing valleys with a variety of fluvial, estuarine, and marine sediments. Fluvial sediments probably fill portions of the base of these valleys; but core data from basal valley sections is generally lacking. Core data from a variety of locations within the valley show that the bulk of the valley-filling rocks, and all oil producing reservoirs, were deposited in estuarine environments. Marine rocks, also present in the valley fill cores, are typically best developed at the top of the Chester section. A cross section that runs up the axis of the deepest of these Chester valleys, from the Oklahoma border to Pleasant Prairie South pool in northwest Haskell county helps to illustrate the cyclic retrogradational nature of the Chester transgressions that filled the valley with vertically stacked estuarine reservoirs (Fig. 3.4). The Chester incised valley was filled with progressively younger sediments in a northerly direction as the Chesterian shoreline advanced from south to north. Pleasant Prairie South Chester sandstone represents the youngest of the three Chester reservoirs being studied.

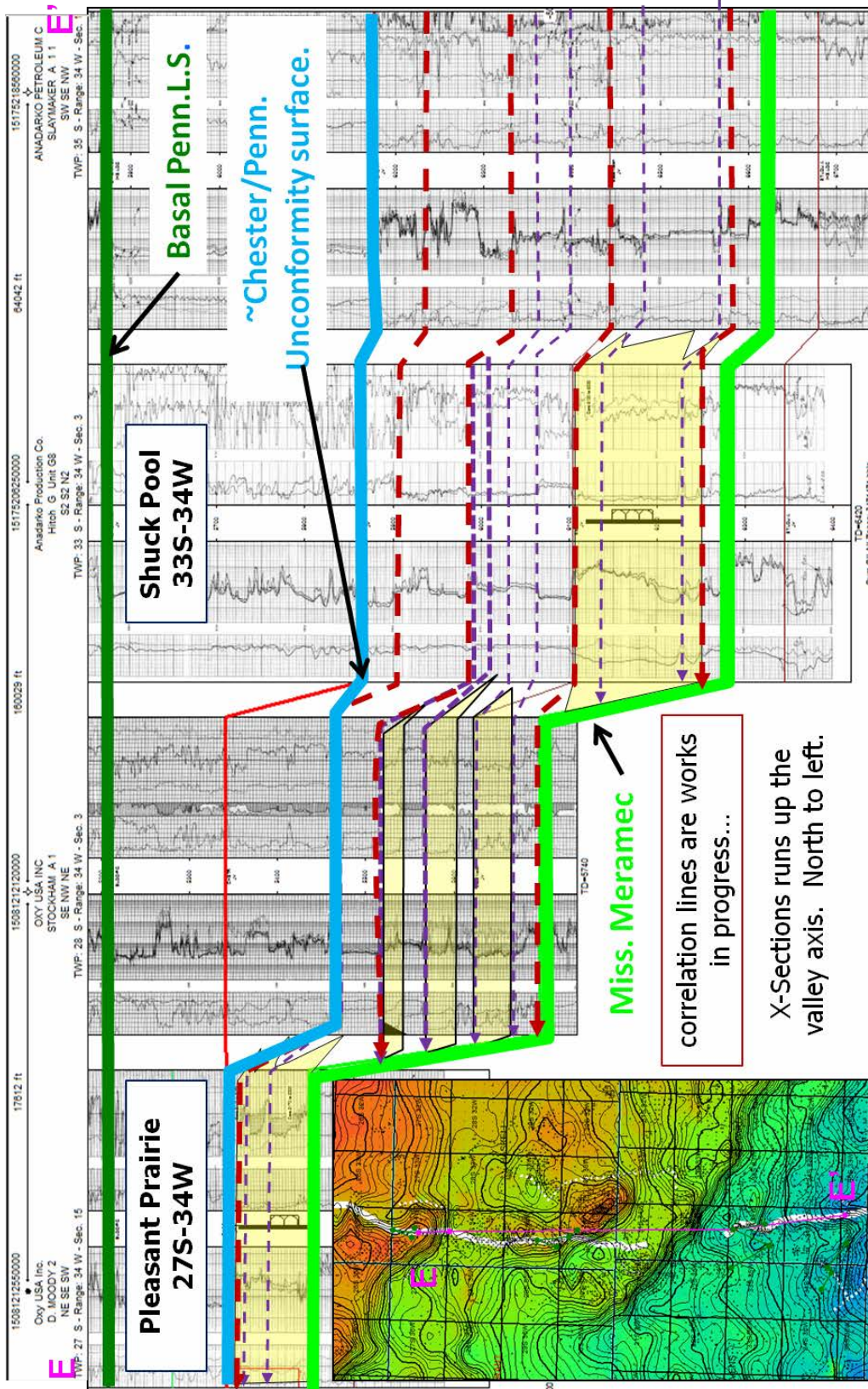


Fig. 3.4. The cyclic retrogradational nature of Chester shoreline advances into Kansas are interpreted to have filled incised valleys with a series of 'back-stepping' stacked estuarine sandstone reservoirs. Red dashed lines are postulated sequence boundaries, and purple lines are possible parasequences.

4. Pleasant Prairie South geology (**Peter R. Senior and Martin K. Dubois**)

The following section summarizes work by Peter Senior in a yet-to-be defended MS thesis in the Department of Geology, University of Kansas. Additional, more detailed geology, will be available when the thesis is completed.

The Chesterian reservoir is a sandstone occupying a narrow, north-south oriented channel in Haskell County, Kansas, and the wells form a line stretching over 4 miles (6 km) (Fig. 2.1). The Chesterian reservoir at Pleasant Prairie South pool is part of a larger trend, an incised paleovalley extending over 50 miles (75 km) from north to south in Kansas and then on into Oklahoma (Figure 3.3). Chesterian sandstones in the paleovalley trend are generally incised into Ste. Genevieve strata, but cut through the Ste. Genevieve and into the older St. Louis in the Pleasant Prairie South.

4.1 Incised valley fill complex

The incised paleovalley developed as a result of subaerial exposure and erosion of Ste. Genevieve and older strata during regression (Severy, 1975; Cirilo, 2002). The location of the paleovalley may have been influenced by block faulting in subjacent strata (Shonfelt, 1988). The paleovalley trends north-south and extends from Haskell County, Kansas in the north, through Seward and Stevens Counties, Kansas, and into Oklahoma.

Sea levels during Late Mississippian time in the area are characterized by overall regression, punctuated by minor cyclical transgressions (Goebel, 1968; Shonfelt, 1988). Transgressive-regressive cycles associated with incised valley-fills can be associated with glacio-eustasy (e.g. Krystinik and Blakeney, 1990; Bowen and Weimer, 2003), and such an association has been proposed for Chesterian incised valley-fills in the Illinois Basin, adjacent to the Oklahoma-Anadarko Basin area (Smith and Read, 2000).

A substantial amount of prior work has been published along the incised valley trend but nothing to date on the Pleasant Prairie South pool. Prior studies from north to south cover South Eubank, Shuck, and Wide-Awake fields. The latter is ten miles south of Shuck, and the Shuck and South Eubank are shown in Figure 3.3. In the South Eubank field, Montgomery and Morrison (1999) identified four facies in core: intertidal flat, storm deposit, tidal-flat/estuarine channel, and sand-wave/tidal bar, and interpreted the suite of facies to represent tide-influenced estuarine deposits. Cirilo (2002) interpreted the Chesterian sediments in the Shuck field area to have been deposited in the central to outer part of a tide-dominated estuary, according to the facies models of

Dalrymple et al. (1992) and probably closer to the estuary mouth than the fluvial-dominated upper or inner estuary zone (Figure 4.1). Shonfelt (1988) interpreted facies defined in core as being deposited in a channel inlet in an estuarine-peritidal strandline complex in the Wide-Awake field. Earlier studies consistently interpreted Chester valley-fill deposits to be of estuarine origin with marine influence generally increasing southward and fluvial influence increasing in a northerly direction.

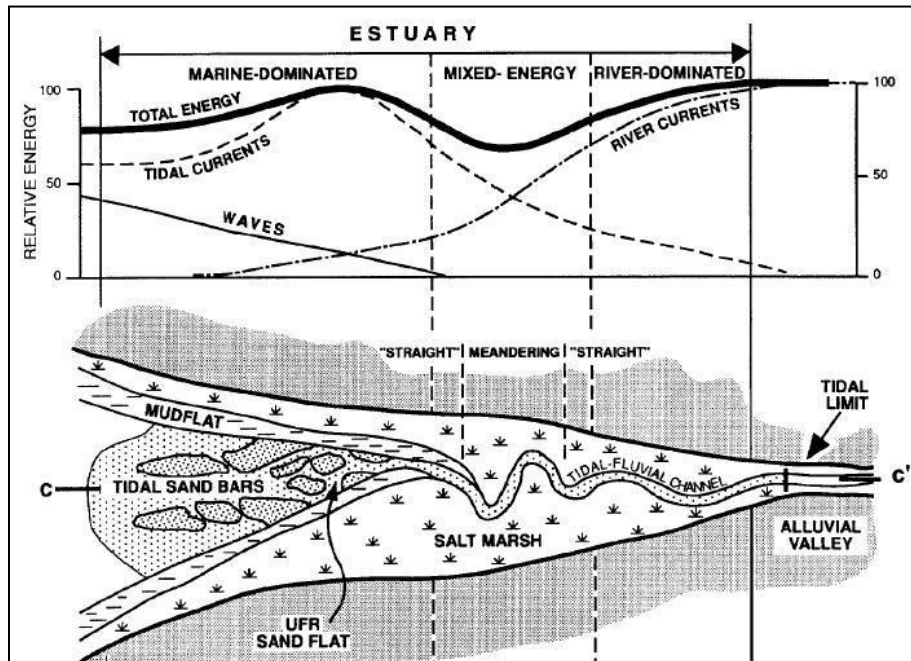


Fig. 4.1 Schematic diagram of a tide-dominated estuary, from Dalrymple et al., (1992).

4.2 Lithofacies defined in core and interpretation

Two wells cored nearly the entire valley-fill reservoir in the Pleasant Prairie South pool and are the subject of this study. Figure 4.2 summarizes the vertical distribution of the core lithofacies and their vertical relationships. The Pleasant Prairie South Chester incised valley fill is predominately sandstone comprised of five major lithofacies (Figure 4.3). Limey conglomerates have large (coarse sand to cobble size) sub-rounded clasts of limestone, chert, and sandstone in a fine-grained sandstone matrix. They were interpreted to be lag deposits at the base of fluvial channel scouring. An alternative interpretation is ravinement caused by a sea-level rise. Both interpretations postulate that the conglomeratic material is derived from valley walls; the fluvial interpretation hypothesizes that the clasts originated updip and were transported down the valley, and the ravinement interpretation hypothesizes an origin related to wave action on the valley

walls during base-level rise. One conglomerate near the middle of the valley-fill sequence is tentatively correlated in most of the 23 wells and is interpreted to be a parasequence boundary. Cross-bedded sandstone is a well-sorted subrounded, fine-medium grained quartzarenite with faint to well-preserved trough cross-bedding and scattered carbonized organic material (wood fragments). This facies is only found in the northern of the two cores and is interpreted as having a fluvial origin, but with minor tidal influence indicated by the presence of mud drapes. Laminated sandstone consists of well sorted very-fine to fine grained quartzarenite with low angle planar cross-bedding. This lithofacies could be associated with deposition either fluvial or tidal bar environment. The weakly stratified sandstone lithofacies was also identified in core and is lumped here with the laminated sandstone lithofacies. The pebbly sandstone lithofacies is a fine-grained, rounded sublitharenite with mm to cm sized mud clasts usually along low angle (10-20°) planar surfaces. Carbonaceous plant material is scattered in the lithofacies. This lithofacies is only found in the southernmost core. It is interpreted to have been deposited in a dune environment a fluvial bar system. Another lithofacies identified in core, but not shown in Figure 4.3 is interbedded sandstone and heterolithic mudstone-sandstone found in the lower part of the incised valley fill. It is lumped with the basal conglomerate facies in the colorfill of the logs. Several wells in the north half of the pool, found in the south half of Section 3 and north half of Section 10, encountered relatively thick intervals identified as shale by wireline logs (Figure 4.4 and 4.5). These could be salt marsh deposits identified in Figure 4.1.

The Chesterian rocks filling the paleovalley in the Pleasant Prairie South are interpreted to have been deposited in an estuarine system having both fluvial and tidal influence. This interpretation is consistent with other published work that documents more marine influence along the valley system in a southerly direction and more fluvial influence in a northerly direction. Additional detailed studies along the paleovalley system (Eubank and Shuck) being conducted in the larger study may better define the depositional environments of the entire system.

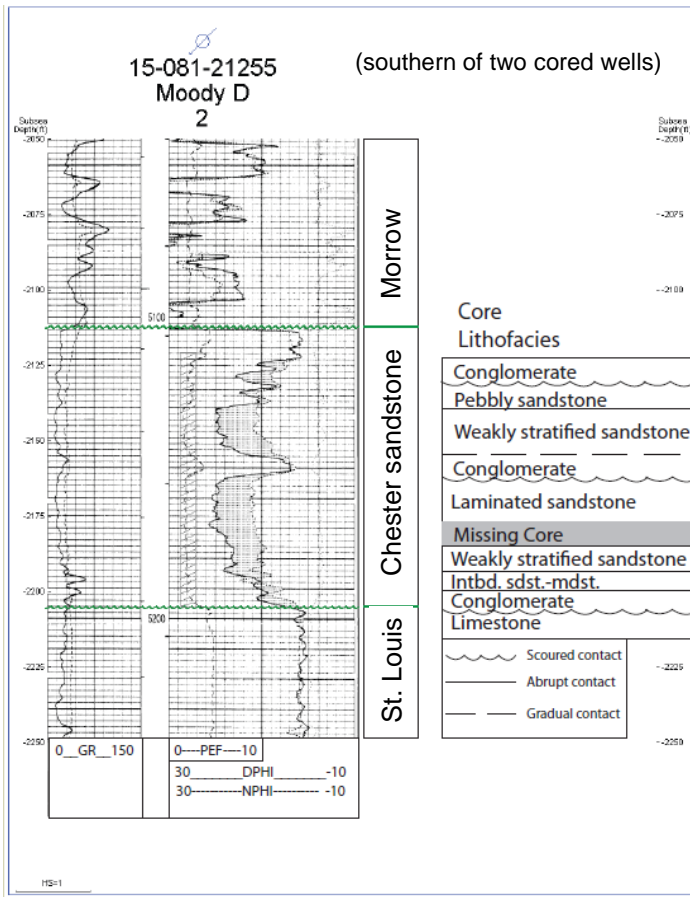


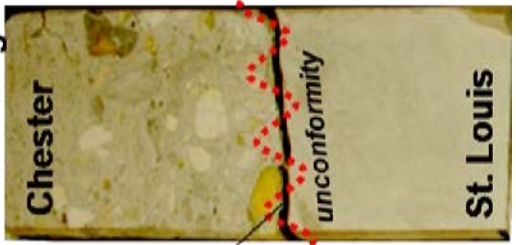
Fig. 4.2 Wireline log and core lithofacies in the southern of the two cores in Pleasant Prairie South.

5218.5 (5213.5)



X-bedded Sandstone

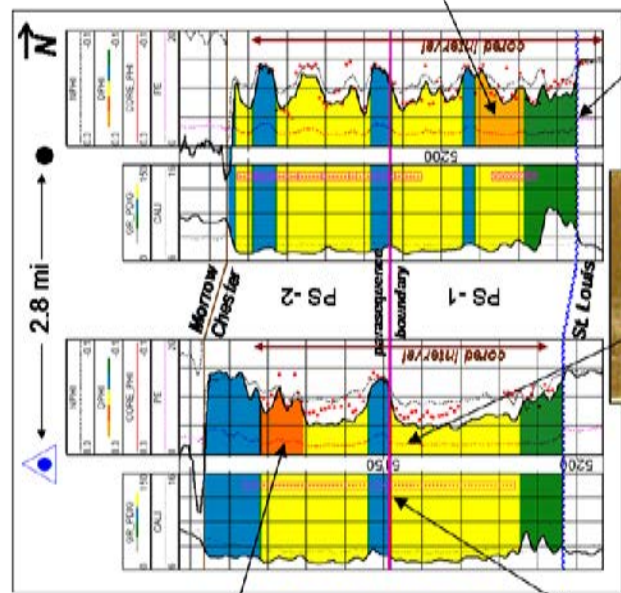
Basal Congl.



5240.5 (5235.5)

unconformity

St. Louis



5148.5 (5156)

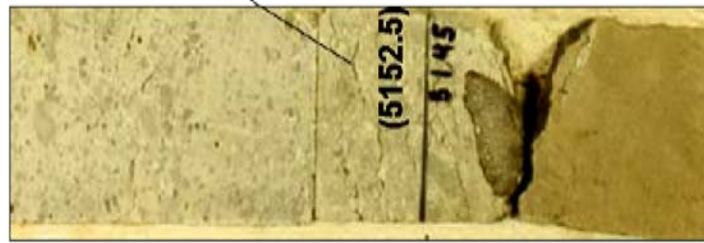
Laminated Sandstone

Pebbly Sandstone



5116 (5124)

Limey Congl.



(5152.5)

5145

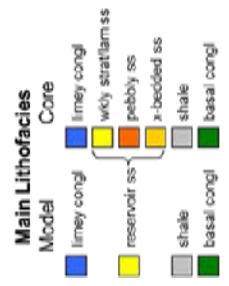
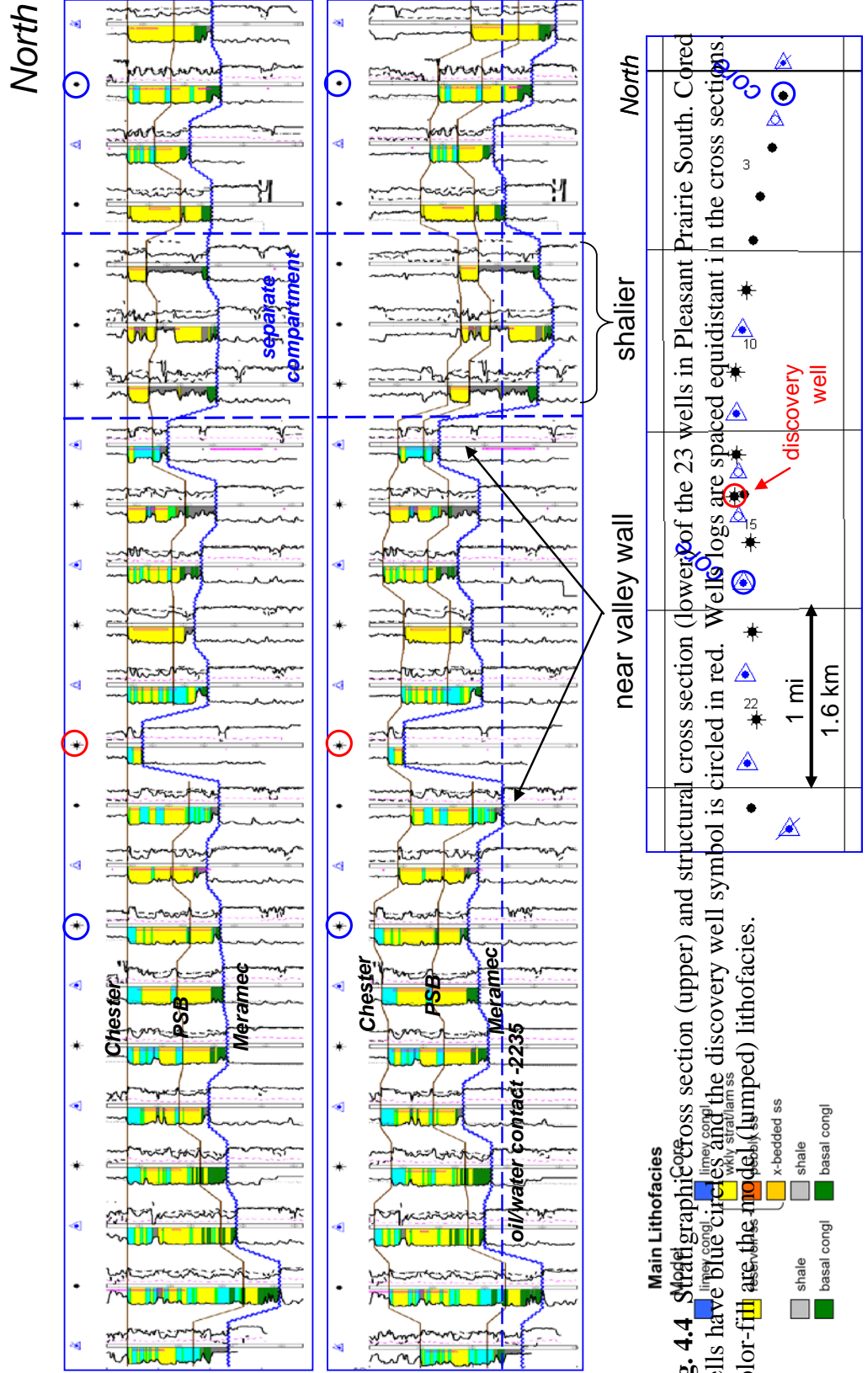
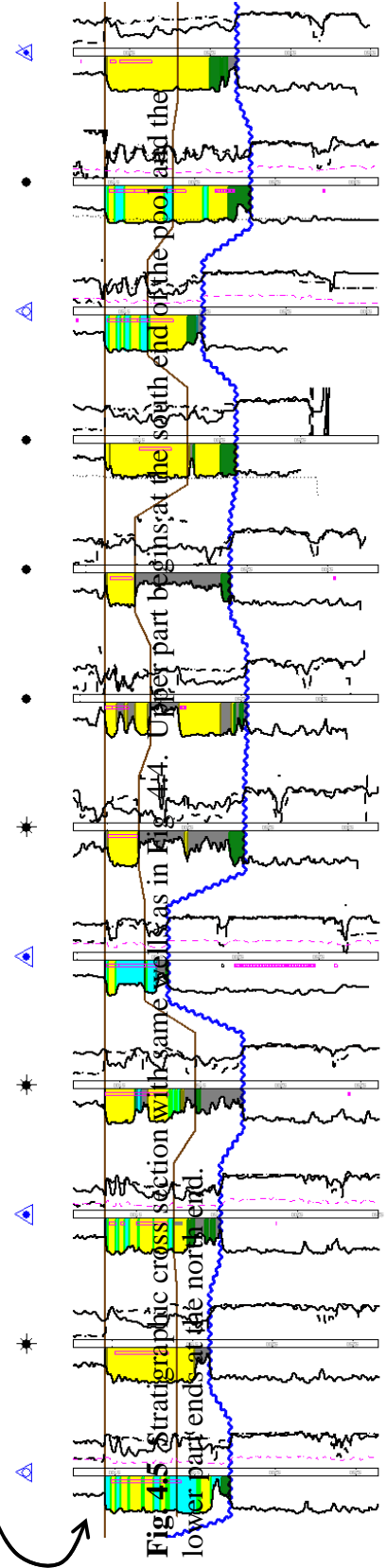
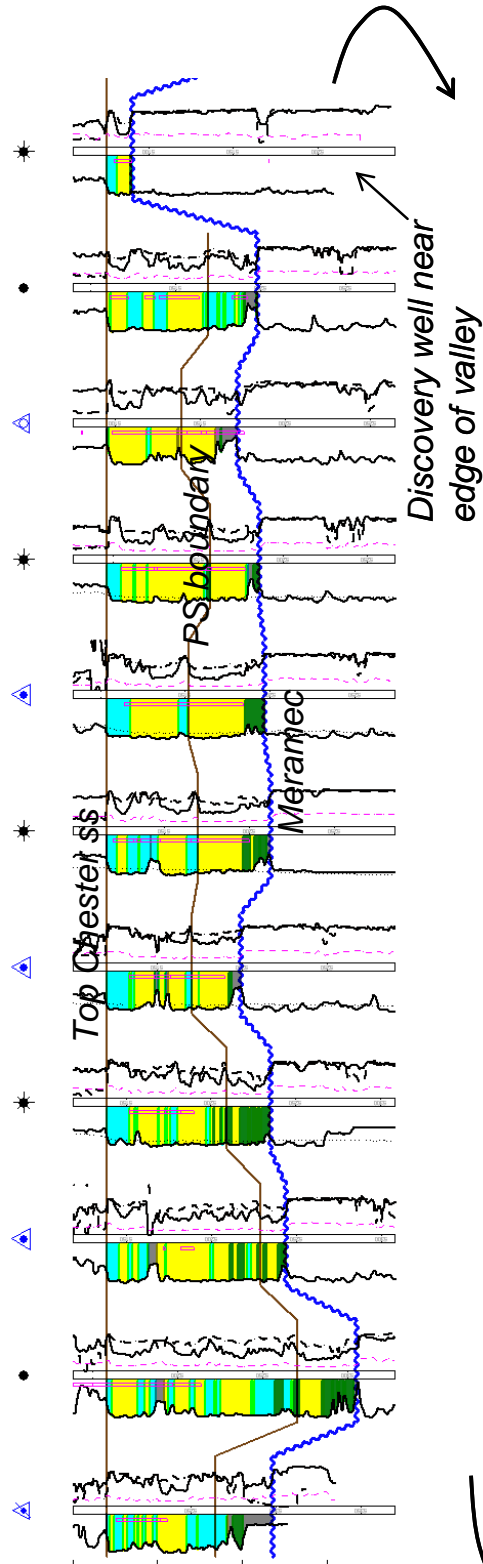


Fig. 4.3 Five sandstone lithofacies defined in core. Numbers in parentheses are wireline log depth whereas the other number is core-measured depth. Wireline logs are color-filled with lithofacies code. On the left are lumped lithofacies in the geomodel and on the right are core lithofacies. Perforations are shown on the left of the borehole. Shale lithofacies was not cored in the two cores described. Abbreviations include X-bedded (cross-bedded) and Congl. (Conglomerate).



North →



5. 3D Seismic Analysis (Dennis E. Hedke)

5.1. Overview

Prior discussion in this report provides the geographic and much of the geologic backdrop for the Pleasant Prairie field. This subset will focus on how the subsurface can be imaged in significant detail, particularly the genetic makeup and evolution of the typical Incised valley fill system (IVF) that contains important oil and gas reservoirs in the study area.

Making full use of data that was acquired approximately 13 years ago involves moving beyond time / amplitude mapping. Multiple attributes, including frequency, discontinuity, volumetric curvature, acoustic impedance, and others provide details that can be useful in better characterizing compartmentalization, flow within modeling units and better reservoir management and recoveries. The goal of the study is to maximize the applications of various available / processed datasets to better understand the complex reservoirs in the IVF systems.

5.2. General Description

Approximately 37.5 square miles of surface template 3-dimensional (3D) seismic data was acquired in the late 1990's. The data was acquired such that the processed bin size is 110' x 110'. It was apparently acquired in at least two sequential geographically overlapping areas. The product that has been the subject of this study was a result of the merging of these two areas, and the merged product is high integrity, with virtually seamless character in the overlapping area. Figure 5.1 illustrates the 'footprint' of the merged total volume, as well as the subset of the data that has been the focus of modeling efforts by other groups in the overall effort, which amounts to about 6 square miles of surface template.

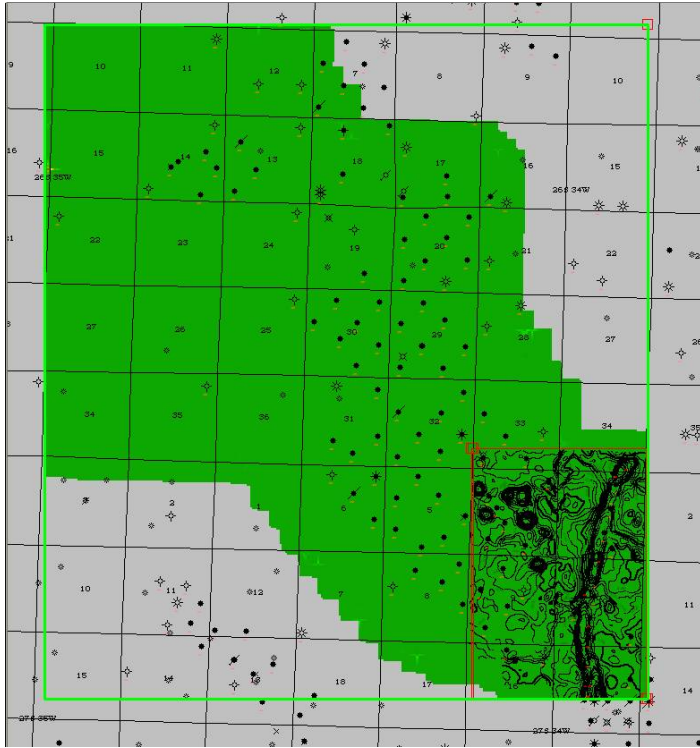


Fig. 5.1 Greater Pleasant Prairie data availability, with modeling focus area lower right. Contours are on the top of the Meramec.

5.3 Definition of major geologic controls on reservoir (IVF)

Seismic imaging is of high quality in the time range of the primary IVF reservoir, which occurs between 840-870 ms. Time Structure at the top Meramecian (total survey included) is illustrated by Figure 5.2. What is immediately evident is that the IVF system is focused in the channel cut within a very tight geographic extent. It is also apparent that Karst dissolution has occurred, as evidenced by the multiple circular features occurring in the regions outside the channel environment. One particular trend runs WNW – ESE across the southern 1/3 of the survey and appears to extend beyond the IVF and in fact becomes a part of it on the east side of the main channel in section 3. While none of these Karst features appear to extend in depth to the magnitude of the IVF, depth conversion mapping indicate that the features in section 4 may reach a datum of (-2200), as compared to the maximum depth in the IVF of approximately (-2275), as illustrated in Figure 5.3.

The fault bounded west edge of the Pleasant Prairie Field proper is very sharply imaged, and vertical profiles confirm that thrust faulting has been at least partly responsible for the structural conditions we see in the present day (Figure 5.4). The west-east offset of the thrust fault, as measured at Morrow time at 814 ms, trace 143, to sub-basement event at 1160 ms, trace 150, is approximately 770 ft. Other features of interest in this arbitrary profile are the karst expression centered at trace 260, which appears to have a core in the basement. In this figure, Further to the east the IVF system appears, with its deepest incisement at trace 306. Note that the time 'relief' below the incised valley at Arbuckle is materially softened, and that by Basement time, the time suppression is very weak. However, one can trace amplitude truncations on the east edge of the IVF well into the basement, implying fault connectivity, at minimum strong joint connectivity as a likely driving force for channel definition / generation. Note also that the Meramec unconformity exhibits a 'V' shaped channel at this particular cut, as opposed to a more vertical 'U' shaped condition that can also appear. More discussion of this point will be offered below.

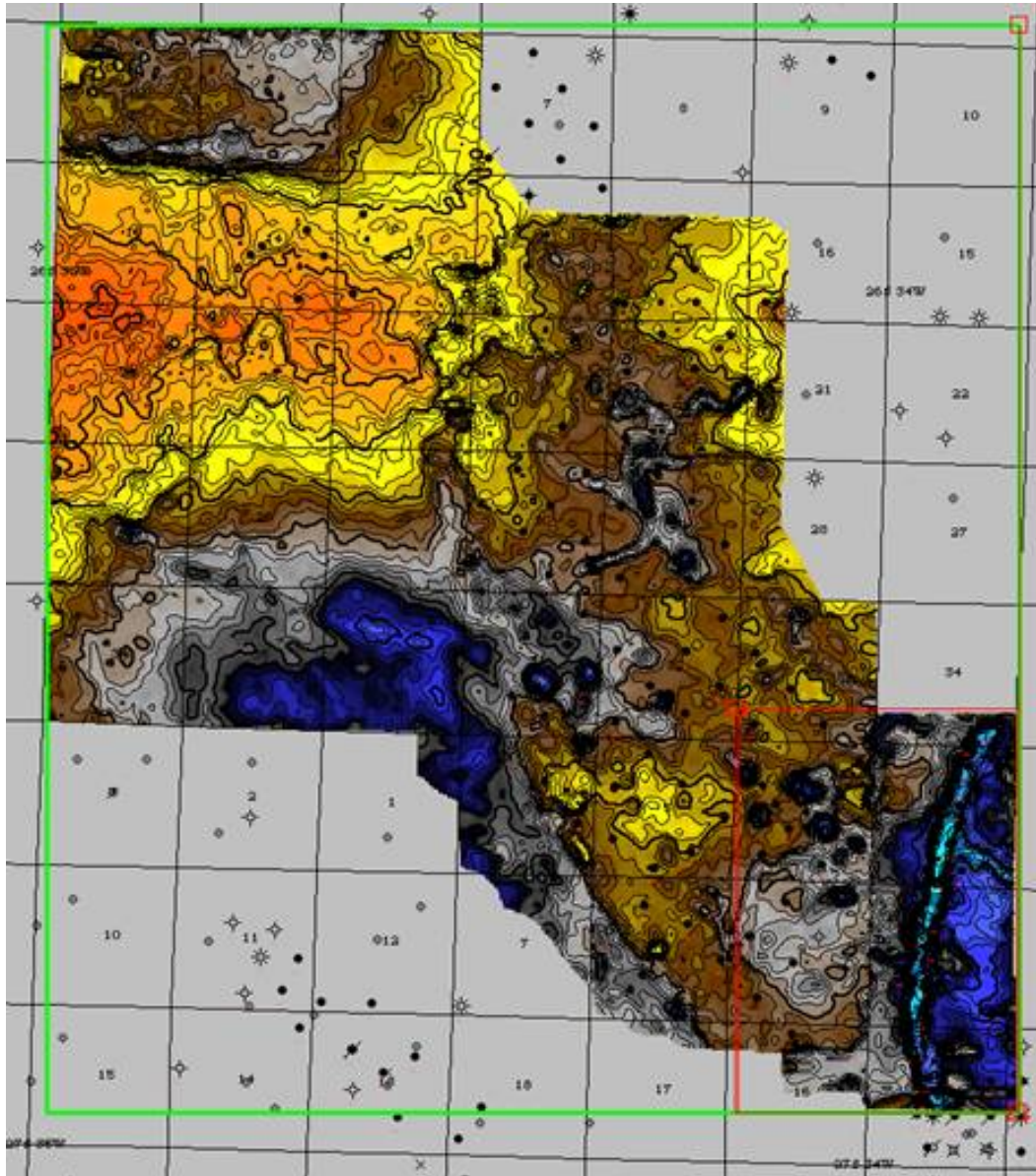


Fig. 5.2 Meramecian time structure, with Chester incised valley lower right.

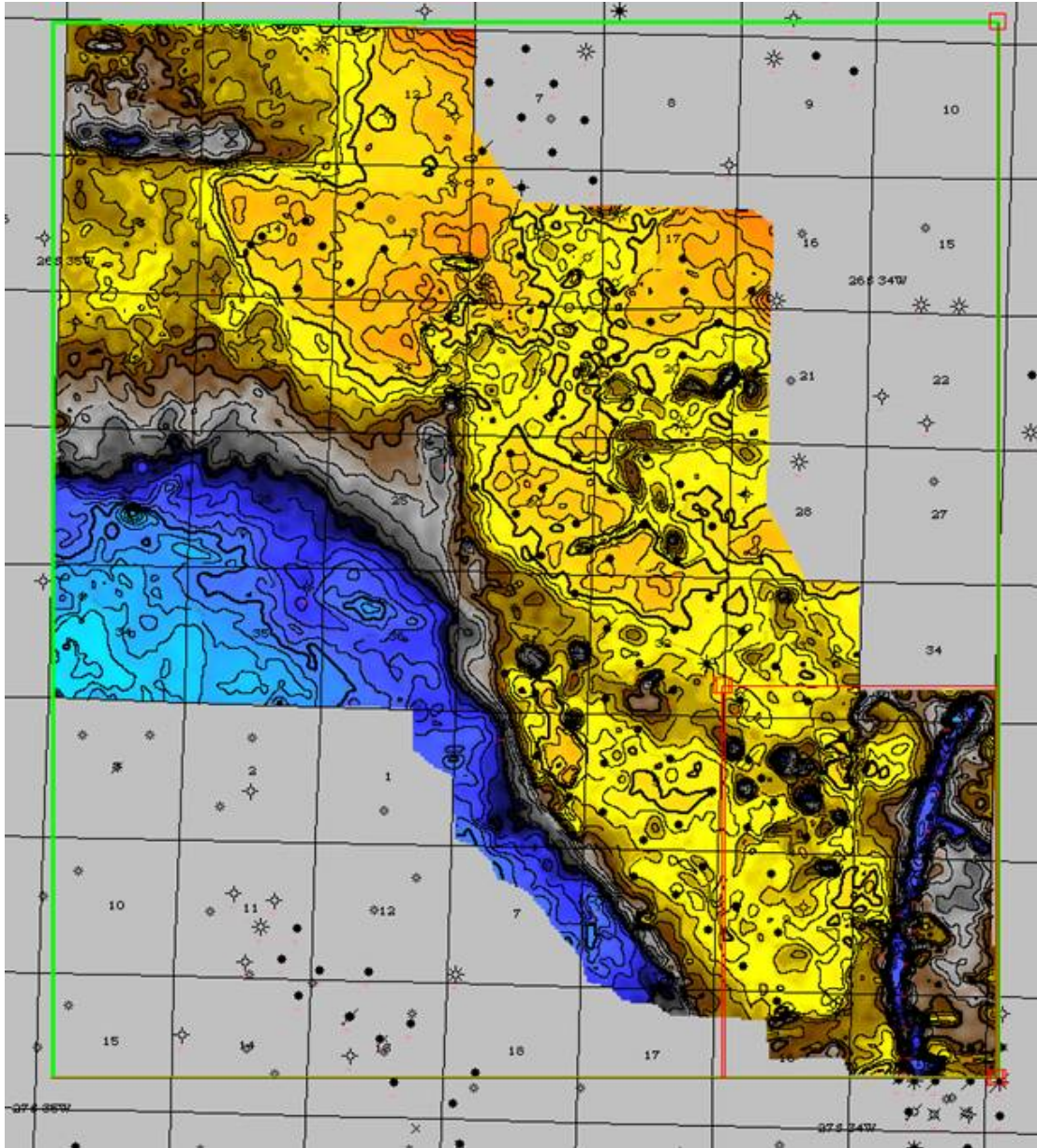


Fig. 5.3 Meramecian depth converted structure, average velocity method.

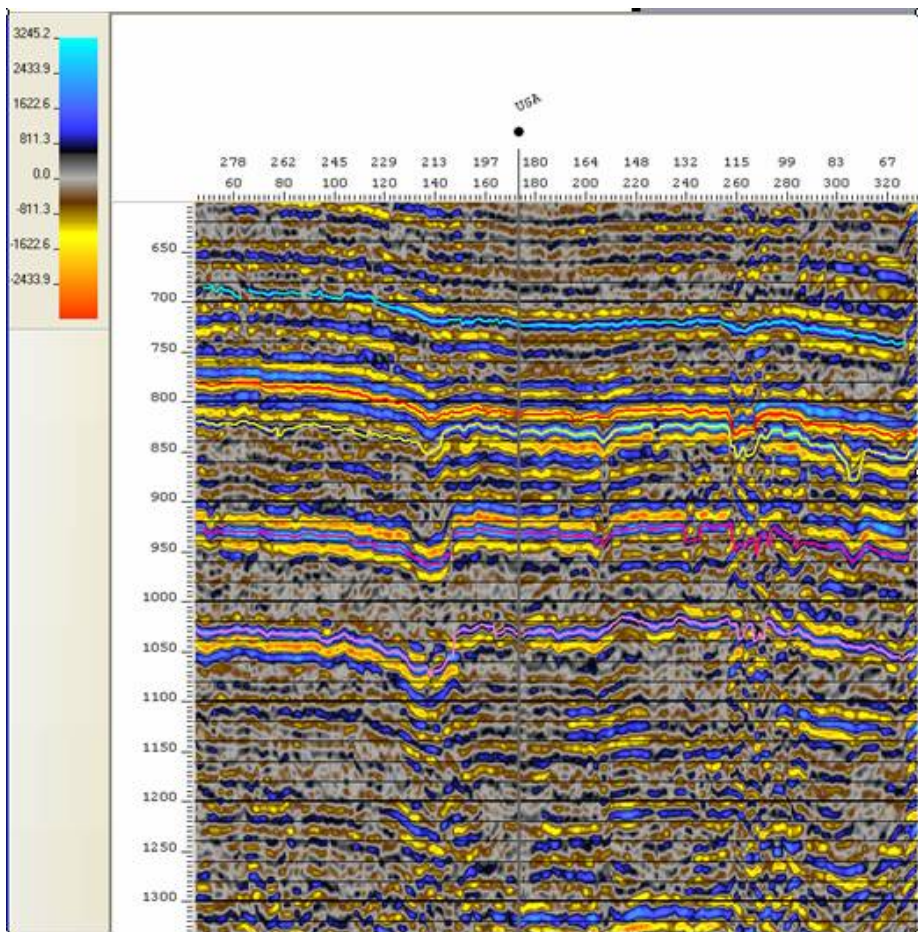
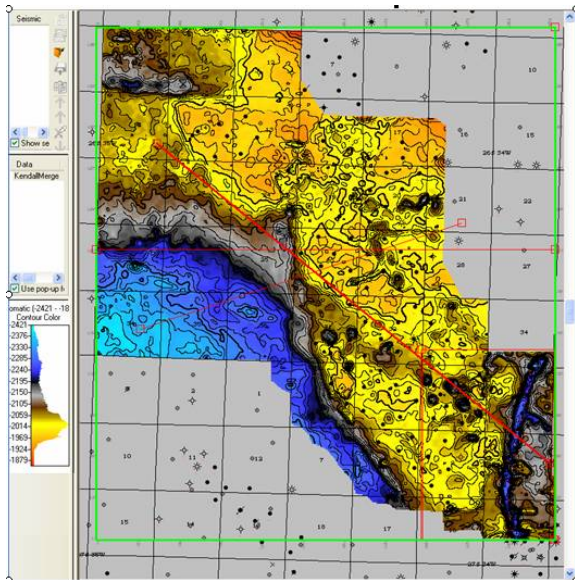


Fig. 5.4 Meramecian depth structure with NW-SE arbitrary profile. The markers highlighted, with the left edge of image as reference, are Morrow at ~780 ms, Meramec at ~820 ms, Arbuckle at ~925 ms, and Basement at ~1030 ms.)

5.4. Seismic attributes and the reservoir

Seismically the IVF is very nicely imaged by two primary characterizing methods. Firstly, the top of Mississippian Meramecian rocks presents well in contrast to the rocks immediately above, Mississippian Chesterian, in both a time and a rock stratigraphic sense. The Meramecian rocks are generally higher density carbonates, while the overlying Chesterian series are generally lower density shales and sandstone, with highly variable velocity as compared to the more regular velocities within the Meramec. This provides a discrete, widely mappable time structure surface that can be depth converted with substantial well control.

Secondly, due to the material variance in stratigraphic content within the Chester rocks, at least as far as the IVF system is concerned, we have opportunity to observe a significant amplitude contrast against the bounding carbonates in the Meramec. This contrast can be observed most conveniently in time slices, either natural, unflattened structural context, or in flattened context (usually hung on Top Morrow), to attempt to examine discrete stratigraphic packages.

In addition to the more conventional methods of structural and stratigraphic characterization mentioned above, we can also examine structural fabric via Volumetric Curvature (VC), and we can look more discretely at stratigraphic indicators by combining amplitude and frequency content, for example via Sweetness Factor (SF), which is defined as instantaneous amplitude divided by the square root of instantaneous frequency [$\text{InstAmp} / \text{InstFreq}^{1/2}$]. Other stratigraphic methods not investigated include acoustic impedance inversion and neural network extraction in search of porosity indicators.

In comparing amplitude to SF, one can see significant correspondence, as illustrated by the map view in Figure 5.5. This depiction draws from a window of stratigraphic content from the Meramec unconformity, upward 15 ms, or a vertical interval of about 90 ft. While the amplitude map does a very good job of discretely defining the IVF system boundary (note contours on depth-converted Meramec), SF character is able to discount the false positive in the northeastern-most portion of the image, correctly associating the blue SF area to non-productive conditions. Also of note is the relatively favorable narrow strip of amplitude indicated in the south half of section 3, which is suggested to be non-productive in the SF mapping. The half-mile long blue oval extending south from the center of section 3 is the location of two poorly performing wells that are not in pressure communication with the balance of the pool. It also may be the case that untapped reserves exist in the western wall of the IVF in the same general vicinity of section 3.

Production data suggests that the region in the north half of section 15 is among the strongest production in the unit, which would seem to be more significantly expressed by SF than amplitude. Finally, it does appear that SF indicators are tracking much more substantially with the karst features on section 2 than are the amplitude indicators. Amplitude and SF have not been quantitatively incorporated in the reservoir modeling but show promise for further study.

The attribute of VC consists of multiple related outputs including Most Negative Curvature, Most Positive Curvature, Dip Magnitude, and a host of others. For purposes of brevity, this discussion will highlight most negative curvature, as it relates most directly to fracture systems, including joints and faults. As was illustrated earlier, the study area is within a region where fracture systems play a fairly significant role in reservoir development. Whether it be focusing of drainage as in the case of IVF genesis, or perhaps conduits for fluid movement (and concomitant diagenesis), understanding these systems will likely bring benefit to understanding hydrocarbon systems.

The map depictions illustrated in Figure 5.6 show the comparison of the same amplitude slice that was presented in Figure 5.5, with the attribute of most negative curvature. Clearly the curvature of the IVF channel is well expressed. In addition, the karst features in section 2, and the tributaries feeding the IVF are also well expressed, and linked to the VC attribute.

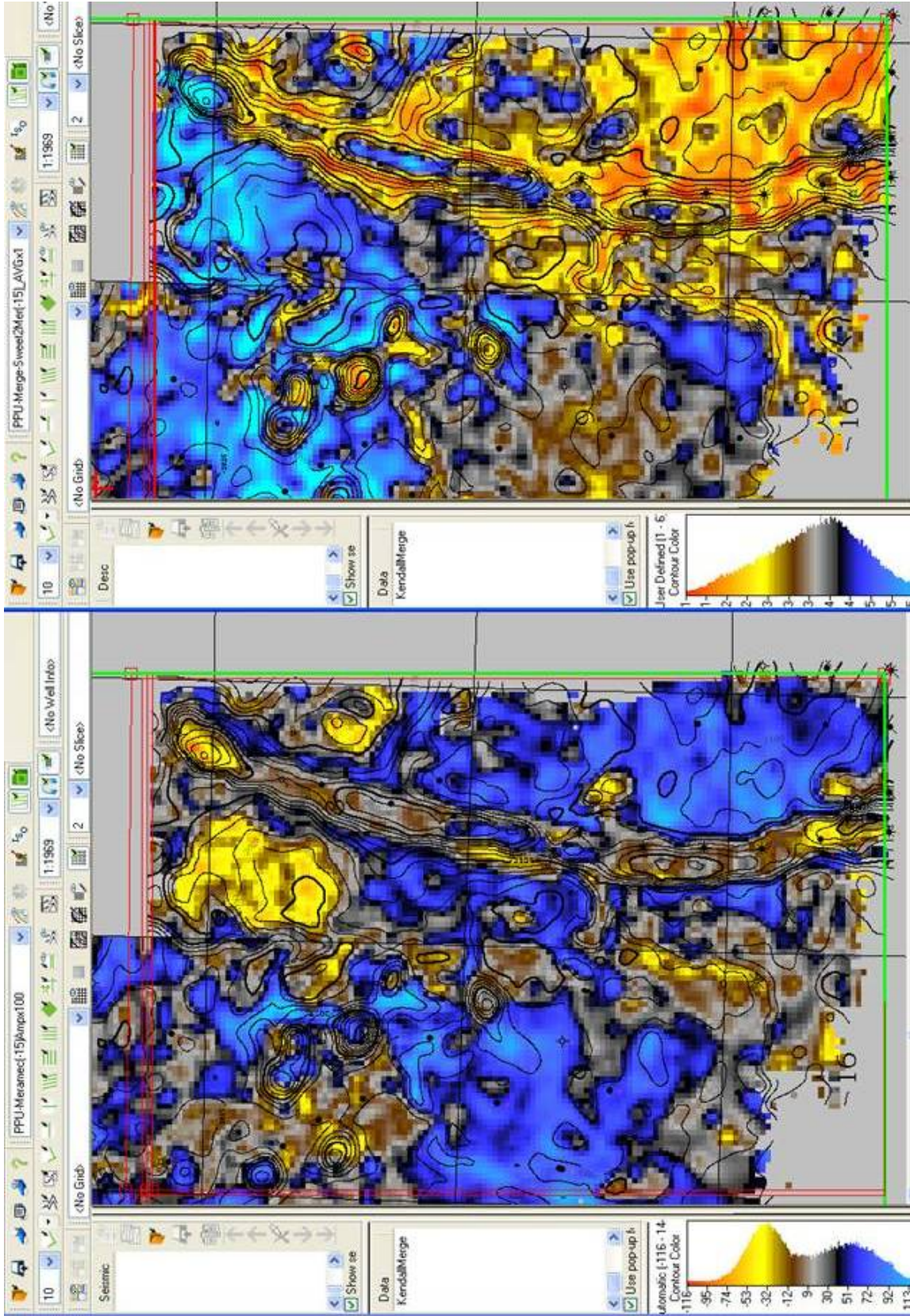


Figure 5.5 Reservoir map / time window illustrating Amplitude (left) and Sweetness factor (right).

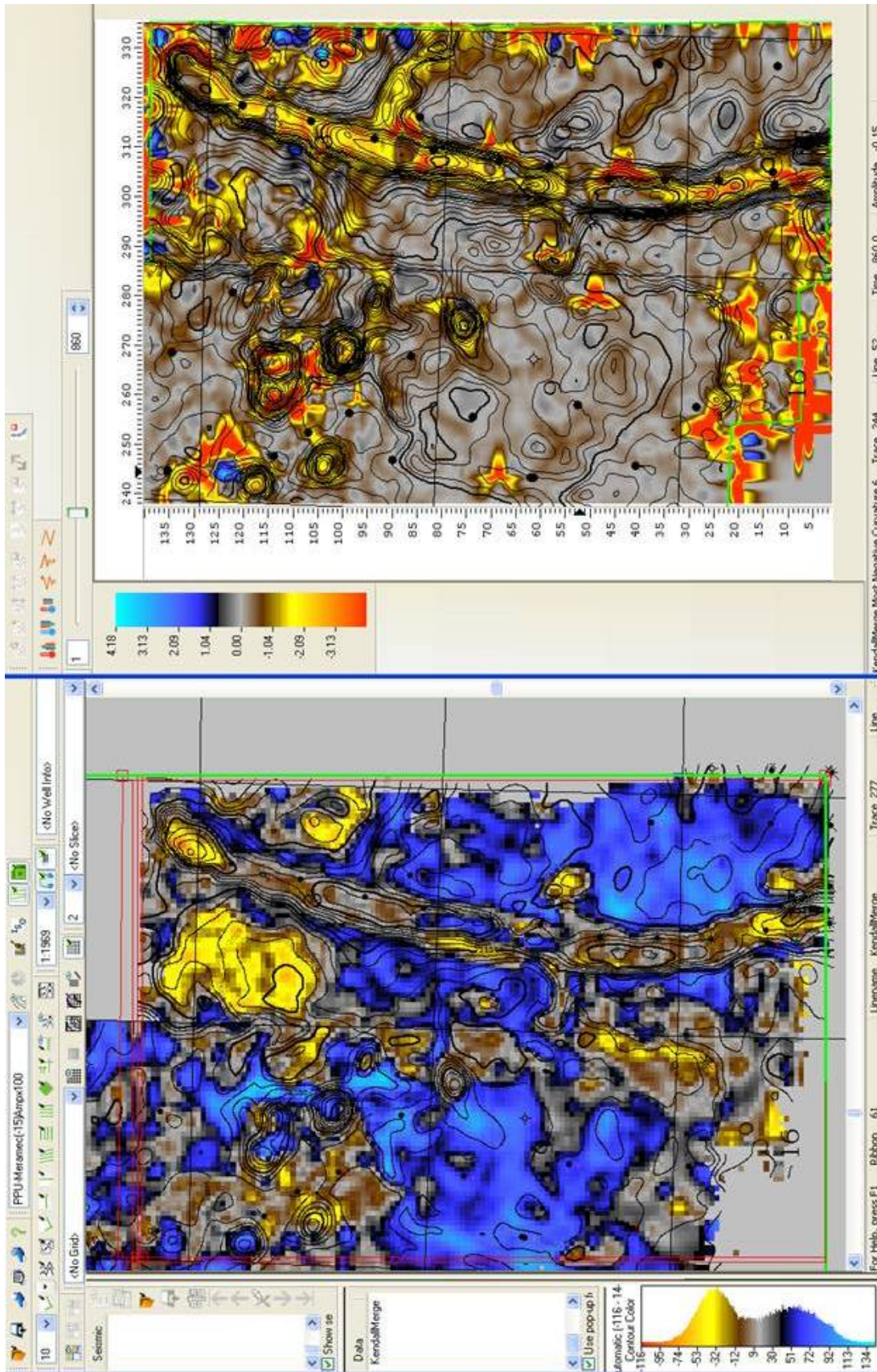


Figure 5.6 Reservoir map / time window illustrating Amplitude (left) and Most Negative Curvature (right).

6. Static model (Martin K. Dubois and Peter R. Senior)

6.1 Overview and workflow

Reservoir characterization and modeling of the Pleasant Prairie South pool is the integration of many disciplines culminating in dynamic reservoir simulation to predict possible outcomes from CO₂ injection (Fig. 6.1). The static geomodel for the Pleasant Prairie South Chester reservoir was constructed in Petrel™ using a standard workflow illustrated in Figure 1.2. A fine-grid model containing 700,000 active cells having cell dimensions of 55ft in XY and ~2ft in Z directions was populated with lithofacies, porosity, permeability, water saturation. A simplified version of the steps to build the model are: 1) identify lithofacies and sequence stratigraphy in core from two wells, 2) relate core petrophysical properties to lithofacies, 3) train a neural network to identify lithofacies in 20 wells without core based on wireline log curve responses 4) build fine-grid structural (wireframe model) using depth-converted seismic surface and well formation tops, 5) populate model with lithofacies using sequential indicator simulation (SIS), 6) populate model with porosity using sequential gaussian simulation (SGS) for each lithofacies, 7) calculate permeability at each cell using lithofacies-based porosity-permeability transform equations, and 8) calculate Sw using Leverett J-Function with Blueback™ plugin. The model was then upscaled in the Z direction to ~10ft layering and the 65,000 active cell coarse-grid model was exported in a rescue format for dynamic modeling.

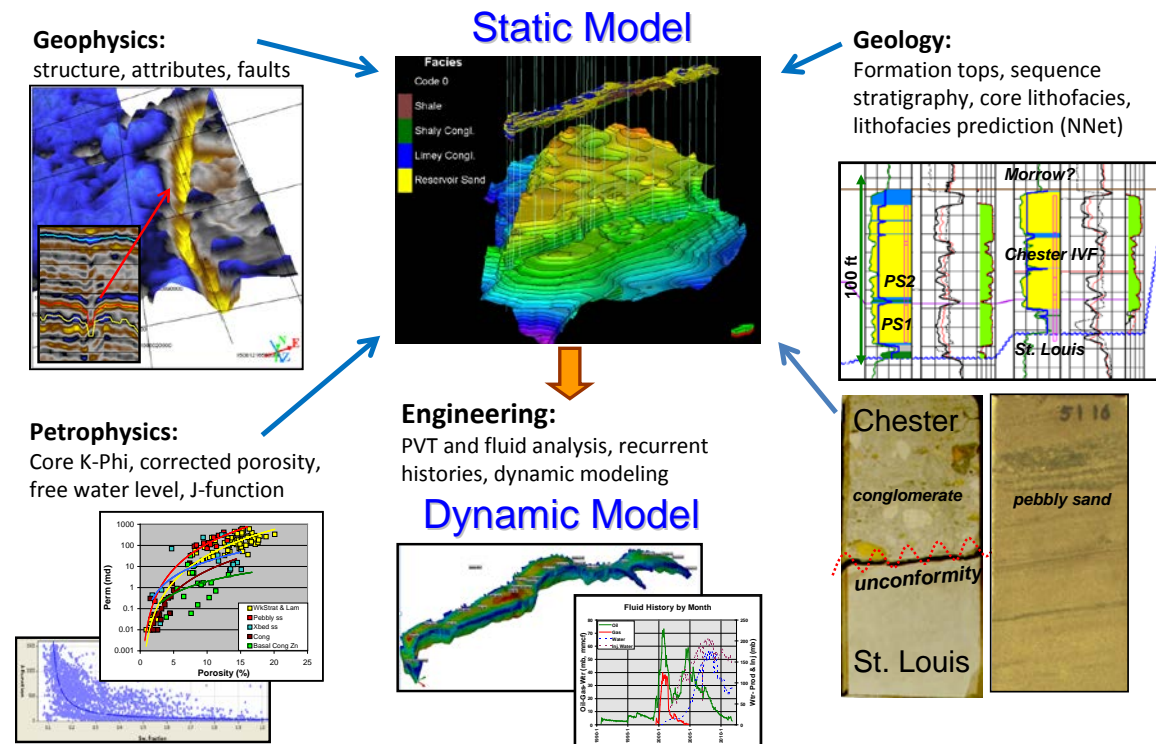


Fig. 6.1 Integration of multiple disciplines for static and dynamic modeling.

Model building is an iterative process with the need to loop back to previous steps throughout the process, rather than the linear flow described in the simple step-by-step process described above. We believe that the present model is adequate, considering the time allocated and the scope of this study, but could be improved with additional iterations as will be discussed.

6.2 Static model data

Although not extensive, the data set for the Pleasant Prairie South static model is adequate for building a reliable model (Table 6.1). The top and base of the reservoir, the Chester sandstone, is well constrained by wells and well log data spaced 1320 ft apart or less. 3D seismic effectively constrains the valley walls and the base of the channel between wells. Modern well logs on each well through the entire Chester interval make for accurate lithofacies and fluid saturation determination. Although there is no special core analysis (SCAL) data available for in situ klinkenberg corrected permeability, the conventional core analysis data is adequate for estimating permeabilities that are proportional to corrected permeabilities. Water saturation calculation parameters m and n were not available in Pleasant Prairie South, but SCAL reports from other similar Chester incised valley sandstone were available from the "larger" project and were used.

Wells	25 wells drilled through the entire Chester and into underlying Meramec 23 in the waterflood 3 directly adjacent too, but not connected to waterflood
Wireline logs	All wells have NPFI, DPFI, RHOB, GR, and deep resistivity 16 wells have PEF, 9 do not
Tops/surfaces	Chester sandstone, parasequence boundary, base Chester sandstone, Meramec
Core	Cores from two wells covering nearly the entire Chester Conventional whole core analysis for 151 samples
SCAL	None in these cores, but limited amount available in other Chester sandstone
Archie parameters	m and n from Chester core SCAL in other fields. R_w from reservoir water.

3D seismic Depth-converted Meramec unconformity structure tied to well data
Sweetness and Mean Amplitude attributes not fully integrated

Table 6.1 Summary of main data inputs to static model. Abbreviations for logs are neutron porosity- NPFI, density porosity - DPFI, bulk density - RHOB, gamma ray - GR, photoelectric effect - PEF.

6.3 Lithofacies and petrophysics

6.3.1 Lithofacies lumping

Classifying rocks into lithofacies is a balancing act between splitting and lumping the continuum into meaningful classes that 1) can be identified accurately with wireline logs in wells without core, and 2) are sufficiently different petrophysically to justify splitting. Initially, six lithofacies were defined in core, limey conglomerate, cross-bedded sandstone, laminated sandstone, weakly stratified sandstone, pebbly sandstone, and interbedded sandstone and heterolithic mudstone-sandstone, and also not in core, but recognized in wireline logs the shale lithofacies. The appropriateness of lumping was revealed by cluster analysis, the neural network training and testing process (Section 6.4), and by analyzing the core petrophysics. Lithofacies were eventually lumped to four lithofacies for modeling: limey conglomerate, reservoir sandstone (weakly stratified and laminated sandstone, pebbly sandstone, cross-bedded sandstone), shale, and basal conglomerate (conglomerate in contact with the Meramec lumped with interbedded sandstone and heterolithic mudstone-sandstone) (Figure 6.2).

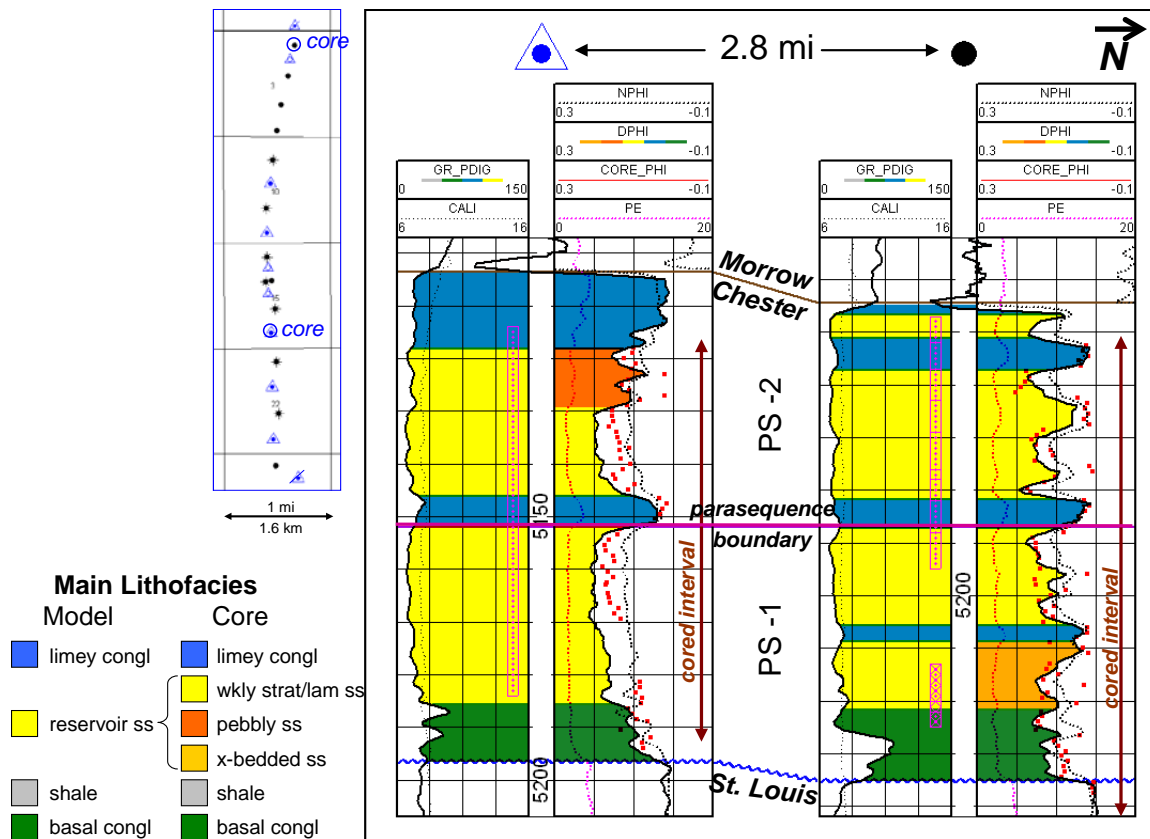


Fig. 6.2 Core lithofacies after initial lumping (right) and model lithofacies. Abbreviations are congl – conglomerate, wklly strat/lam ss – weakly stratified or laminated sandstone, and x-bedded – cross-bedded.

6.3.1 Petrophysics

Conventional whole core analysis data was available for two wells (Figure 6.2). Statistical summary of that data by lithofacies is in Table 1. No special core analysis data, including in situ porosity and permeability and relative permeability, was available from wells in the pool for this study. The difference between porosity in conventional core analysis data and that under in situ conditions is minimal at the depths for these wells, under 5200 ft. However absolute permeability under in situ conditions would be significantly reduced, and if Klinkenberg correction was applied the permeability would be further reduced. In building the model we have assumed that corrections to permeability would be proportional to the conventional core analysis and would be taken into account in the dynamic modeling process.

Lithofacies:	Avg Φ (%)	Avg k (md)	Range Φ (%)	Range k (md)
All conglomerate	5.14	13.92	1.5 - 10.6	0.01 - 72
Basal conglomerate only	7.98	17.96	7.5 - 10.6	0.06 - 32.5
Non-basal conglomerate only	4.19	12.57	1.50 - 7.40	0.01 - 72
Pebbly sandstone	10.15	172.95	2.2 - 13	0.224 - 418
Weakly stratified sandstone	10.44	141.60	1.6 - 20.10	0.03 - 629
Laminated sandstone	13.76	159.92	0.90 - 17.9	0.01 - 535
Cross-bedded sandstone	9.98	66.02	1.80 - 15-10	0.04 - 316
Interbedded sandstone & heterolithic sandstone-mudstone	9.11	2.54	5.5 - 13.2	0.334 - 10.0

Table 6.2 Core-derived porosity and permeability by lithofacies.

Core porosity and permeability relationships by lithofacies are shown in Figure 6.3. Partially lumped core lithofacies demonstrate different porosity/permeability relationships as would be expected due to difference in pore geometry as a function of grain size, clay content and cementation. However, there is insufficient data to reliably separate the data set to five classes (Fig. 6.3A). Higher R^2 correlations were attained by lumping all the sandstone lithofacies into the "reservoir sandstone" lithofacies and lumping the two conglomerate lithofacies (Fig. 6.3B).

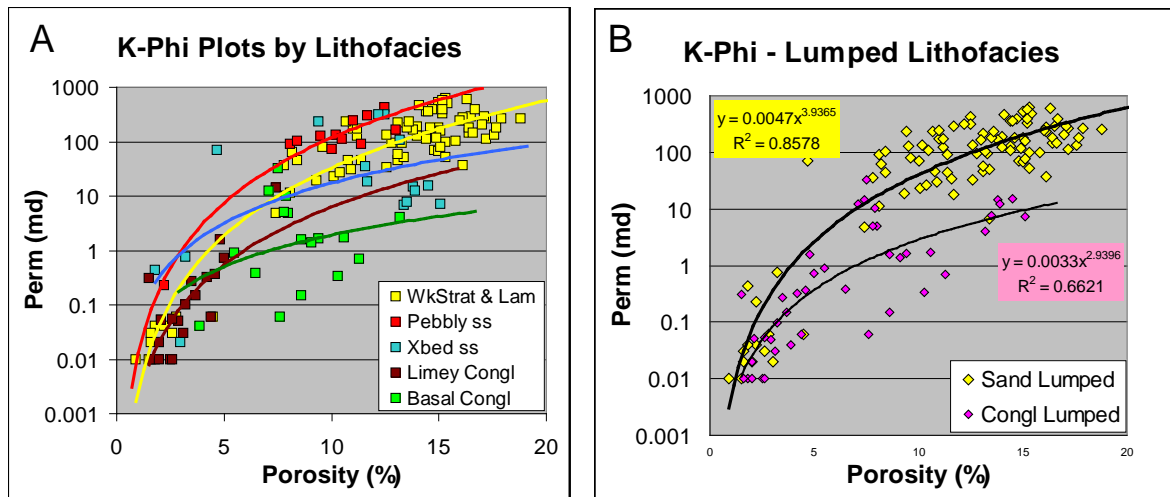


Fig. 6.3 Porosity-permeability cross plots by core lithofacies not lumped (A) and model lithofacies lumped (B). Abbreviations are the same as in Fig. 6.1.

In the geomodel, the power-law equations in Fig. 6.3B were applied to reservoir sandstones and each of the conglomerate lithofacies. A permeability of 0.01 was arbitrarily assigned to the model shale lithofacies, not identified in core. Below are the equations:

Sandstone $K(\text{md}) = 0.0047 \cdot \text{PHI}^{3.9365}$

Conglomerate $K(\text{md}) = 0.0033 \cdot \text{PHI}^{2.9396}$

Shale $K(\text{md}) = 0.01$

Corrections to wireline log porosity or using wireline log measurements to more closely match core derived porosity was completed with the assistance of John Doveton, Kansas Geological Survey. Neutron and Density porosity (NPHI and DPHI) and Bulk Density (RHOB) curves were available in the cored wells and the balance of the 23 wells in the pool. Lithofacies were not split for the analysis, mostly due to the relatively small data set for the conglomerate lithofacies. Core depths were carefully matched to wireline log depths and three approaches were tested: 1) regression analysis considering RHOB and the average of NPHI and DPHI, 2) average of NPHI and DPHI, 3) varying matrix density (RHOMA). Results of the testing are illustrated in Table 6.3.

Method tested	R ²
1. Regression analysis	
RHOB	0.6932
NPHI DPHI	0.6497
2. NPHI-DPHI Average	0.6199
3. PHI = (Rhoma-RHOB)/(Rhoma-Rhof) **Rhof = 1.0 g/cc	
Rhoma = 2.68 g/cc	0.6239
Rhoma = avg rhob from core repts (2.65)	0.6239
Rhoma = NPHI-DPHI Average	0.6199
Rhoma = rhob from core rept at each step	0.4748

Table 6.3 Results of testing three methods for matching wireline log-derived properties to core porosity.

Using RHOB directly to match core porosity proved most effective, having an $R^2 = 0.6932$. The equation for estimating porosity from RHOB is

$$\text{Porosity (\%)} = -46.775 * \text{RHOB} + 126.992$$

Predicted porosity is compared with core porosity in Figure 6.4. Core porosity deviations from the predicted may be explained by sample interval and slight variations in RHOMA. The core porosity is the average porosity over a half-foot interval, whereas the wireline log measured RHOB is the average over up to 2 ft. Slight variations in RHOMA due calcite cement and limestone clasts (in conglomerates) can impact RHOB significantly. Had more data been available more than one equation would have been developed and they would most likely have had better correlations.

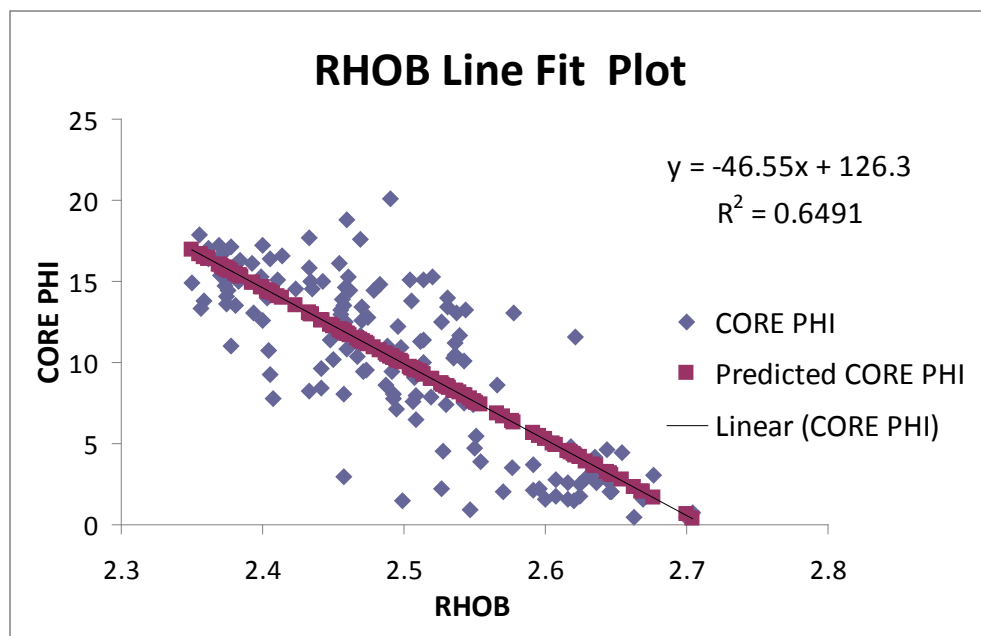


Fig. 6.4 Cross-plot of RHOB and core porosity illustrating the relationship of measured core porosity and predicted porosity.

6.4 Predict lithofacies in wells without core

Key to modeling lithofacies in the static model is establishing relationships between wireline log curve to lithofacies where known and applying these relationships to wells without core using their wireline log curves. Fortunately in this study each of the 23 wells have relatively modern logs. As part of Senior's MS thesis work, he chose to evaluate the effectiveness of artificial neural networks (ANN) to estimate lithofacies in wells without core utilizing the core from two wells as a training set. We had hoped to be able to differentiate lithofacies at a fine scale, rather than lumped. As we worked through the process it became readily evident that it was appropriate to lump the main sandstone lithofacies, the main reservoir lithofacies, because of a combination of 1) multivariate statistical cluster analysis (Agglomerated Hierarchical Clustering), 2) core petrophysical data indicated lumping was appropriate, and 3) the ANN approach was not effective in delineating the finer classes of sandstone lithofacies because their wireline log characteristics were similar and overlapping. In the current study of the Chester reservoir Eubank field, 6 miles south of Pleasant Prairie South pool, John Youle arrived at a similar conclusion, lumping the reservoir sandstone lithofacies. Furthermore he has concluded that a simpler approach of applying ranges and cutoffs to key wireline log curves is effective in defining lithofacies in wells without core. Following is a brief summary of Senior's work.

A simple description of the process of defining lithofacies in wells without core is to 1) define lithofacies in core, 2) tie lithofacies to log attributes (several log curves, 3) train and test a neural network with the lithofacies in cored wells, and 4) predict lithofacies in wells without core. Optimization for the appropriate set of log curves used as predictor variables, neural network parameters (nodes in hidden layer and damping), and the balance between splitting and lumping are all part of an iterative, trial and error process.

6.4.1 Neural network structure

Artificial Neural Network (ANN) modeling to predict lithofacies in wells without core was performed using Kipling.xla, an add-in for Microsoft Excel developed by Bohling and Doveton (2000). The Kipling.xla add-in was used to generate well logs of predicted lithofacies in wells without core. ANNs are so named because of the similarity of their intricately connected system of nodes to the structure of the human brain. An ANN consists of an input layer, hidden layers, and an output layer, with each layer made up of nodes. Figure 6.5 is a schematic of the organization of an ANN. Each node in the input layer corresponds to a variable used in prediction, the number of nodes in the hidden layer or layers is set by the user, and the number of output layer nodes corresponds to the number of possible outcomes. An ANN made with Kipling.xla has a single hidden layer, although theoretically an ANN can have multiple layers. In the case of the present study, each input layer node corresponds to a log variable (e.g. Gamma Ray) and each output layer node represents a lithofacies class. Outputs are generated in the form of statistical probabilities; for each depth interval with a set of input (log) variables a statistical probability is generated for each of the possible lithofacies classes, and the ANN assigns the highest probability as the predicted lithofacies at each depth interval. Prediction of lithofacies using Kipling.xla is an iterative process of training and testing ANN using different values for the number of hidden layer nodes and a damping parameter.

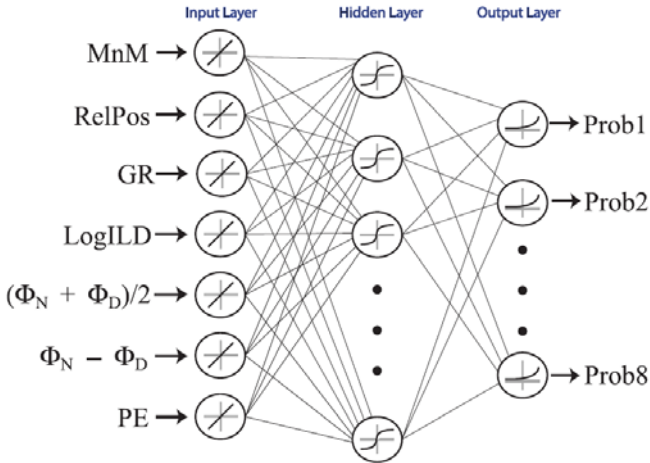


Fig. 6.5 Schematic diagram of the organization of an Artificial Neural Network (ANN), from Dubois et al., (2006). The same input variables were used in this study, except the MnM (marine-non-marine indicator, which was not. On the output side, probabilities of four lithofacies are defined rather than eight.

6.4.2 Training and testing

After determining that the lithofacies should be lumped, four core lithofacies, shale, basal (shaly) conglomerate, non-basal (limey) conglomerate, and reservoir sandstone defined at the half-foot scale, same as the sample rate for the wireline logs. No shale lithofacies are present in the core wells so a shale interval from one of the wells with shale in the northern half of the field was inserted into the training set. Log variables used to train the network included gamma ray, neutron-density porosity average, neutron porosity minus density porosity, log10 of deep induction, and a relative position log, and photoelectric (PE) log. The relative position log assigns a number between zero (deepest) and one (shallowest) for each depth interval and was generated in Microsoft Excel. This group of variables is common to all wells used in the study, and was also used in ANN prediction of lithofacies in other studies (e.g. Dubois et al., 2006). In wells without PE estimated apparent grain density logs were generated using the equation

$$RHOMAA=(Rho_b-\Phi X)/(Rho_b-Rho_f)$$

where Rho_b is the value from the bulk density log, ΦX is porosity, calculated using the RHOB regression analysis equation in section 6.3, and Rho_f is the density of pore fluid, set to the density of water, 1.00 g/cc. Two sets of porosity logs were used: ΦX as the best match to core

porosity as outlined in the Petrophysics section above. Generating the estimated apparent grain density logs allowed an additional variable to be used in all wells, while the PE log was only available on a subset of wells in the field.

Optimal neural network controls, number of hidden layer nodes (HLN) and damping parameter, were determined parametrically by running tests on each combination of the ANN variables HLN (10, 20, 40, and 80 nodes) and Damping (0.01, 0.1, 1, and 10). A modified jackknife training and testing process was used, whereby the training set was randomly split 50-50, half for training and half for testing. Optimal parameters were determined by the best overall results. Results did not vary much, and were above 90% overall correct in most test cases, and the "winner" had a 94.5% overall accuracy rate. As a general rule-of-thumb, it is desirable to use the fewest hidden layer nodes and the highest damping parameter to prevent overtraining the ANN. Overtraining results in the ANN becoming so attuned to the training dataset that inaccurate results are obtained when predictions are made on other datasets. This process was run for the case with PE curve and the case without a PE curve where RHOMAA was substituted. Optimal ANN parameters for HLN and damping for the PE case are 10 and 0.001, and for the no PE case are 80 and 1. Because each ANN is unique given a unique seed number, five examples for each case (PE and no PE) were then run using the optimal parameters and one of the five for each was chosen on the basis of best results when training on all examples and predicting on all examples. The chosen ANNs were then used to predict lithofacies for wells without core. Resulting lithofacies can be viewed in cross-section view of the main 23 wells in Figure 4.4.

6.5 Build structural (wireframe) model

The goal of the modeling process is to represent the reservoir as accurately as possible given the limitations of the facies and property data (well-scale), structural data (tops, surfaces, and seismic Meramec structure), and the inherent limitations of the modeling computer application. Another key limitation is the limited time available for the task. The current model has some shortcomings, as will be described, that could be mitigated in additional iterations.

6.5.1 Basic building blocks

Layering scale was set at an average of two feet to adequately capture the vertical heterogeneity found in core lithofacies, porosity and permeability. Cell scale in the XY direction was set at 55 ft to ensure that the lateral heterogeneity would be captured. The relatively small cell size also helped reduce edge effects where the modeling application is limited in areas with rapid changes in thickness (e.g.: steep valley walls). The foundation for the model is the seismic depth map on the top of the Meramec surface tied to well control (Figure 5.3). The seismic map, along with well control, forms the base and the sides to the incised valley. The surface on the top of the Chester sandstone is the top of the reservoir body and is identified on well logs. The parasequence surface defined in core and correlated throughout the reservoir by wireline well logs separates the reservoir into an upper and lower interval. It has not been determined whether the parasequence boundary, marked by the limey conglomerate lithofacies in most wells, is a flow barrier, but it is likely a vertical baffle at a minimum, unless there are regularly spaced vertical fractures in the reservoir. Open vertical fractures were observed scattered throughout the core, but they were not quantified.

6.5.2 Construct wireframe (structural model)

The cellular model was constructed in four steps:

Step 1: Import seismic depth structure map of the Meramec and modify as appropriate (Fig. 6.6A). The Meramec structure map was smoothed slightly and the surface was locally "dragged" up or down to more closely conform to the Meramec tops picked from well logs. In the first iteration the valley walls were not modified. In later versions, after a volumetric analysis by model segments, the valley walls were locally steepened to allow for more reservoir volume when it appeared there was insufficient reservoir volume, or flattened slightly when it appeared there was too much reservoir volume.

Step 2: Construct the upper Chester sandstone and parasequence boundary (PSB) surfaces and import into modeling application (Figure 6.6 BC). Two simple monoclinial surfaces were constructed using the Chester sandstone top and parasequence top from wireline logs. These surfaces were artificially extended beyond the valley in all directions so that they would intersect the valley wall. After import, the surfaces were smoothed slightly and accurately tied to the tops at the wells.

Step 3: Layer the lower parasequence with the top being the parasequence surface and the base and sides of the volume bounded by the Meramec structural surface. This interval was layered with 2-ft layers, conformable to the top (PSB), resulting in a layering that mimics fill of an incised valley with a rising sea level (Figure 6.7).

Step 4: Layer the upper parasequence with the top being the Chester sandstone top surface, and the base being the PSB, and sides of the volume bounded by the Meramec structural surface. This interval was layered with 2-ft layers, conformable to the base (PSB).

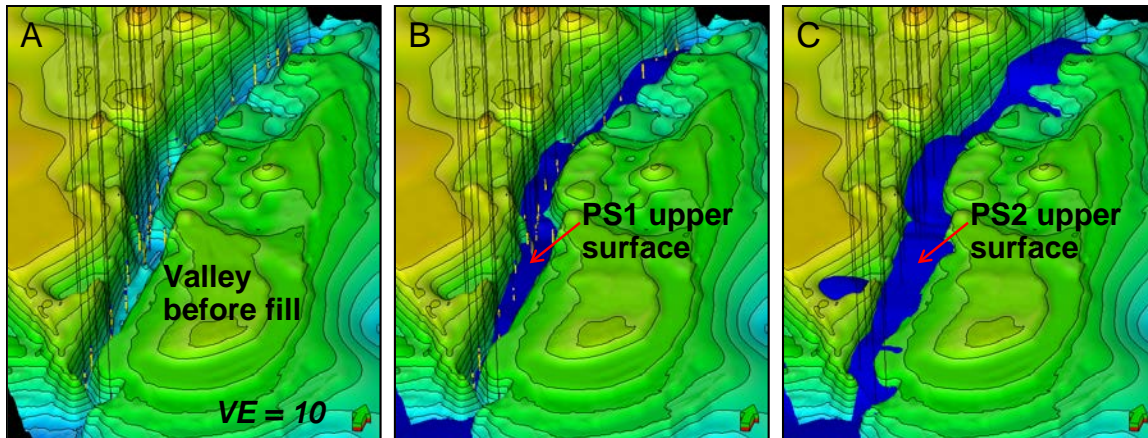


Fig. 6.6 Filling stages in the incised valley

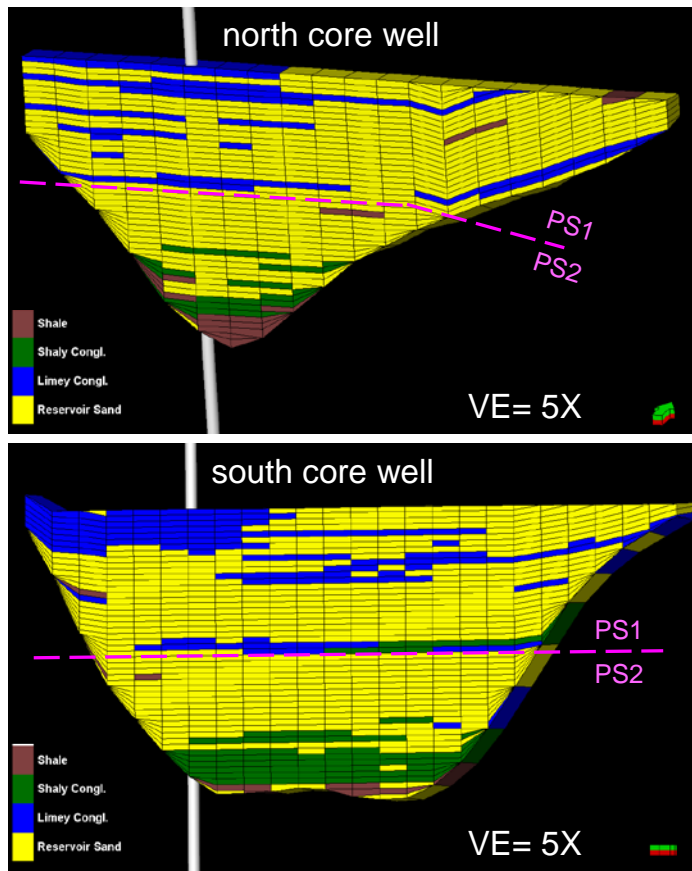


Fig. 6.7 Cross-sections through cored wells roughly perpendicular to the long axis of the valley.

6.6 Populate cellular model with properties

Porosity, permeability and water saturation are all lithofacies dependent due to varying pore volume and pore geometry with grain size, clay content and cementation. Porosity derived from wireline logs using measured RHOB and lithofacies estimated by the ANN procedure are the two main inputs. After lithofacies and porosity modeling, permeability is a direct calculation. Water saturation was calculated using Leverett J-Function with BluebackTM plugin.

6.6.1 General modeling discussion

One of the main goals of modeling is to obtain a cellular model that best represents the actual reservoir relying on data available such as wireline well logs, seismic, cores and core analysis. It is also important to take into account engineering data such as pressure through time, productivity, and waterflood performance. Based on these data alone we have the following understanding of the reservoir:

1. Chester sandstone is deposited in a narrow, relatively steep-walled, flattened nearly V-shaped, but slightly U-shaped valley that ranges from 150-200 ft from valley rim to the deepest incision. Widths at the rim average about 1400 ft, but are as narrow as 800 ft (Figure 6.8).
2. The Chester sandstone fills the valley to within approximately 2/3rd from the base of the valley.
3. Sand and conglomerate sandstone lithofacies dominates the valley fill and appears to fill the valley from wall-to-wall.
4. Individual flow units range from 10-30 ft thick and most can be traced from well to well (Figures 4.3, 4.4, 6.2) for up to half of the pool's 4-mile length.
5. Two of the wells in the northern half of the pool (shalier wells) are isolated from the rest of the pool - not pressure connected.
6. Otherwise, waterflood performance suggests the reservoir has relatively good lateral continuity in a north-south direction.

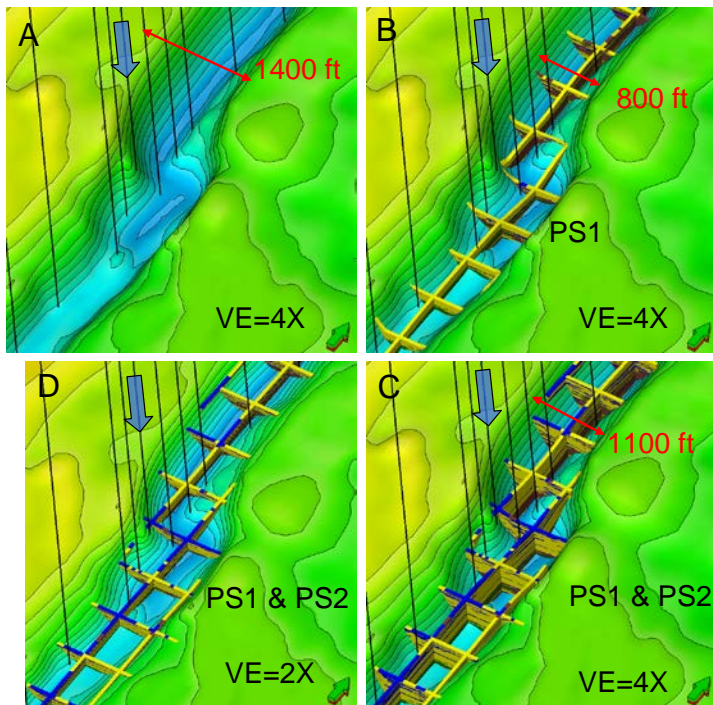


Fig. 6.8 Chester incised valley and fill. A point of reference is the discovery well indicated by a blue arrow. (Clockwise) A. Meramec structure CI=20ft. Width at valley rim = 1400 ft. B. Valley partially filled with parasequence 1. Width of fill = 800 ft. C. Valley partially filled with parasequence 2. Width of fill = 1100 ft. D. Same view as (C), but VE = 2x.

In light of the observations listed above, we guided the modeling process to reflect the observed flow unit thicknesses and lateral continuity. Data analysis and variogram analysis modeling tools confirmed lateral continuity. Long north-south variogram ranges and narrow east-west ranges resulted in more-or-less deterministic models because well spacing (1320 ft) was significantly shorter than the ranges.

6.6.1 Data preparation

Much of the well-scale data preparation was managed in Petra™, a geologic database and mapping application. Lithofacies estimated using the ANN by numerical code (Lithofacies1-4) were imported into Petra™. Using the log calculation tool in Petra™, porosity was calculated from RHOB using the equation defined in section 6.3:

$$\text{Porosity (\%)} = -46.775 * \text{RHOB} + 126.992$$

and permeability was calculated by lithofacies by applying the equations defined in Section 6.3:

Reservoir Sandstone $K(\text{md}) = 0.0047 * \text{PHI}^{3.9365}$

Conglomerate $K(\text{md}) = 0.0033 * \text{PHI}^{2.9396}$

Shale $K(\text{md}) = 0.01$

Again using the log calculation tool in Petra™, water saturation was computed using the Archie equation for all lithofacies except shale. Shale lithofacies was assigned an $S_w = 1$ by default:

$$S_w^n = a * R_w / (R_t * \text{Phi}^m)$$

where, S_w water saturation
 Phi porosity (from RHOB calculation)
 R_w formation water resistivity = 0.04

Rt	true resistivity (measured deep resistivity)
a	tortuosity exponent = 1
m	cementation exponent = 1.8
n	saturation exponent = 1.9

Cementation and saturation exponents for the Chester Sandstone were not measured in core in the Pleasant Prairie South, but were in core from the Eubank field eight miles to the south and used in a proprietary petrophysics report (Gray, 2001). The study was part of the pre-waterflood unitization study for the Eubank North Unit. The Chester sandstone in the Eubank, also being studied as part of the "larger project" is very similar to that in the Pleasant Prairie South and cementation and saturation exponents should be very similar.

Formation water resistivity used in the Pleasant Prairie South study is 0.04, the same as in Gray (2001) which was stated as being based on measured formation water in the Eubank field. At the time when the study was begun, measured R_w for the study area was not available. Since then water analysis data, five samples from four wells, taken prior to water flood were provided by one of the operators (Table 6.3). Total dissolved solids (mg/l) was converted to Total dissolved solids (ppm) by multiplying the former by the specific gravity. R_w at 125°F was read from a Schlumberger chart (Schlumberger, 1986). Temperature at 5200 ft, reservoir depth, is the average bottomhole temperature from four drill stem tests in the Chester sandstone in the study area (two were 122 and two were 128). Mean R_w for the five samples is 0.0388. However, when the two samples from the same well are averaged and four R_w values are considered, the mean value is 0.0376. Lowering the R_w to 0.038 would decrease S_w ever so slightly and increase oil in place by about 1%.

Well	Sample Date	TDS (mg/l)	Sp. Gr	TDS (ppm)	R_w at 125°F
Lease A well 1	6/21/1996	97,650	1.065	103,997	0.045
Lease A well 1	8/20/1999	104,815	1.065	111,628	0.042
Lease A well 2	3/22/2001	128,532	1.075	138,172	0.037
Lease B well 1	11/30/2000	143,768	1.09	156,707	0.035
Lease B well 2	11/30/2000	133,721	1.085	145,087	0.035

Table 6.3 Water analysis data from four wells on two leases

6.6.2 Data inputs and upscaling

Lithofacies (code 1-4), porosity, permeability, and water saturation were exported from Petra™ in the digital format LAS2, sampled at 0.5 ft sample rate, for the interval from the top of the Chester sandstone to the top of the Meramec, and imported into Petrel™. Lithofacies and porosity were then upscaled from the half-foot scale to model layer scale (average 2 ft), lithofacies by "most of" and porosity arithmetically. Permeability and Sw were not upscaled because data at well scale was not involved in their calculation in the model.

6.6.3 Lithofacies modeling

The four lithofacies modeled include shale (lithofacies code 1), basal (or shaly) conglomerate (2) limey conglomerate (3), and reservoir sandstone (4). Lithofacies upscaled to layer scale at 25 wells with data were used to develop variograms for stochastic modeling. Variogram type was set as exponential, with the nugget and sill set at 0.0001 and 1, respectively. Variogram curves were fit for each lithofacies in the two parasequences to derive variogram ranges in the major (north-south), minor (east-west), and vertical directions Table 6.4. Major azimuth was set as North-South because of the orientation of the incised valley and the presumed dominant direction of currents.

		Major Range (ft)	Minor Range (ft)	Vertical Range (ft)	Major Azimuth (degrees)	Minor Azimuth (degrees)
Parasequence 2	1 - Shale	4500	1200	6	0	270
	2 - Shaly congl	10000	2000	10	0	270
	3 - Limey congl	13000	2000	10	0	270
	4 - Sandstone	14000	1800	15	0	270
Parasequence 1	1 - Shale	5000	1600	16	0	270
	2 - Shaly congl	14635	1600	10	0	270
	3 - Limey congl	9000	900	10	0	270

	4 - Sandstone	10981	1200	13	0	270
--	---------------	-------	------	----	---	-----

Table 6.4 Variogram range parameters used in modeling lithofacies.

Three realizations of the Sequential Indicator Simulation (SIS) were run using the same variograms but with different initializing seeds to yield three unique, but very similar solutions. SIS is a stochastic process, but because of the ranges of the variograms in the major direction relative to the well control (7X), the layering process, and the apparent lateral continuity of the flow units, the modeling process was somewhat deterministic. Of the three realization, the one chosen for the balance of the modeling was the one with lithofacies volume ratios most similar to the upscaled lithofacies at the wells. Lithofacies at three scales are shown in Fig. 6.9.

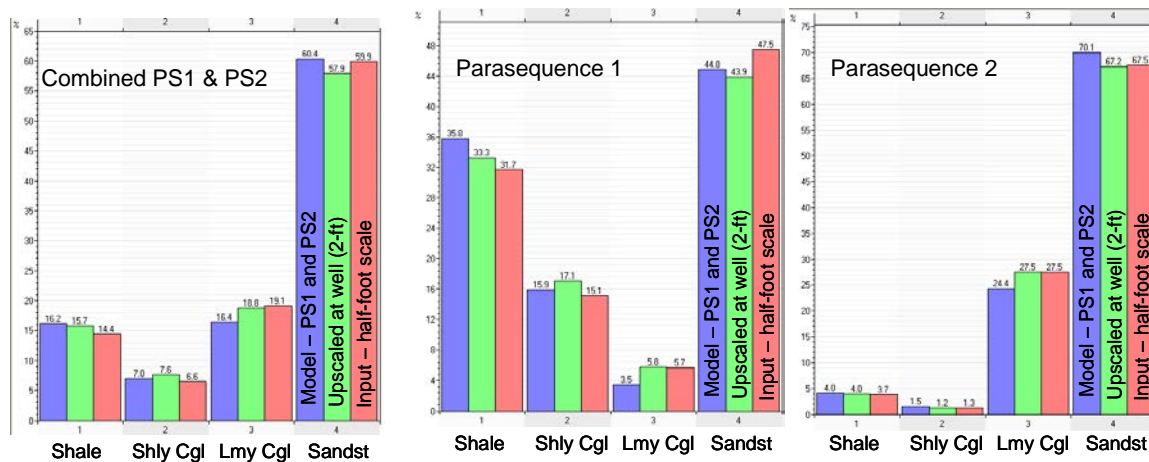


Fig. 6.9 Lithofacies distribution in the model at well (half-foot), upscaled to layer (2 ft average), and in the model.

Lithofacies distribution in the model is illustrated in 2D cross sections in Figure 6.10. Wells with symbols, except the two pseudowells, are the same 23 wells shown in earlier Figures 4.4 and 4.5. Two pseudowells (pink) were added to help fill-out the valley in a critical area and will be discussed later in this report. The area labeled "compartment" comprises an area of the pool where two wells are not in pressure communication with the waterfloods to the north and to the south. Figure 6.11 is a 3D view of the model split approximately the same as in Figure 6.10.

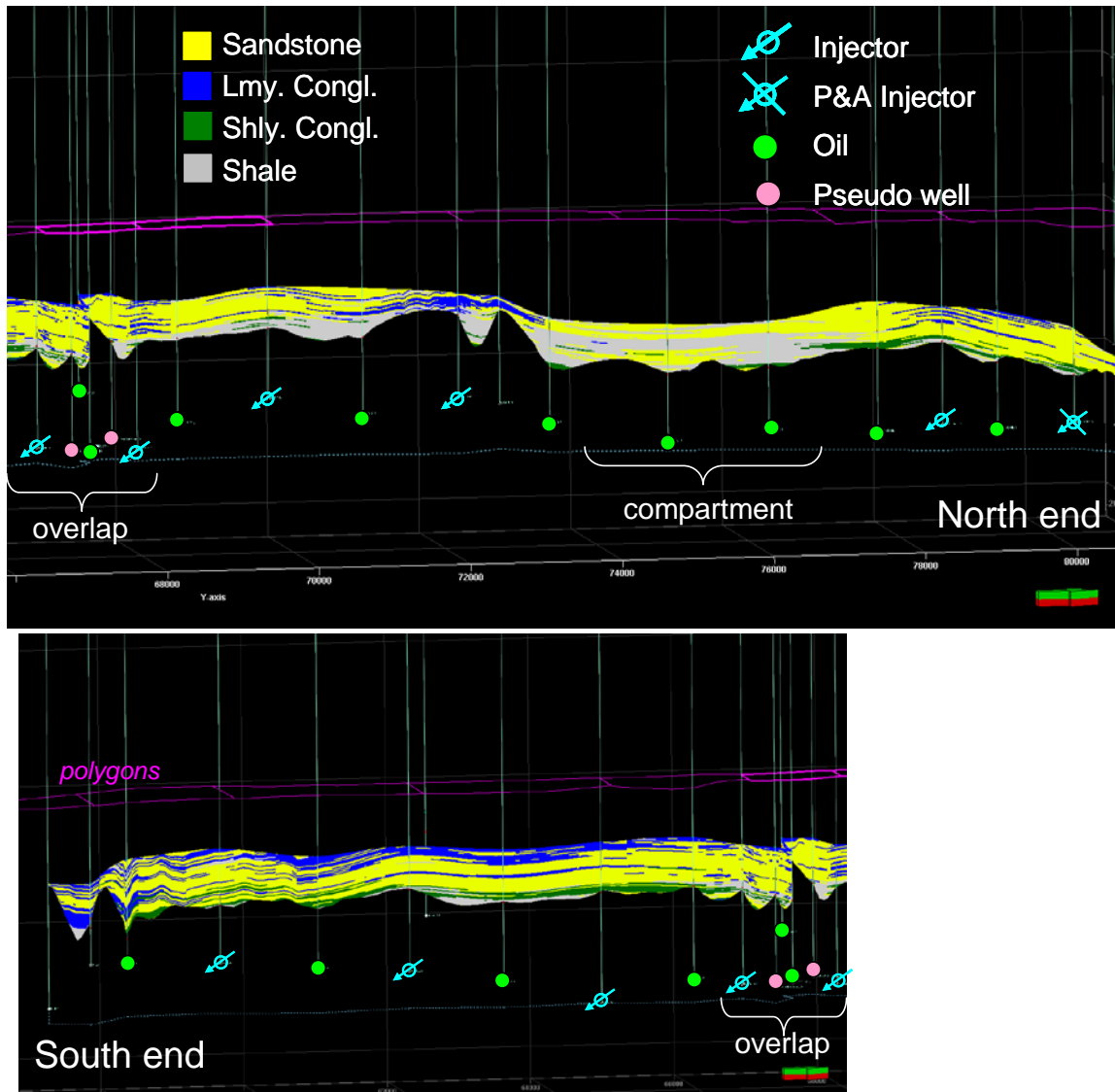


Fig. 6.10 South-North cross-section up the valley showing the Chester valley-fill lithofacies. Upper figure is the upper part of the pool and lower is the lower part. Wells with symbols are the 23 wells in the Pleasant Prairie South waterflood and correspond to the wells in cross-sections in Figures 4.4 and 4.5.

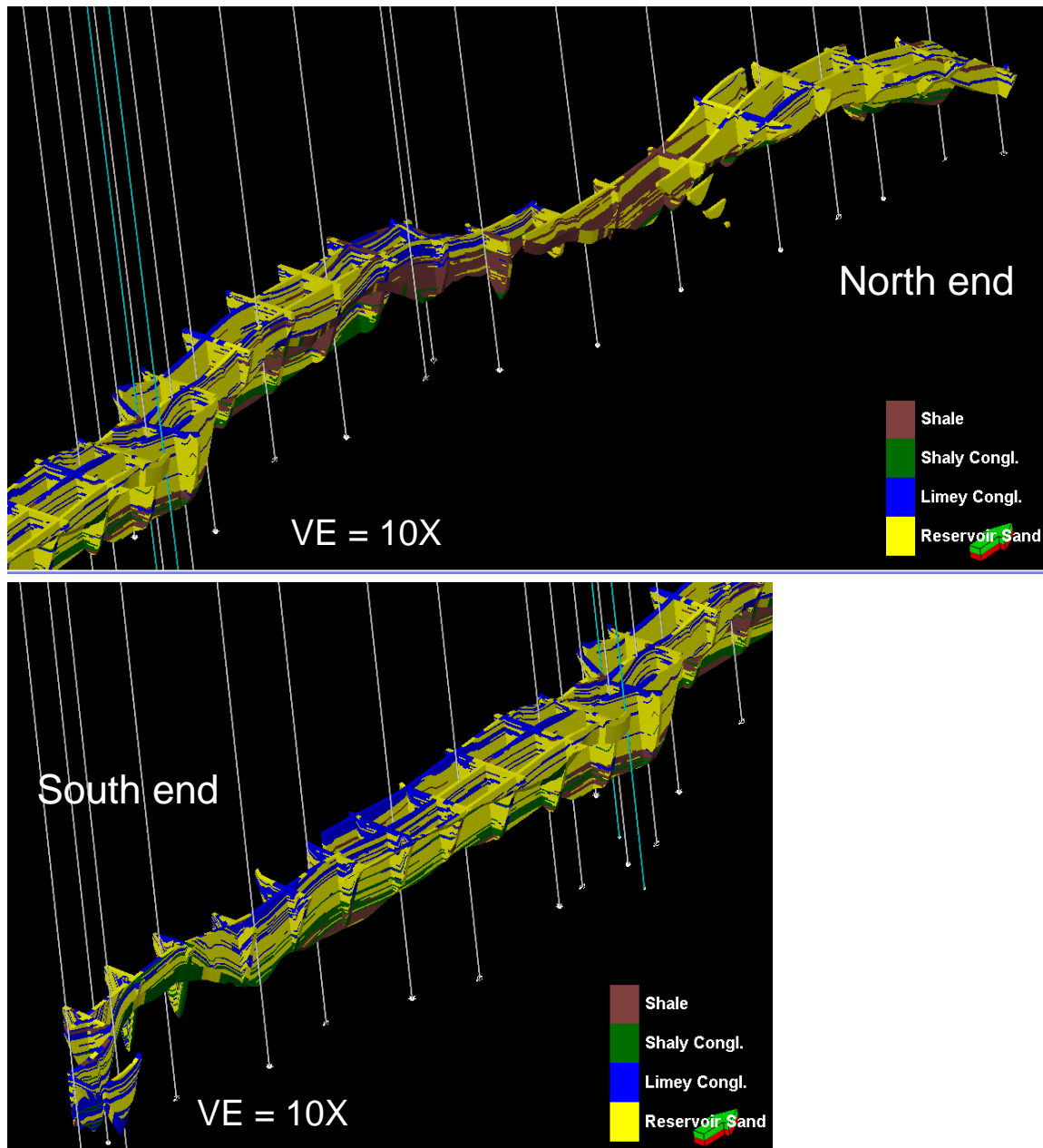


Fig. 6.11 3D view of lithofacies covering approximately the same areas in Fig. 6.10

6.6.4 Porosity and permeability model

Because porosity is linked to lithofacies, porosity was modeled separately for each lithofacies. Data analysis and variograms parameters were established for each of the four lithofacies for

each of the two parasequences. Porosity upscaled to layer scale at 25 wells with data were used to develop variograms for stochastic modeling. Variogram type was set as exponential, with the nugget and sill set at 0.0001 and 1, respectively. Variogram range parameters set by analysis are provided in Table 6.5

		Major Range (ft)	Minor Range (ft)	Vertical Range (ft)	Major Azimuth (degrees)	Minor Azimuth (degrees)
Parasequence 2	1 - Shale	5000	500	20	0	270
	2 - Shaly congl	5800	2500	20	0	270
	3 - Limey congl	8000	500	20	0	270
	4 - Sandstone	4000	500	20	0	270
Parasequence 1	1 - Shale	5500	500	20	0	270
	2 - Shaly congl	5000	1200	20	0	270
	3 - Limey congl	3800	500	20	0	270
	4 - Sandstone	4000	700	20	0	270

Table 6.5 Variogram range parameters used in modeling porosity by lithofacies.

Five realizations using Sequential Gaussian Simulation (SGS) were run using the same variograms but with different initializing seeds to yield five unique, but very similar solutions. As with the lithofacies, each of the solutions were similar, but different enough to have a clear choice as to which porosity model to use. The model was chosen by comparing pore volumes by lithofacies and parasequence, and total pore volume (Fig. 6.12). Realization 5 was most consistently close to the mean of the five realizations and was used.

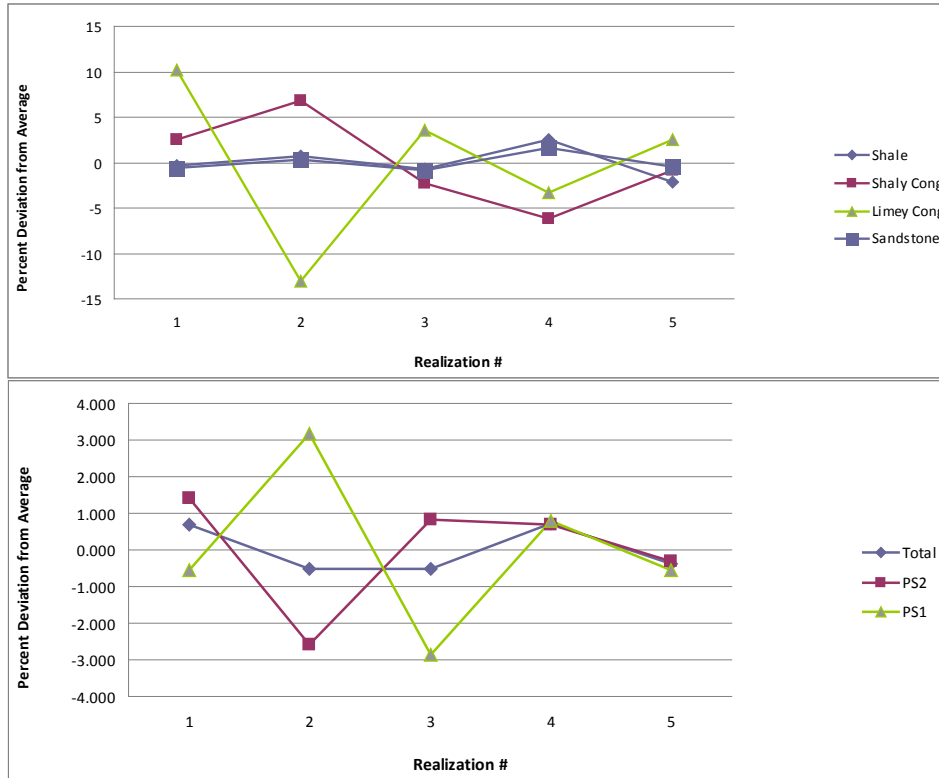


Fig. 6.12 Deviation from average pore volume for five realizations by lithofacies (upper) and by parasequence and total model (lower).

Permeability in the XY directions was then calculated at each cell by lithofacies used these equations:

Sandstone $K(\text{md}) = 0.0047 * \text{PHI}^{3.9365}$

Conglomerate $K(\text{md}) = 0.0033 * \text{PHI}^{2.9396}$

Shale $K(\text{md}) = 0.01$

6.6.5 Water saturation model

The usual method for estimating water saturation (S_w) in reservoir models is by a Leverett J-function which requires measured capillary pressure data (P_c , interfacial tension, contact angle). We do not have these data in the study area but instead have used the PetrelTM plugin tool from the Blueback Reservoir Engineering Toolbox for estimating J-curves based on wireline log S_w and estimated permeability (Figure 6.13). The J-curves were then applied in the model at the cell

scale. Inputs to the plugin are Free Water Level (FWL) = -2245, irreducible water saturation (Swirr) = 0.15, porosity, permeability and Sw at the log scale (half-foot). FWL is estimated to be 10 ft below the oil/water contact (-2235) provided by one of the pool operators. There is no clear oil/water contact in the pool, but a transition in two wells supports -2235. Swirr is a measured SCAL property and is not available in cores in the study area. However, SCAL data from Chester core in the Eubank field eight miles south of the study has an average Swirr for three samples of 0.17, and a low value of 0.12; and a Swirr of 0.15 estimated by a capillary pressure curve for a different sample. Calculation of Sw and permeability by lithofacies was discussed in earlier sections.

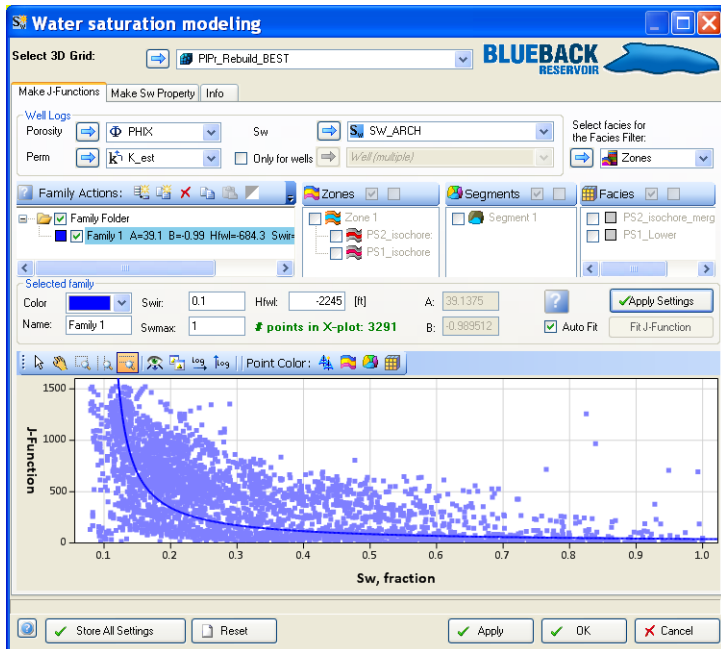


Fig. 6.13 Blueback Reservoir input tab and J-Function scatter plot for the model input data. Swi eventually used was 0.15, not the 0.1 shown.

6.6.6 Property model views and statistics

Figures 6.14 through 6.17 illustrate the fully populated property model.

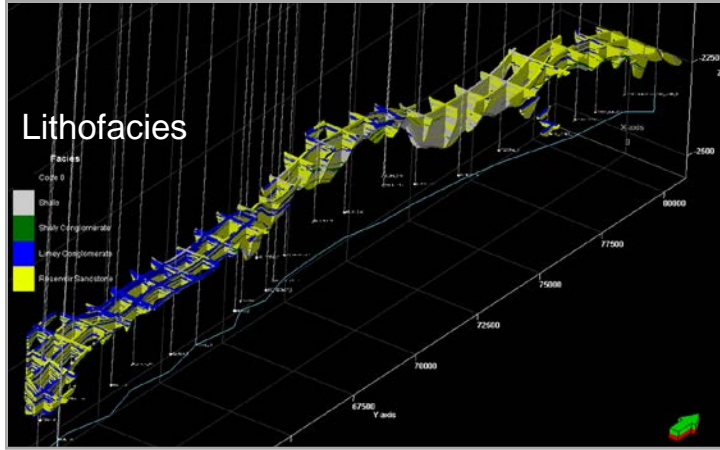


Fig. 6.14 Lithofacies model

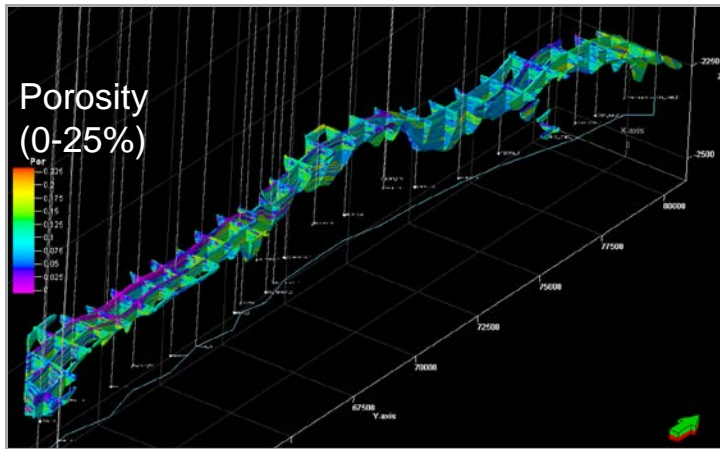


Fig. 6.15 Porosity model

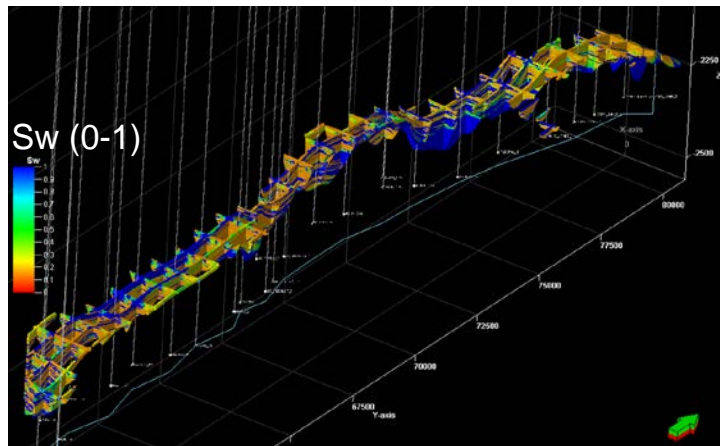


Fig. 6.16 Water saturation model

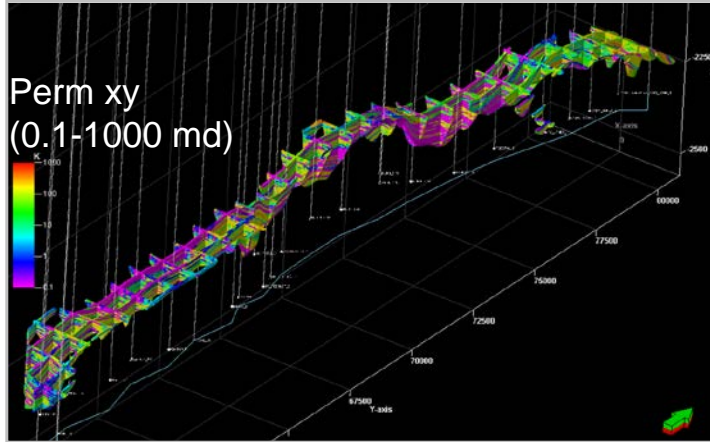


Fig. 6.17 Permeability XY model

Figure 6.18 shows statistical data for lithofacies and porosity properties at varying scales, half-foot log scale (for the raw inputs), those data upscaled to layer scale (average 2 feet), fine-grid model cells before upscaling and fine grid model cells after upscaling to the coarse grid for simulation. Figure 6.19 shows statistics for Sw and permeability, calculated at the cell level in the fine-grid model compared to the distribution in the coarse grid model after upscaling.

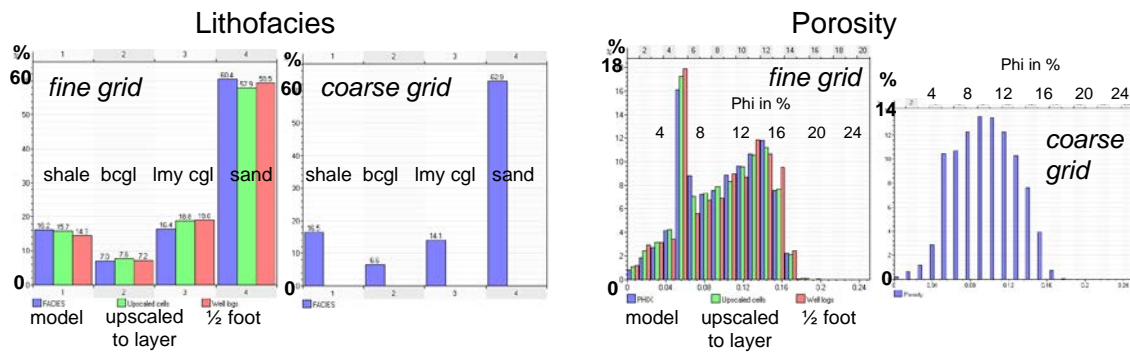


Fig. 6-18 Lithofacies and porosity histograms. For each, the fine-grid statistics are on the left and the upscaled coarse-grid statistics are on the right.

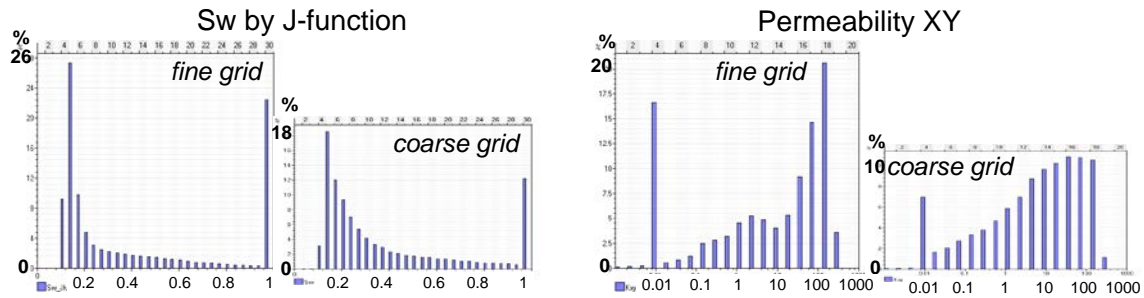


Fig. 6-19 Water saturation and permeability histograms. For each, the fine-grid statistics are on the left and the upscaled coarse-grid statistics are on the right.

6.6.7 Prepare model for dynamic simulation

The fine-grid model property model was upscaled from 700,000 active cells to 65,000 active cells, or in effect, from an average of 2-foot layers to 10-foot layers. Upscaling involves reducing a vertical column of cells within the model interval by averaging over the interval being upscaled, in this case, 5 cells on average. Properties upscaled and their upscaling method is shown in Table 6.6.

Property	Method	Weighting
Lithofacies	Most of	
Porosity	Arithmetic	
Permeability XY	Geometric	
Water Saturation	Arithmetic	Volume (porosity)

Table 6.6 Property upscaling methods by property.

Lithofacies is not required in the simulation model, but it was run to better understand the effect of upscaling. Comparison between the fine and coarse grids is shown in Fig. 6.20. After upscaling the model framework, wells and the four upscaled properties were exported in a rescue format for simulation.

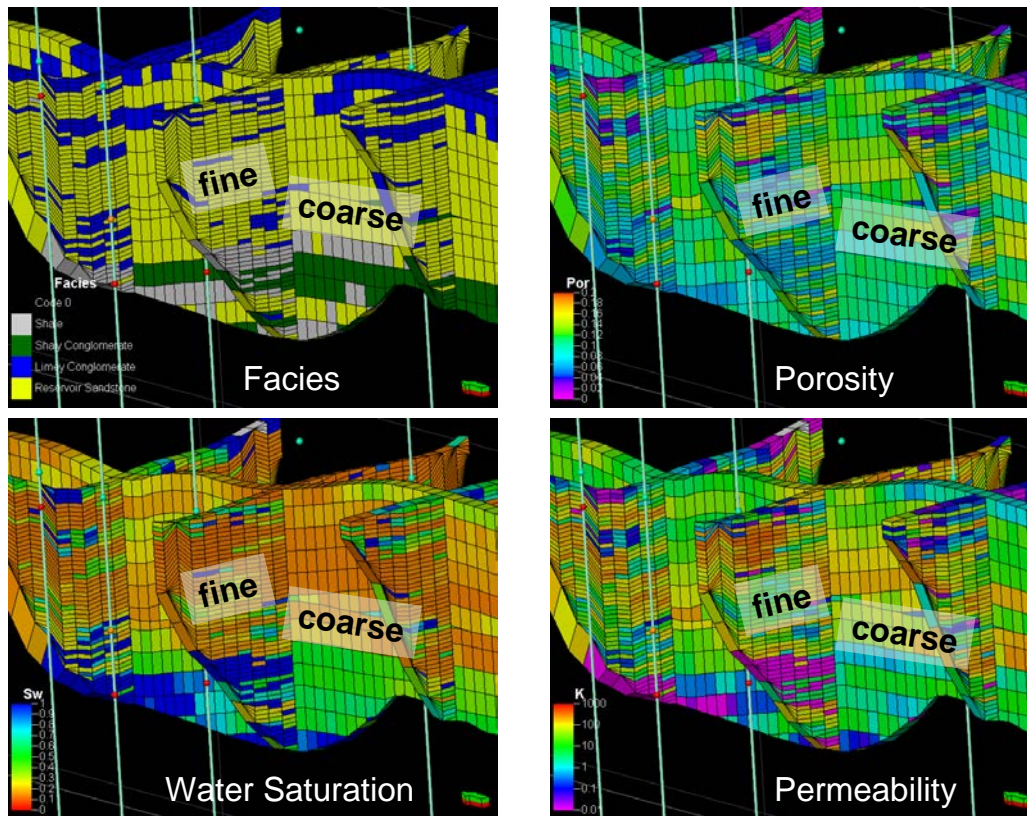


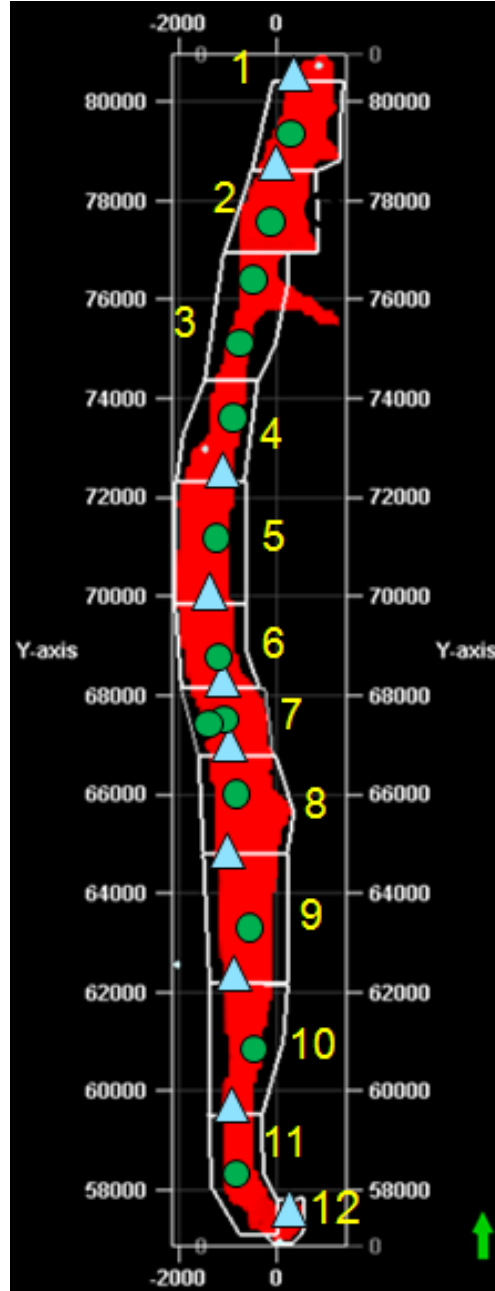
Fig. 6.20 Comparison between fine grid and upscaled coarse gridded properties.

6.7 Discussion: model iterations, modifications and additional work to consider

Two full iterations of static model building were performed, the first with a seismic depth-converted Meramec structure provided by the operator and the second with an interpretation by Hedke (see Section 5). Modeled reservoir volumes were compared with production histories for a first-pass material balance analysis and adjustments made to the model to more closely approximate recovery factors expected for the region and reservoir.

6.7.1 Volumetric comparisons

For volumetric analysis the modeled area was divided into regions by polygons. The east-west polygon boundaries were placed at the injection (Figure 6.21). Five of the current injectors were originally oil wells and four were drilled as injection wells (Fig. 2.1). Production was allocated to each polygon region, with the production for the oil wells converted to injectors being split equally between the adjacent polygons. Polygon 12 contains a well reservoir is not in communication with the rest incised valley. The furthest north injection well plugged and did not contribute significantly to waterflood. Production was then compared to reservoir volumes from the static model (Table



wells

whose
of the
is
the
the
6.7)

Fig. 6.21 Polygons, regions 1-12, and wells in the static model. Red indicated the incised valley. Oil wells are the green dots and water injection wells are the blue triangles.

Parameters

Geomod Build 2

FVF	1.18
Swir	0.15
Phi cut-off	0.06
FWL	-2245

Region	BV [*10 ³ RB]	PV [*10 ³ RB]	HCPV [*10 ³ RB]	STOIP [*10 ³ STB]	Cum Oil [*10 ³ STB]	RF	Poly- gon	Start Date (yr)	PV Multi- plier
Polygon1	14,258	1,529	990	840	202	24.0%	1	2000	0.6
Polygon2	15,742	1,639	1,184	1,004	310	30.8%	2	2000	0.7
Polygon3	11,531	1,132	547	464	36	7.7%	3	2001	0.7
Polygon4	9,396	915	515	437	140	32.0%	4	1996	0.75
Polygon5	24,363	2,757	1,915	1,623	597	36.8%	5	1995	0.8
Polygon6	19,645	2,193	1,640	1,390	512	36.8%	6	1995	0.7
Polygon7	22,854	2,618	1,955	1,656	728	44.0%	7	1992	0.85
Polygon8	29,898	3,732	2,958	2,506	717	28.6%	8	1999	0.8
Polygon9	28,098	3,334	2,603	2,206	755	34.2%	9	2000	0.8
Polygon10	16,751	1,870	1,462	1,239	332	26.8%	10	1999	0.8
Polygon11	15,600	1,849	1,385	1,173	121	10.3%	11	1999	1
Polygon12	1,788	183	122	103	0	0.0%	12	2000	0.8
	209,924	23,751	17,276	14,641	4,449	30.4%			

Geomod Build 1

FVF	1.15
Swir	0.15
Phi cut-off	0.06
FWL	-2250

Region	BV [*10 ³ RB]	PV [*10 ³ RB]	HCPV [*10 ³ RB]	STOIP [*10 ³ STB]	Cum Oil [*10 ³ STB]	RF	Poly- gon	Start Date (yr)	PV Multi- plier
Polygon1	18,661	2,119	1,391	1,159	202	17.4%	1	2000	0.6
Polygon2	13,957	1,475	1,074	895	310	34.6%	2	2000	0.7
Polygon3	17,477	1,713	972	810	36	4.4%	3	2001	0.7
Polygon4	9,244	942	623	519	140	26.9%	4	1996	0.75
Polygon5	19,272	2,148	1,571	1,309	597	45.6%	5	1995	0.8
Polygon6	10,610	1,209	948	790	512	64.8%	6	1995	0.7
Polygon7	6,224	709	554	462	728	157.6%	7	1992	0.85
Polygon8	17,052	2,048	1,644	1,370	717	52.3%	8	1999	0.8
Polygon9	20,226	2,366	1,899	1,583	755	47.7%	9	2000	0.8
Polygon10	19,905	2,346	1,909	1,591	332	20.9%	10	1999	0.8
Polygon11	26,321	2,982	2,204	1,836	121	6.6%	11	1999	1
Polygon12	8,914	893	609	507	0	0.0%	12	2000	0.8
	187,863	20,950	15,398	12,831	4,449	34.7%			

Table 6.7 Summary of volumetric reservoir data, oil production, recovery factor and other variables by polygon region for two static model iterations. Polygons 1-7 are in the northern part of the model and 8-12 in the southern. Abbreviations include BV - bulk volume, RB - reservoir barrels, PV - pore volume, HCPV - hydrocarbon pore volume, STB - stock tank barrels, OIPO - oil in place, Cum Oil - cumulative oil produced through December 2011, and RF - recovery factor.

Geomod Build 1, the first model iteration appeared to have too little reservoir volume in polygons 6 and 7, and possibly too much in polygons 1, 2, 11, and 12, based on the recovery factors (volume of oil produced / volume of oil in the polygon). Volumetric relationships to RF were improved in Geomod Build 2, but the volumes may have been overly "corrected."

6.7.2 Modifications to the static model (Geomod 1 to Geomod 2)

Two major modifications were made in the second model build, adjustments to the valley wall slope and the insertion of two pseudo wells. A second interpretation of the Meramec seismic surface provided a slightly improved volumetric balance, but not judged to be sufficient. The valley edge was adjusted locally, widened with respect to one or the other seismic interpretation, but generally not adjusted outside the bounds of one or the other of the interpretations. Figure 6.22 illustrates an area of the model with the most modification, the area around polygon 7. Valley walls were moderately steepened and widened and two pseudowells were inserted. Pseudowells are stretched or shrunken "copies" of the southernmost well in Figure 6.22. The cross section illustrates the continuity between wells up the valley. Insertion of two pseudo wells helped assure that those portions of the valley would be populated with similar properties.

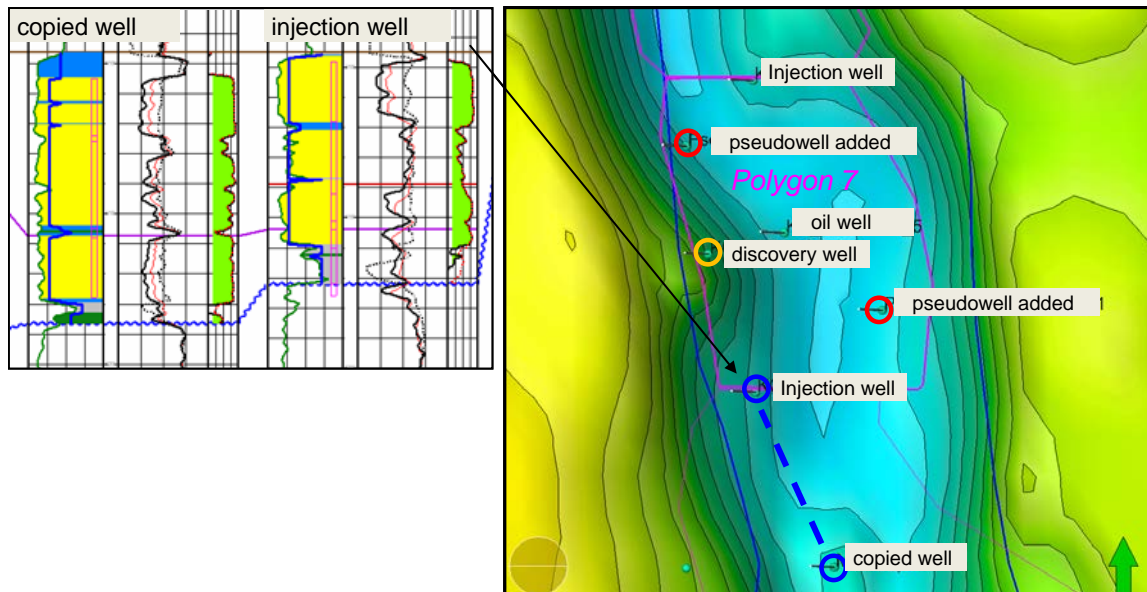


Fig. 6.22 Portion of the valley around polygon 7 and two-well cross section of wireline logs. The contoured surface is the modified Meramec structural surface.

6.7.3 Recovery factor and comparison with similar waterfloods

One method for evaluating a reservoir study is the comparison with the performance of similar reservoirs (e.g.: Shuck and Eubank Fields). Very late in the life of the Shuck field's two waterflood units it was estimated that the average estimated ultimate recovery (primary + secondary) would be 33.6% of OOIP, although one unit was predicted to recovery 31.1% and the other 39.7% of OOIP (Eubank North Unit technical committee report, 2001). The low recovery factor in of one of the units may be explained by relatively thick intervals of bitumen saturation (Sorenson et al., 1999) being included in the OOIP. The Eubank North Unit report estimated that the yet-to-be-installed Eubank North Unit waterflood would recover approximately 41% of OOIP through primary and secondary operations. The flood was initiated in 2004, is currently at 36% of OOIP, and appears to be on track to meet the projections. In the Shuck Field the waterfloods have recovered 55% of the total oil produced whereas in the Etzold North Unit secondary methods are projected to be responsible for 49% of the ultimate recovery. Based on comparisons with analog fields, the projected 30.5% recovery factor for the Pleasant Prairie South pool is 10-34% lower than the two analog fields. If all other factors are assumed to be constant (reservoir properties, field operations, and fluid properties) then the OOIP would need to be reduced by 9-26% to match the recovery factors of the two analog fields.

As discussed above, the geomodel modifications may have "over corrected" and added too much volume. However, it should be pointed out that several regions of the model may have underperformed for reasons other than having too much OOIP. Wells in polygons 1, 2, and 11 are under the influence of only one injector whereas the ideal case with the geometry of the reservoir would be to have injectors on either side. The effect is that up to half the reservoir volume in each of these polygons is not being swept. Polygon 3 is not in pressure communication with the IVF reservoir. Polygon 12 does not have a producer located in the polygon. An injection well in that polygon injected a mere 153 mbw between 2001 and 2006 before it was discontinued, 9% of the average injector, and it is not believed to be very well connected with the incised valley reservoir. When these regions (1, 2, 3, 11, and 12) are removed from the volumetric comparison the recovery factor for the balance of the waterflood increases to 34.2%, more in line with the larger waterfloods in fields to the south.

7. Dynamic model and simulation (Eugene T. Williams)

A numerical simulation model was created for the Pleasant Prairie Chester sandstone to evaluate the potential of this reservoir as a CO₂ sequestration site. The purpose of the simulation model is to demonstrate incremental volume of oil that might be generated with CO₂ injection and to determine the volume of CO₂ that might be sequestered.

The model has been validated as a predictive tool by history matching field performance over the period from initial oil production in September 1990 through December 2011. Secondary recovery waterflood operations were initiated in the southern region (Pleasant Prairie unit) in September 2001 and in the northern portion of the field in December 2002. This section describes the simulation model, the history matching process and results, and the prediction calculations.

7.1 Simulation modeling workflow

Numerical simulation modeling is carried out utilizing the Computer Modeling Group simulation tools IMEX (black oil) and GEM (compositional). The model input parameters are nearly identical except that the black oil model utilizes standard oil and gas PVT values, whereas the compositional models uses composition and an equation of state.

During the historical period of the field, the Pleasant Prairie Chester Reservoir was depleted by primary and waterflood methods. Both of these processes are adequately modeled using black oil simulations. For the CO₂ depletion and sequestration predictions, a compositional (or EOS) model method is required.

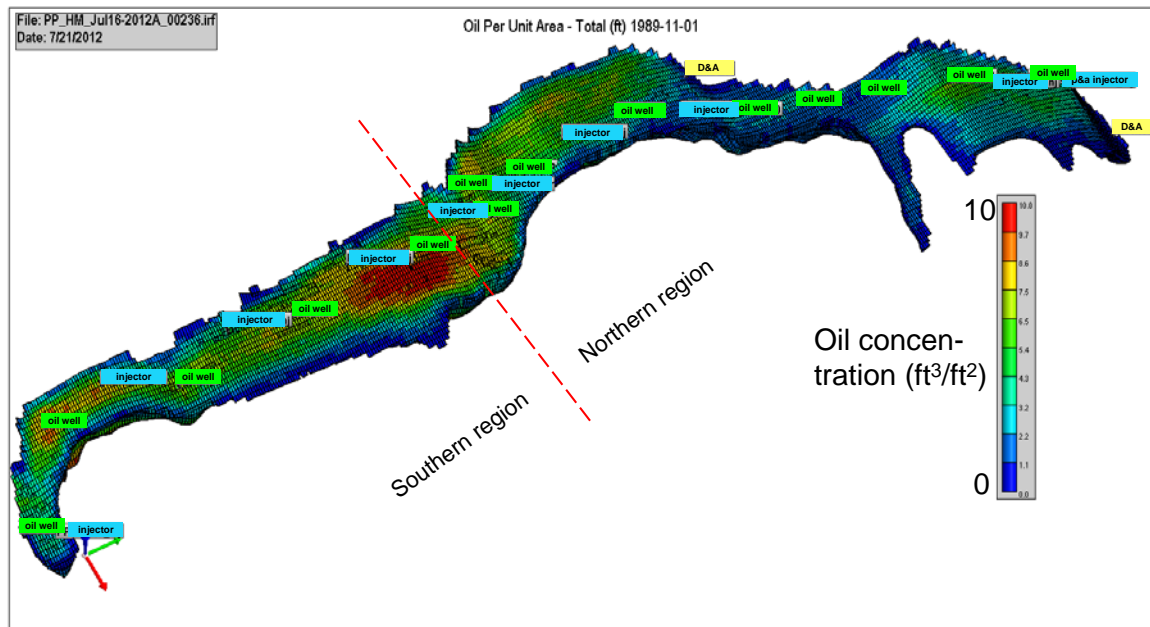
In these studies, the reservoir is modeled and history matched using the black-oil simulator. Once an acceptable match was achieved, the relevant modeling modifications were applied with an equation of state in place of the PVT properties. The EOS model yielded a very similar match as the Black Oil model through primary and secondary production and therefore the EOS model was considered suitable for the status quo (NFA - no further action) and CO₂ injection projections.

7.2 Model input data

The static model was created in Petrel as described in report Section 6, and then exported in RESCUE format. The RESCUE file was imported into CMG software program BUILDER. The parameters imported were:

- Simulation grid: corner point geometry
 - 81×451×25 – total cells 913,275
 - Each cell is 55 ft by 55 ft aerially and variable in thickness (from 0-10 ft)
- Cell porosity
- Cell permeability
- Null (Inactive) cells
- Initial water saturation
- Well trajectory

After the import of the static model, additional factors were applied to inactivate cells that were not relevant to the modeling. Cells with pore volumes of less than 100 ft³, or with porosity less than 6% were inactivated. After these modifications, the total number of active cells in the dynamic model was 64,670. The dynamic simulation model is illustrated in Figure 7.1.



Figure

7.1 – Pleasant Prairie dynamic model oil concentration (ft³/ft²).

Other simulation grid values assigned to the dynamic model are

- Rock compressibility $5.0E-6 \text{ psi}^{-1}$ at 1850 psi.

The oil PVT was derived using an equation of state (EOS) software program, CMG's WINPROP. The EOS was derived using PVT reports from the following wells (field name highlighted):

- **Eubanks:** Owens A-2
- **Eubanks South:** ML Clawson #3-34
- **Pleasant Prairie:** Mary Jones #1
- **Wellington:** Dead Oil Tank Sample for CO2 swelling tests
- **Shuck:** Fincham A-3

Both black oil PVT and EOS were exported from WINPROP for application in the Pleasant Prairie simulation model. PVT values for gas oil ratio, formation volume factor and viscosity are illustrated in Figures 7.2 and 7.3. For simulation modeling the oil at initial conditions, in the reservoir was assumed to be slightly under-saturated and a bubble point pressure of 1300 psi was selected.

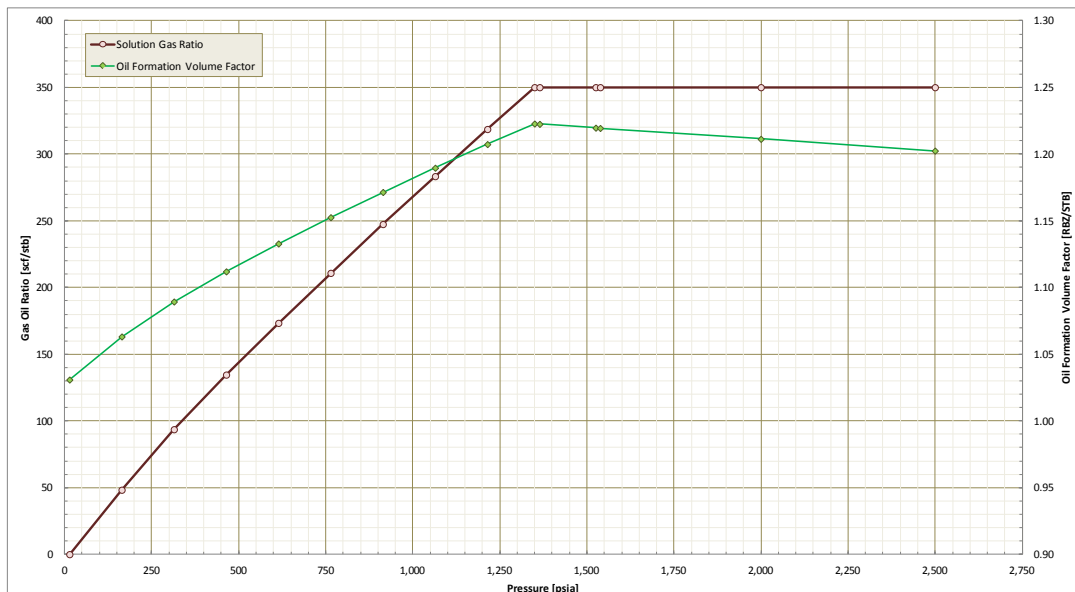


Figure 7.2 Oil PVT (R_s and B_o). Solution gas ratio (left axis) in red. Oil FVF on right axis (green).

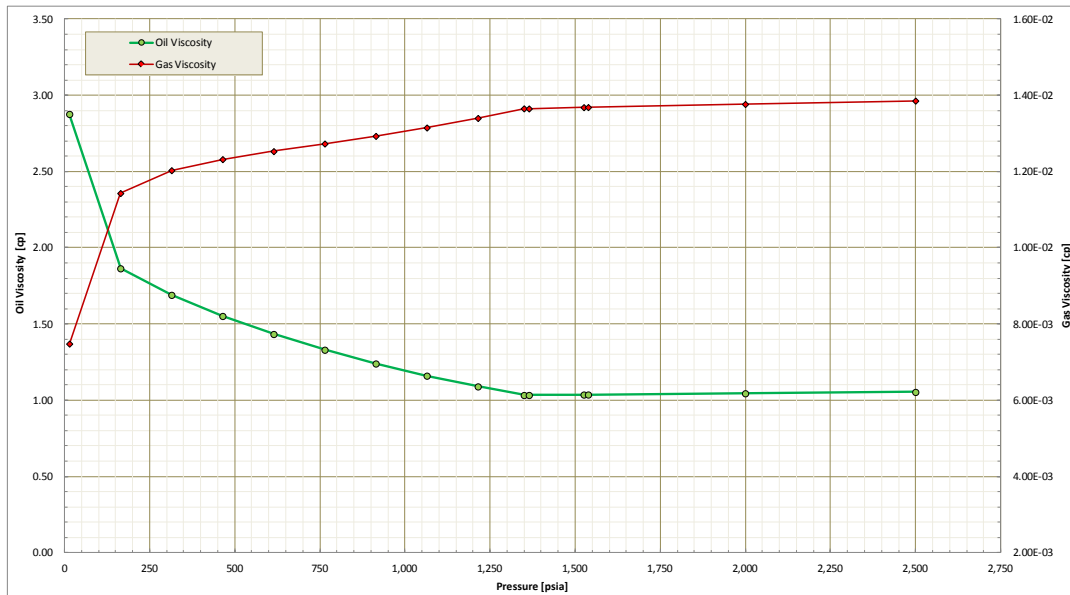


Figure 7.3 Viscosity: Oil viscosity scale on left in cp (green line). Gas viscosity on right (cp) is red line.

SCAL was not available for the Pleasant Prairie reservoir but typical values for similar clastic reservoirs were applied. For the reference case a residual oil saturation of 25%, a connate water saturation of 15%, and a K_{rw} at residual oil of 0.5 were assumed. These values were compared to published values for the Eubank waterflood report and the Shuck waterflood report. Note that these endpoints are history matching variables and the values assumed were selected to ensure that they would serve as limiting values.

The simulation model was initialized assuming capillary equilibrium. That is, a capillary pressure curve was estimated as illustrated in Figure 7.4 to encompass the initial water saturations as imported from the static model. This capillary pressure function was applied to an original Free Water Level (FWL) of 2245 ft subsea. Original oil water contact in the pool was estimated at 2235 subsea by the operator of the northern portion of the field. The simulation model calculates an initial cell pressure based on height above the contact and density differences between the oil and water. With this pressure the model, as set up, internally calculates a capillary pressure shift to match the input water saturation and ensure that the model is initially in equilibrium.

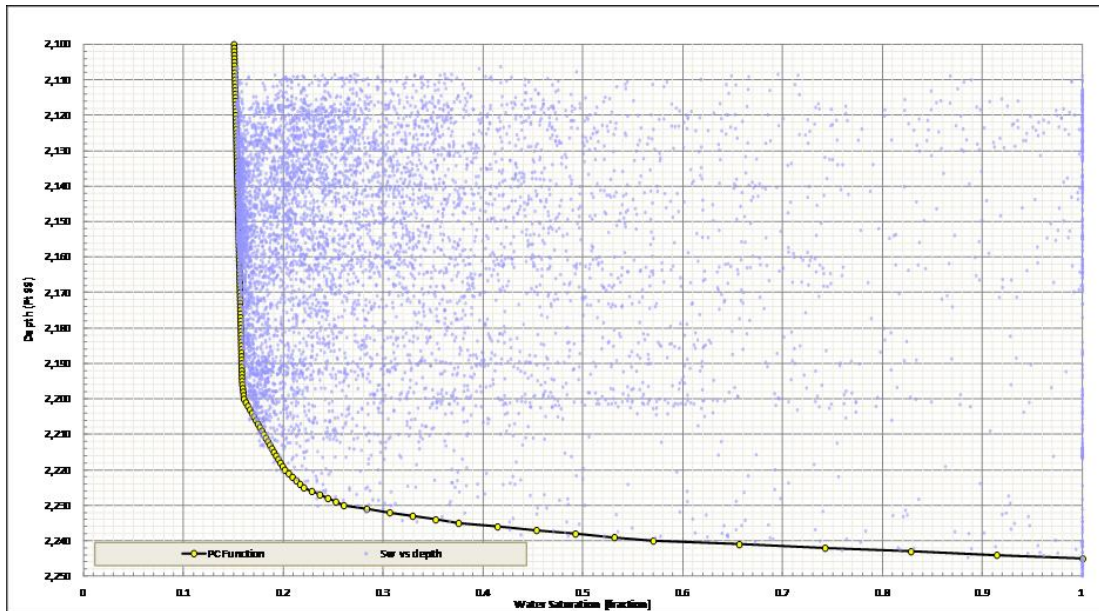


Figure 7.4 Limiting capillary pressure function (yellow). Subsea datum (ft) on left. Blue dots are individual data points for Sw 0-1 (left-right) on x-axis.

In order to account for variability in the reservoir, the model was segmented into 13 working polygons. These polygons were selected for the static model based on injection well locations and are not represented as having any specific unique reservoir characteristic. The polygon regions are illustrated in Figure 7.5. Polygon 13 has no wells. The pool is separated into two regions on the basis of field operations, South and North. The South region is unitized (Pleasant Prairie Unit (PPU)) and has 4 oil producers, 4 water injectors and shares a water injector with the North Region. The North region has 9 oil producers, 4 injectors and one shared injector.

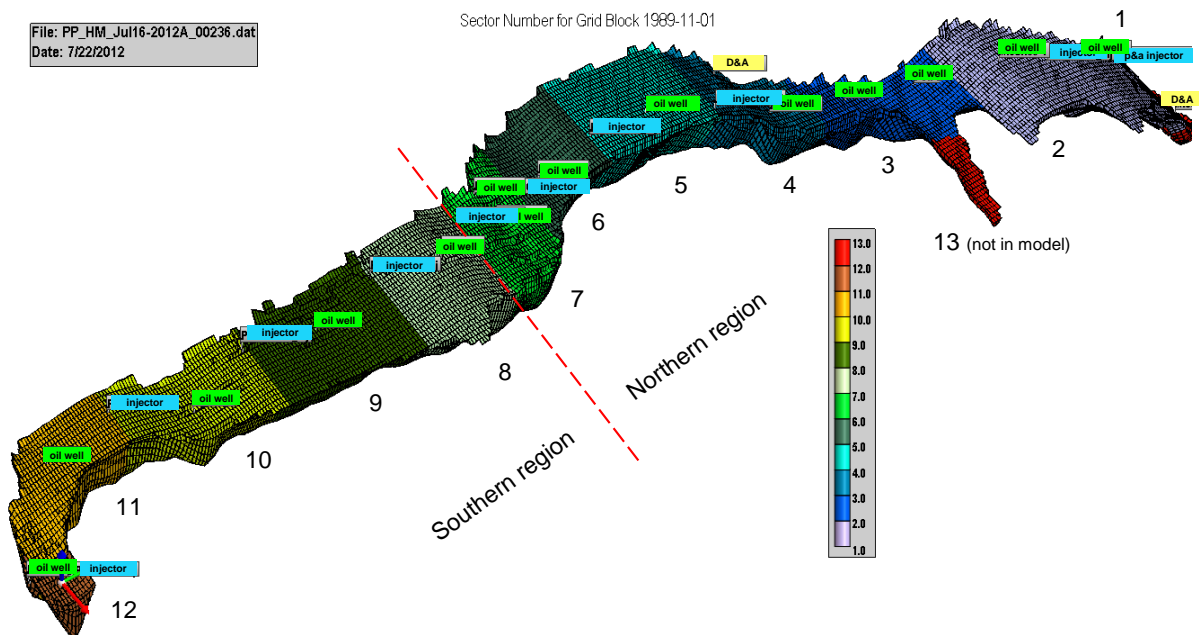


Figure 7.5 Sector numbers. Oil wells are labeled in green and water injectors in blue. Dry holes are yellow.

The model was initialized and initial pore volume (PV) and hydrocarbon PV (HCPV) calculated. The calculated volumes were compared to the volumes calculated in the static model. A volume modifier was applied to each polygon to ensure that the starting HCPV and stock tank barrels initially in place (STOIP) were identical in the dynamic model as they were in the static model. The STOIP and volume modifiers in the static model and dynamic model are presented in Table 7.1. The multiplier shown in this table is applied to each region in the dynamic model to ensure that the starting volumes are identical to the static model volumes.

	Entire Field	Sector 01	Sector 02	Sector 03	Sector 04	Sector 05	Sector 06	Sector 07	Sector 08	Sector 09	Sector 10	Sector 11	Sector 12
Total Pore Volume.	M rbbl	1,630	1,828	1,331	1,206	3,384	2,444	2,717	3,880	3,517	2,010	1,955	226
HC. Pore Volume	M rbbl	1,008	1,244	558	540	1,981	1,668	1,969	3,000	2,658	1,521	1,411	132
Fluids in Place													
Petrel Stock Tank Oil	M STB	840	1,004	464	437	1,623	1,390	1,656	2,506	2,206	1,239	1,173	103
IMEX Stock Tank Oil	M STB	829	1,023	459	444	1,629	1,372	1,619	2,467	2,186	1,251	1,160	109
Multiplier	%	101.28%	98.10%	101.04%	98.34%	99.63%	101.34%	102.29%	101.60%	100.91%	99.03%	101.09%	94.53%
Mobile STO	M STB	531	673	274	264	1,023	907	1,080	1,673	1,470	840	769	68
Total Gas	MM SCF	281	346	155	150	551	464	548	835	740	423	393	37
Free Gas	MM SCF												
Water	M STB	613	575	762	657	1,383	765	738	868	846	481	536	92
Reservoir Oil	M rbbl	1,008	1,244	558	540	1,981	1,668	1,969	3,000	2,658	1,521	1,411	132
Reservoir Gas	M rbbl												
Reservoir Water	M rbbl	622	584	773	666	1,403	776	749	881	858	488	543	93

Table 7.1 Comparison of Static and Dynamic Model STOPIP

The perforation history of each well is matched to the static model trajectories to determine when and which layers in the model will be open to flow for each well.

Production data was available by month for each producing and injection well from the first production date, September 1990, through December 2011. However, wells in the Pleasant Prairie Unit (PPU) had production and injection allocated by well only to May 2009. After that period only total PPU oil values were available by month. For the period May 2009 to December 2011, it was assumed that total liquid production and total water injection remained constant at the April 2009 rates. The production history for the Pleasant Prairie unit is illustrated in Figure 7.6. It is apparent from this figure that liquid production had been relatively constant from 2006 to the end of allocated production in May 2009.

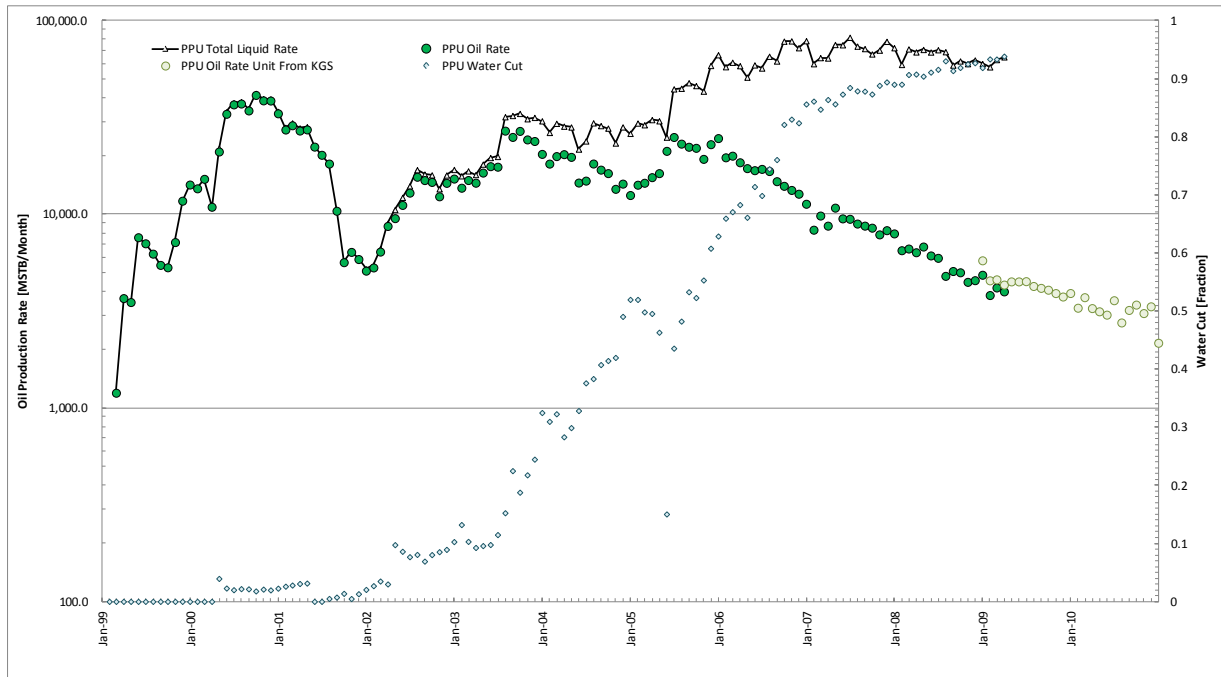


Figure 7.6 South region (Pleasant Prairie Unit) production history. Black line - total fluids, green and yellow - monthly oil production, blue dots - water/total fluid ratio. Green dots are operator data and yellow are combined operator and Kansas Geological Survey database.

Figure 7.7 illustrates the injection history for the field. For the Pleasant Prairie Unit (PPU) water injection had been relatively constant from 2006 to the end of allocated injection history in May 2009. The assumed value for water injection is shown in this figure.

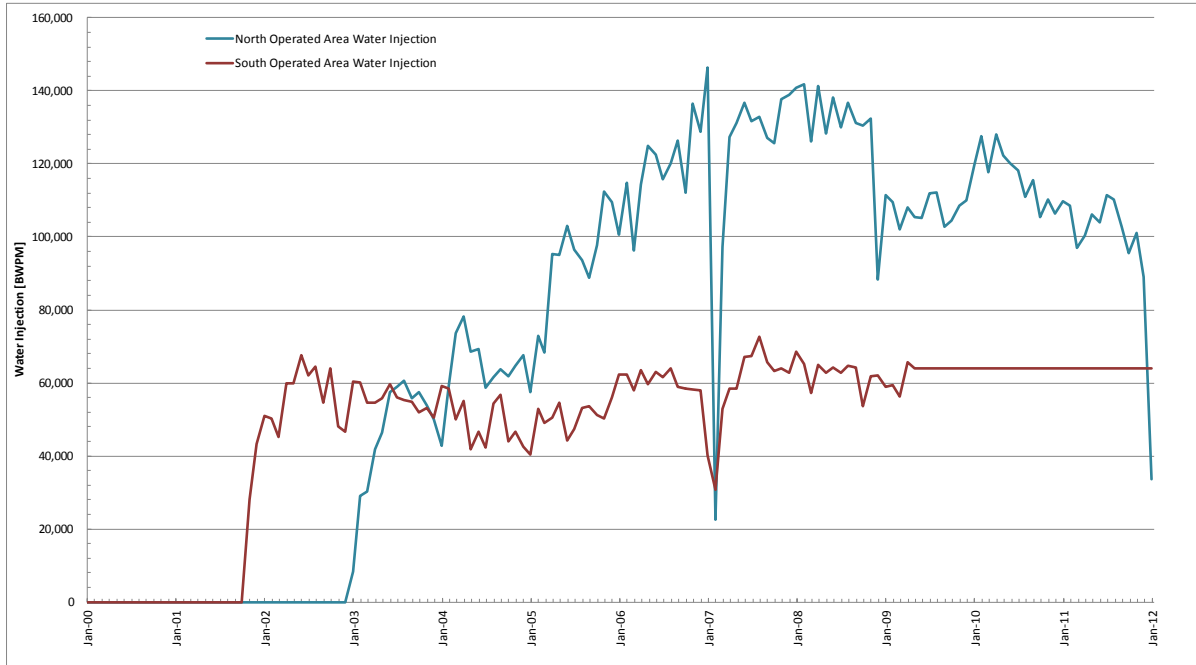


Figure 7.7 Pleasant Prairie water injection history. Blue is northern region and red is southern region.

For producing wells during the historical period, total liquid production rate (stock tank oil plus stock tank water) was applied to each well as the principal constraint. A minimum bottomhole pressure of 25 psi was applied as an additional constraint on each producing well.

For injection wells during the historical period, water injection rate was applied to each well as the principal constraint. A maximum bottom hole pressure of 2600 psi, the maximum injection pressure reported by the operator of the northern region, was applied as an additional constraint on each injection well.

Production control for the PPU over the period without allocated production -- May 2009 to December 2011 -- used as a group rate control, total liquid. The model allocates production and injection to individual wells based on well production and injection indices.

For the historical period, the actual flowing bottom hole pressure and well productivity index (PI or II) were not matched. Instead, in order to ensure that the reported fluids would be produced or injected, each well productivity index (PI) or injectivity index (II) was multiplied by 10.0. This

assumption is used with automatic history matching to ensure that an comparable material balance can be calculated for each realization.

7.3 Black oil history match

History matching was carried out using the CMG automatic history matching software program CMOST. Uncertain history matching parameters include:

- Pore volume multipliers by sector
- Global horizontal permeability multiplier
- Horizontal transmissibility modifiers by sector
- Residual Oil saturation modifier by region
- Critical Water Saturation modifier by region
- Relative permeability function (Corey, VE, stratified) by sector
- Water relative permeability
- Vertical Perm modifier
- Anisotropy (I-direction transmissibility relative to J-direction transmissibility)

In the dynamic model J-direction is in the direction of the channel, I-direction is orthogonal to the channel.

Parameter	Potential Values or Ranges
Relative Permeability: Independent for 13 Polygons	Rock type 1, 2, 3, or 4
Pore Volume Modifier: Independent for 13 Polygons	0.6 to 1.2
Residual Oil Saturation: 4 Independent Regions	0.25, 0.30, 0.35, 0.40
Critical Water Saturation: 4 Independent Regions	0.15, 0.2, 0.25, 0.3, 0.35
Permeability Multiplier: Global	0.1 to 100
Transmissibility Modifier: Independent for 13 Polygons	0.1 to 10.0
Water Relative Permeability at SOR	0.25, 0.35, 0.50
Vertical Perm to Horizontal Perm ratio: Global	0.001, 0.01, 0.10
Areal Heterogeneity (K_x/K_y): Global	0.1, 1.0, 10.0

Table 7.2 History matching uncertainty.

The objective functions for the history matching included total field production (monthly liquid and oil rates), north end and south end production (monthly liquid and oil rates), and individual well oil rates for all wells that had cumulative oil production greater than 75,000 bbls. There were also a few wells that had pressure data which was included as individual well objectives.

The history matching process involved several thousand simulation runs and used both CMOST DECE and Latin Hypercube with proxy approximation objective methods. During the process, response surface modeling using the software program JMP was applied to evaluate the significance of the uncertainty parameters and to accelerate the history matching process. The results of the history match, comparing the simulation model calculated values to historical measurements are illustrated in the following figures:

Figure 7.8: Liquid match

Figure 7.9: Oil match

Figure 7.10: Water production and water cut match

Figure 7.11: Water Injection match

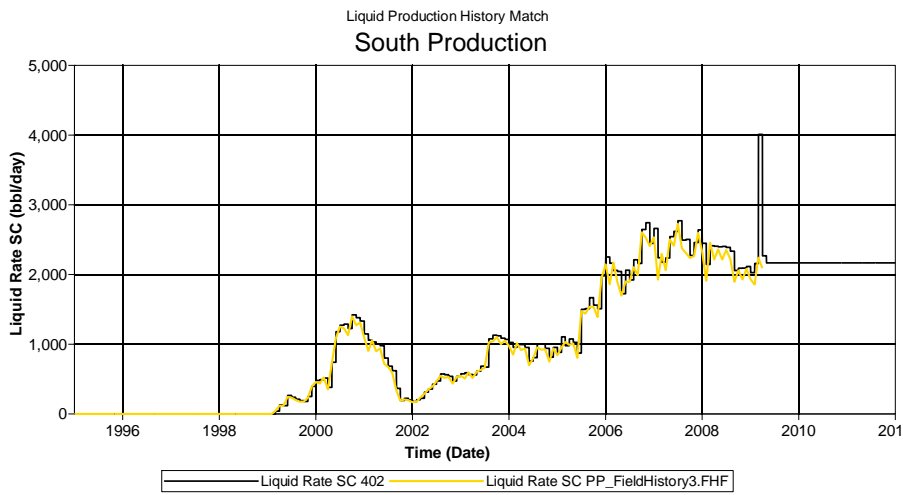
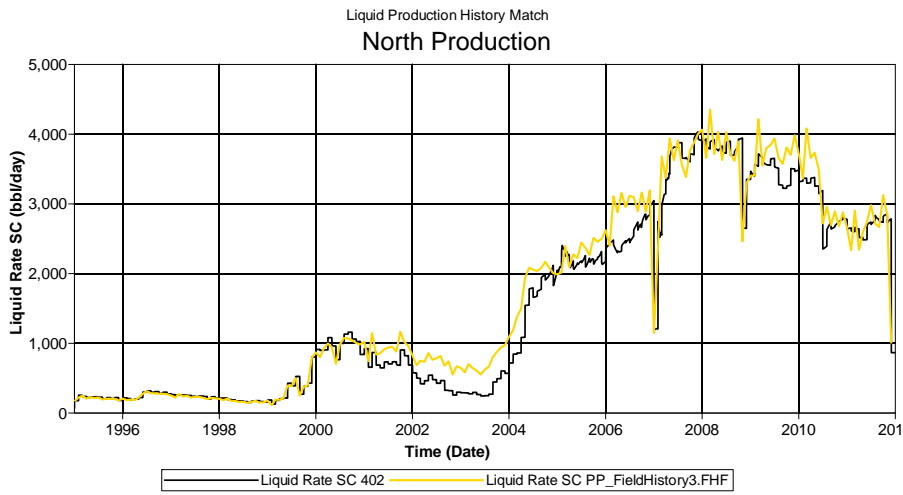
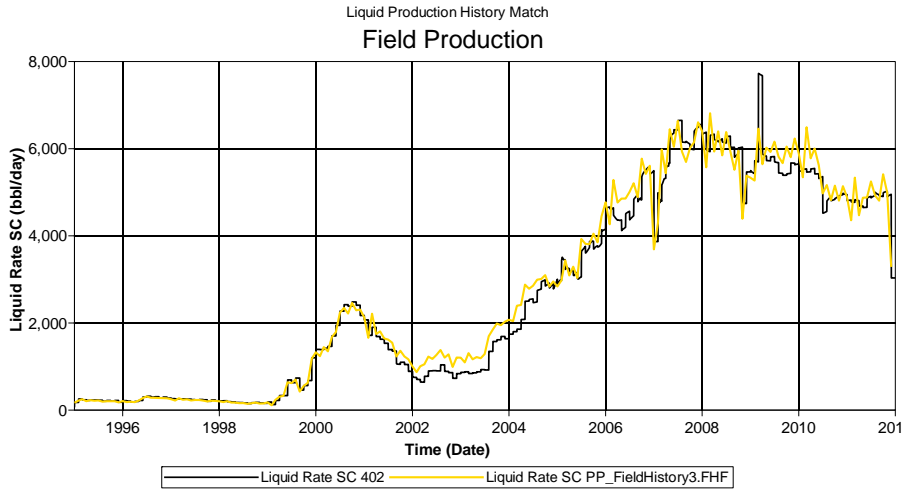


Figure 7.8 History matched total liquids produced. Model fluids are black lines. Yellow lines represent actual fluids reported. Liquid rate is used as well control so expect an exact match. South operated unit is assumed to continue after May 2009 at then current rate of total liquid production

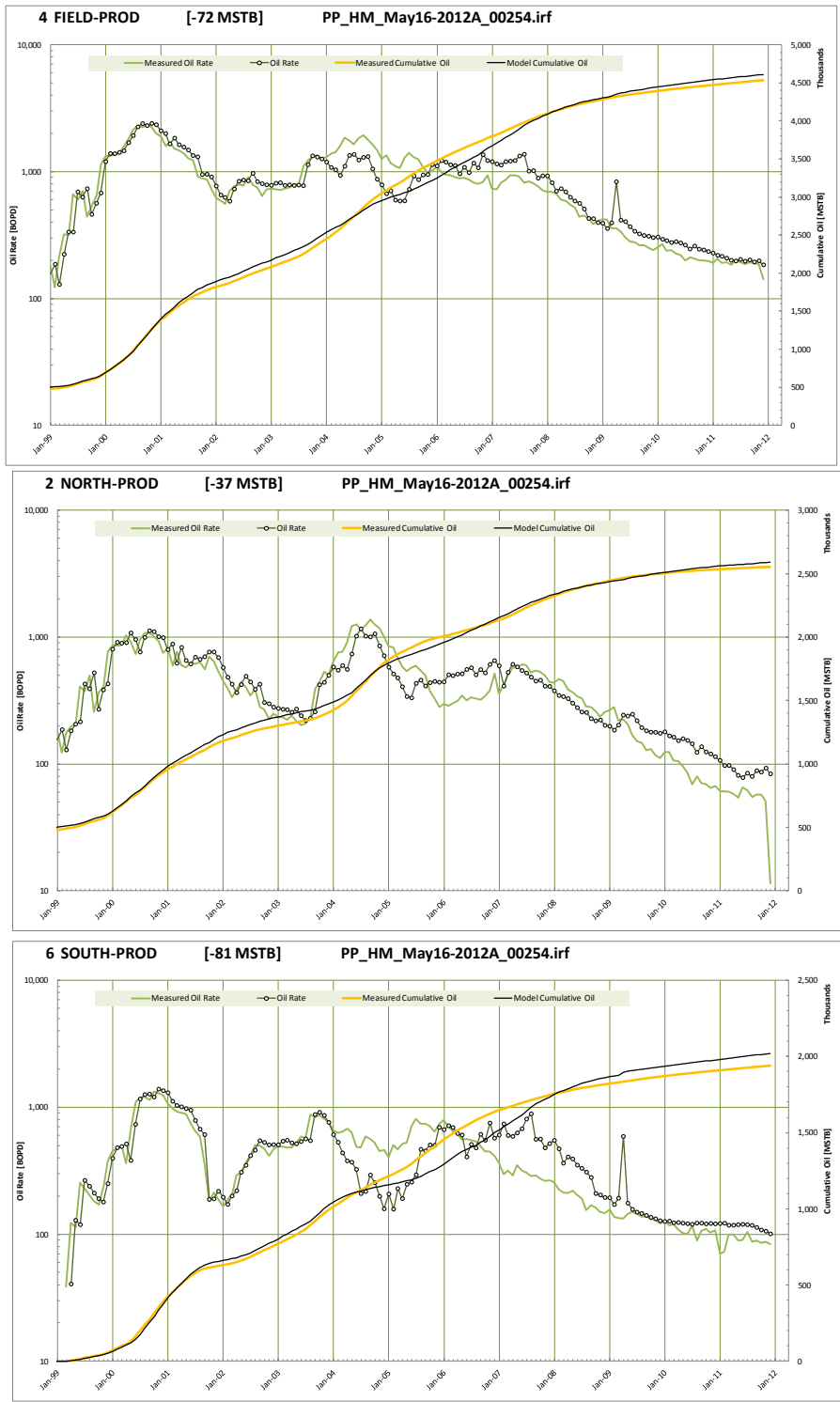


Figure 7.9 Oil production match. Rate in barrels/day are on the left axis and cumulative oil in stock tank MBO are on the right axis. Model rates are in black and actual rates are colored lines.

Overall match of oil production by group is relatively good. Difficulty matching period of water breakthrough in 2005.

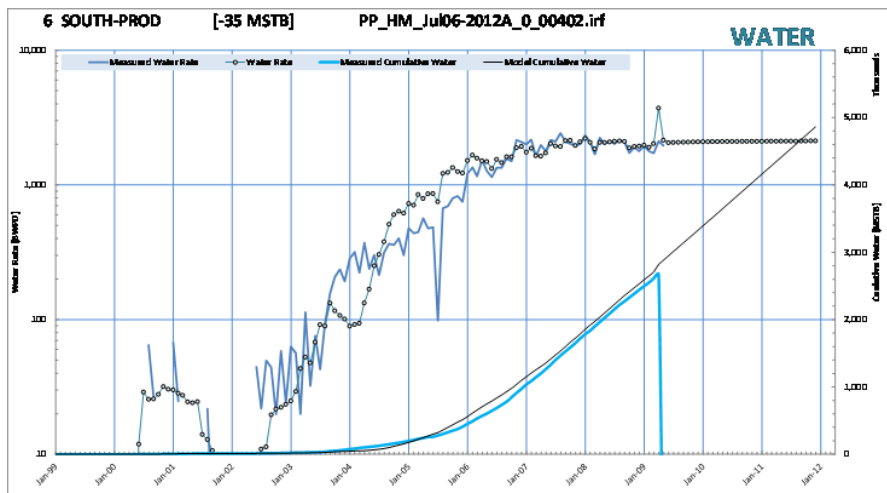
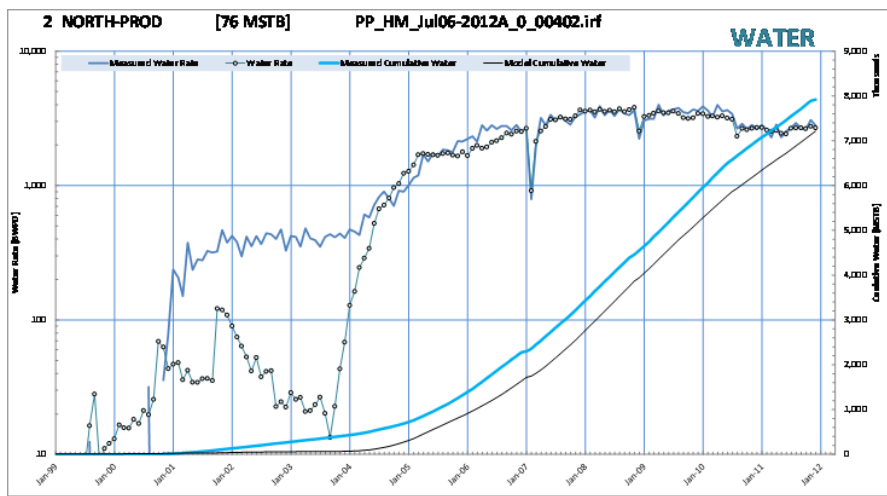
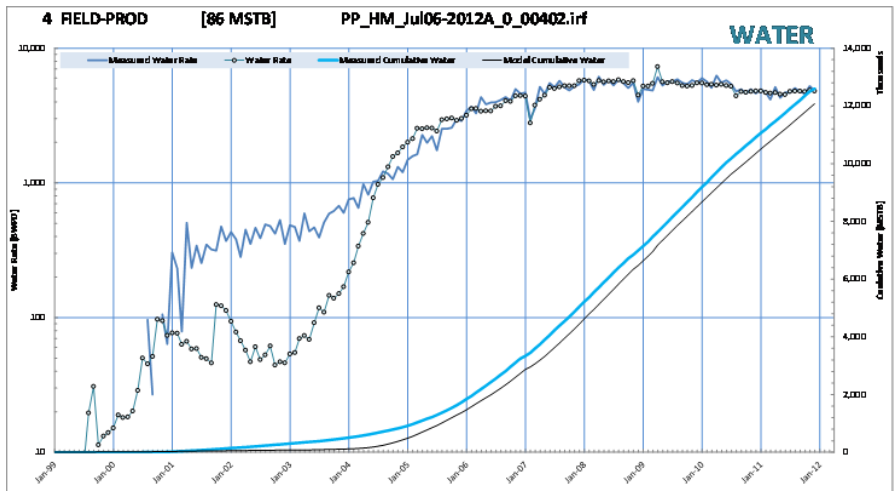


Figure 7.10 Water production match. Rate in barrels/day are on the left axis and cumulative water in MBW are on the right axis. Model rates are in black and actual rates are colored lines. Water match is relatively good with respect to timing and magnitude.

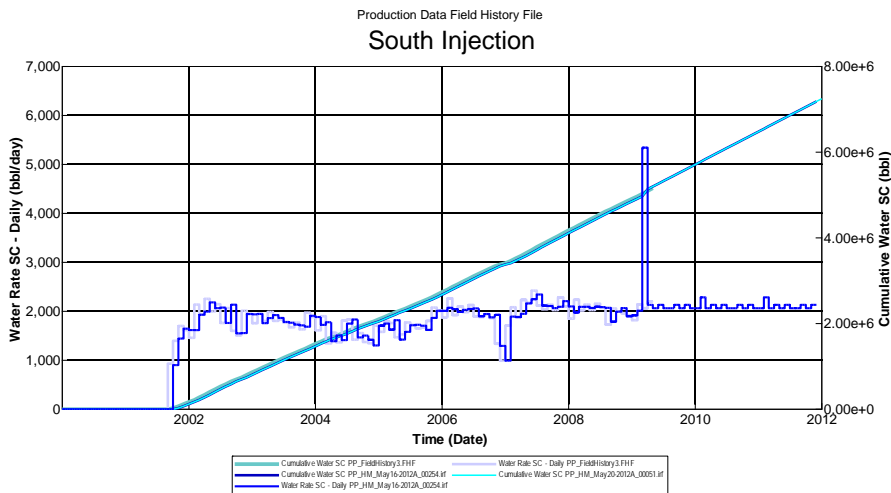
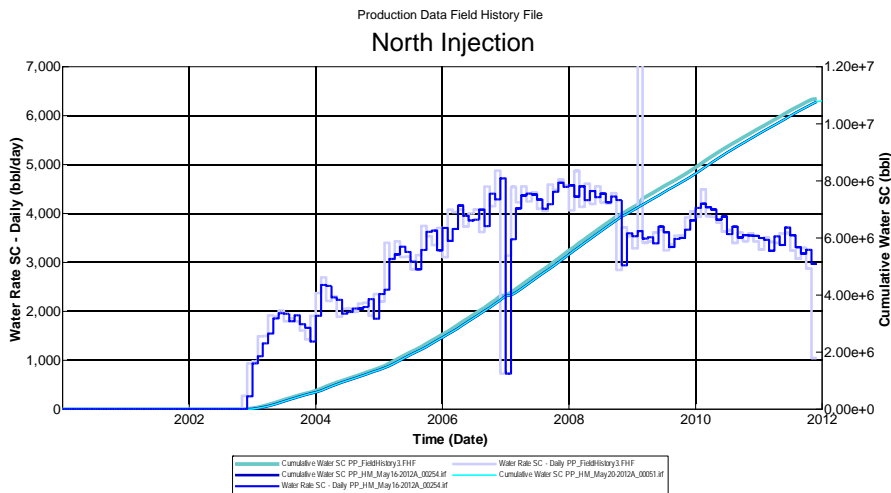
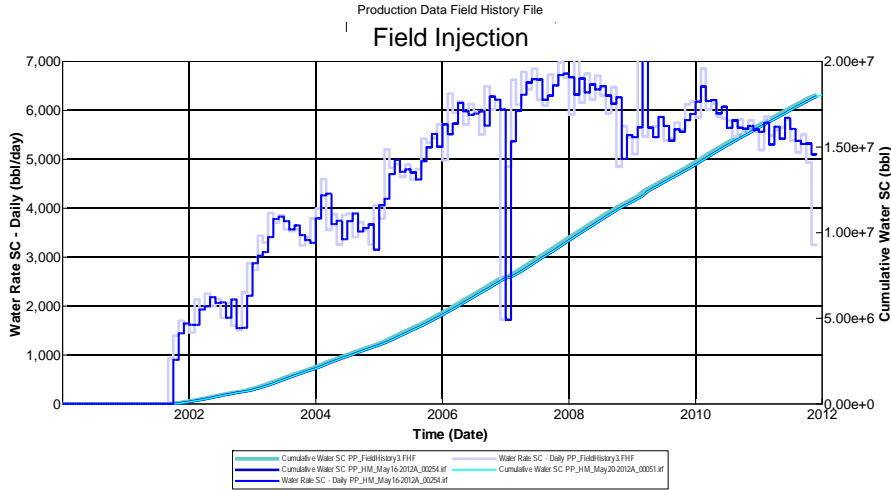


Figure 7.11 Water injection match. Rate in barrels/day are on the left axis and cumulative water injected in bbl are on the right axis. Model rates are in black and actual rates are colored lines.

Water injection rate is specified but there is a maximum BHP limitation that causes some wells to not meet objective. South Operated unit wells are assumed to continue injection rates after may 2009 at then current rates.

Total liquid match in each case should be nearly perfect in all cases as liquid rate was the primary well control. The oil production and water production are very reasonable

Considering that well control was based on total liquid, allowing the model to allocate between oil and water production, the history match realized validates that the simulation model will provide representative forecasts for analyzing alternate development programs.

Certain conclusions can be derived from the history matching process.

- A global multiplier on permeability was necessary to allow production and injection of the historical values. The global multiplier that was derived from history matching was 10x. It is likely that it is only the low permeability cells that benefit from the permeability multiplier. In order to keep permeabilities in a reasonable range, a maximum permeability for any cell is restricted to 3.2 Darcy.
- Modifications to the volumes of mobile oil available for production was necessary, although there is not a unique method for reducing mobile oil volume in the model. That is the mobile oil can be effected in models using several methods:
 1. **Pore Volume Modifiers:** these affect the STOIP adjustments affect assumptions about porosity, NTG, or connected reservoir volume. The volume modifiers that determined in history matching are illustrated in Figure 7.12. The overall volume-weighted pore volume multiplier for the model is 0.79.
 2. **Transmissibility Modifiers:** These affect the areal conformance and can cause oil in cells not on direct flow paths to be bypassed.
 3. **Relative permeability (Rock Tables):** The shape of relative permeability functions will affect the implied vertical conformance.
 4. **Relative Permeability end points:** The assumed residual oil saturations defines the fraction of oil that can be displaced by water.

It cannot be proven with the history matching which factor is most appropriate for the Pleasant Prairie reservoir. Yet each method might result in somewhat different projections for the volumes of oil that might be recovered by CO₂, and the volume of CO₂ that might be sequestered. Sensitivity analysis to multiple history matching solutions is beyond the scope of this study.

01:81	396:428	01:25	*	0.6	** POLY Region 1
01:81	366:395	01:25	*	0.7	** POLY Region 2
01:81	319:365	01:25	*	0.7	** POLY Region 3
01:81	282:318	01:25	*	0.75	** POLY Region 4
01:81	237:281	01:25	*	0.8	** POLY Region 5
01:81	206:236	01:25	*	0.7	** POLY Region 6
01:81	181:205	01:25	*	0.85	** POLY Region 7
01:81	145:180	01:25	*	0.8	** POLY Region 8
01:81	097:144	01:25	*	0.8	** POLY Region 9
01:81	049:096	01:25	*	0.8	** POLY Region 10
01:81	018:048	01:25	*	1	** POLY Region 11
01:81	001:011	01:25	*	0.8	** POLY Region 12

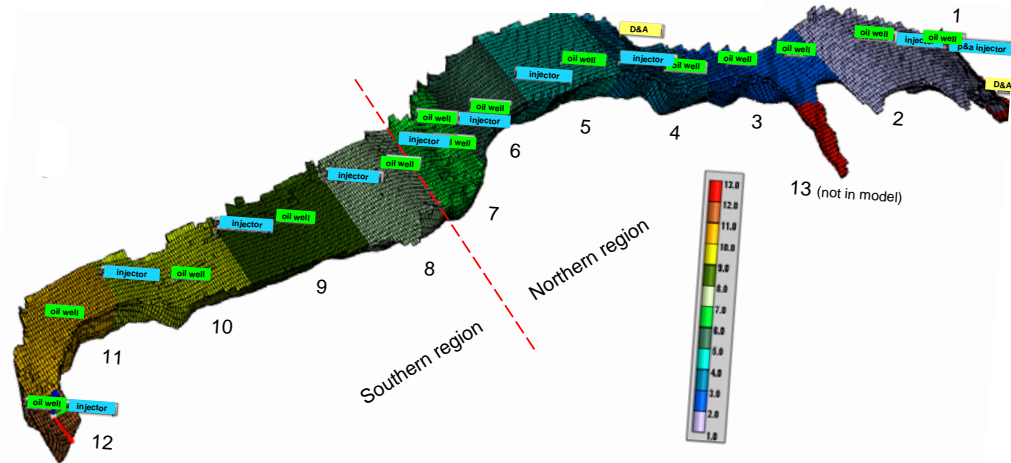


Figure 7.12 Volume modifiers at end of history match by polygon.

7.4 Dynamic model for predictions

For the CO₂ injection analysis, it is necessary to use a compositional (EOS) simulation program. To illustrate that the EOS simulation is consistent with the Black Oil model, the history match is repeated for the compositional model and compared to the black oil in Figure 7.12. From this figure, it is clear that the EOS model is also validated by the history match.

An initial baseline simulation is carried out to forecast Pleasant Prairie production assuming operations maintained status quo. That is, the No Further Activity (NFA) case assumes that total liquid production and injection will continue at current rates, and that oil cut will continue to decline. A fifteen year period is forecast (i.e. to Jan 2027). Note that economics are not considered in this forecast. Individual wells in the forecast might continue to produce at very low oil rates.

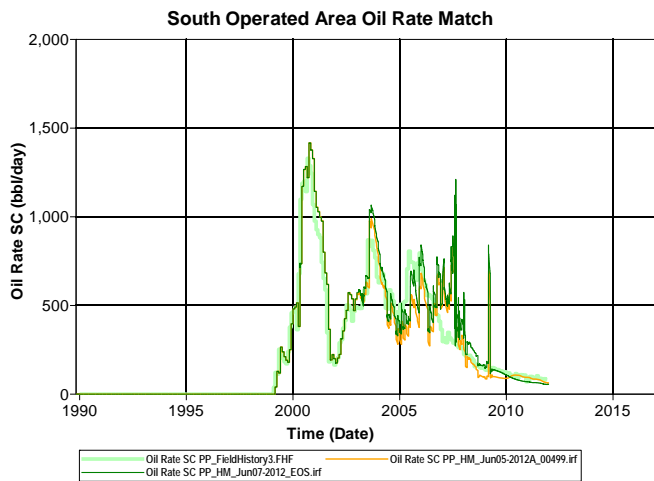
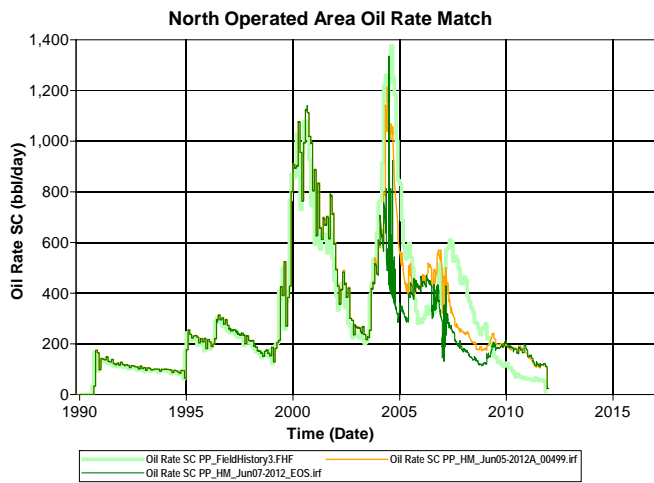
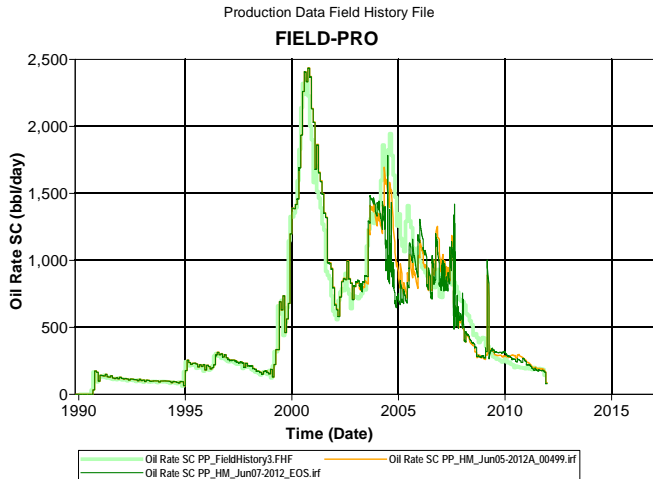


Figure 7.13 EOS oil production model match. Rate in barrels/day are on the left axis. EOS model rates are dark green, black oil rates are orange, and actual rates are light green colored

lines. The EOS model provides nearly the same production match as the Black Oil. Simulation time is much longer (1.5 day for EOS).

CO₂ sequestration modeling scoping cases were then carried out to evaluate the potential incremental oil that might be realized and to determine the volumes of CO₂ that might be sequestered in the Pleasant Prairie Chester reservoir. For the CO₂ injection cases, the following assumptions were applied:

- Status quo liquid production and water injection were continued from Dec 2011 rates until July 1, 2013
- All producing wells were shut in on July 1, 2013
- All water injection wells were converted to CO₂ injection wells on July 1, 2013
- Injection wells were assigned a maximum bottomhole injection pressure of 2600 psia.
- Sensitivity to several injection rates were carried out, ranging from 100 MCFD CO₂ per well to 1.5 MMCFD CO₂ per well.
- All producing wells were placed back on production when the average pressure within its polygon reaches 1500 psi.
- Total field production rate is constrained to a voidage replacement ratio of 1.0. That is, total reservoir fluid out is limited to the total reservoir volume being injected.
- A maximum gas production rate for each producing well is assigned at 100 MCFD.
- CO₂ injection and well liquid and gas production is forecast to 7/1/2026.

Note that objective of analyses was to maximize sequestration. Wells were allowed to produce mostly or all water, even if this might not be economic, in order to allow maximum sequestration of CO₂. There was no consideration for optimizing the oil recovery by investigating pattern efficiency or by modeling WAG processes.

Several cases were carried out. The case for CO₂ injection rate of 5 MMCFD is presented in this report. Volume converted to tons is 290 tons/day, using a conversion factor of 17.23 mcf/ton (Dubois, etal, 2002). For reference, 50 million gallon per year ethanol plants, a typical size in Kansas, yield approximately 7 MMCFD CO₂ from the fermentation process.

A comparison of oil recovery under the NFA and the CO₂ injection cases is presented in Figure 7.14. Both oil production and cumulative recovery are presented in the figure. It is calculated with these models that remaining oil under the NFA case is about 4.64 MMSTB. With CO₂ sequestration, this volume is expected to increase 6.59 MMSTB with an increase in EUR

(incremental oil due to CO₂ injection) of 1.95 MMSTB under the 5 MMCFD CO₂ injection case.

The estimated volumes of CO₂ sequestration is presented in Figure 7.16. Both the CO₂ volumes injected and CO₂ volumes produced are illustrated. About 0.61 million tons (1 ton = 2000 lb) of CO₂ will be sequestered. When the CO₂ injection and fluid production at the wells cease at the end of 2026, average reservoir pressure is 1574 psia.

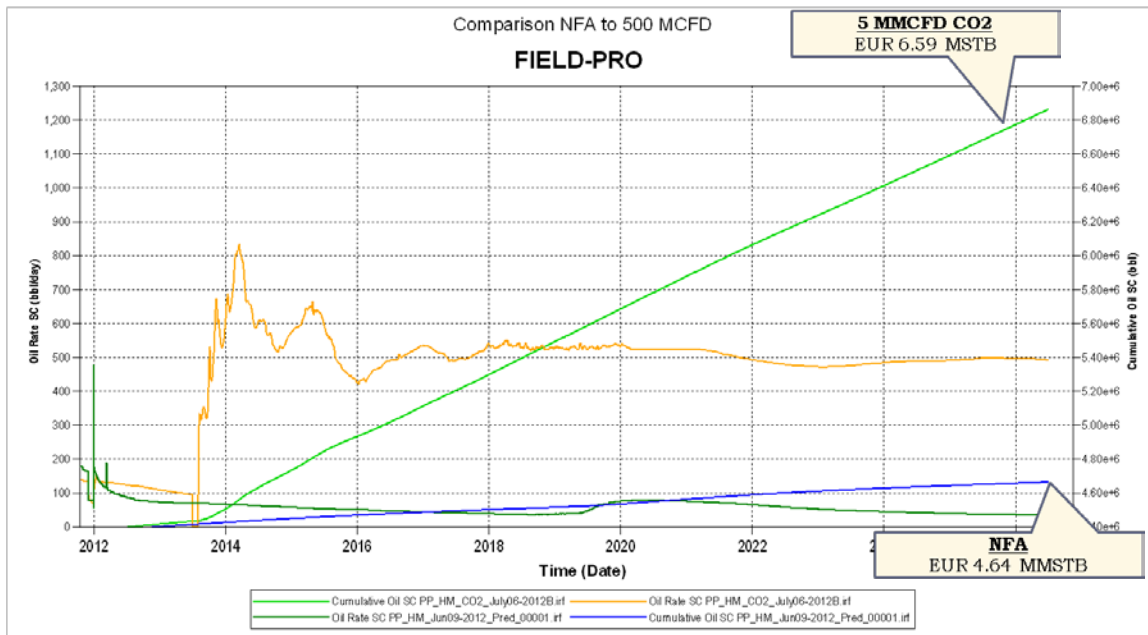


Figure 7.14 Oil production for the CO₂ injection case compared to NFA. Yellow is oil rate in CO₂ case, green diagonal line is cumulative CO₂-related oil, lower green is a NFA case, and blue line is cumulative oil for the NFA case.

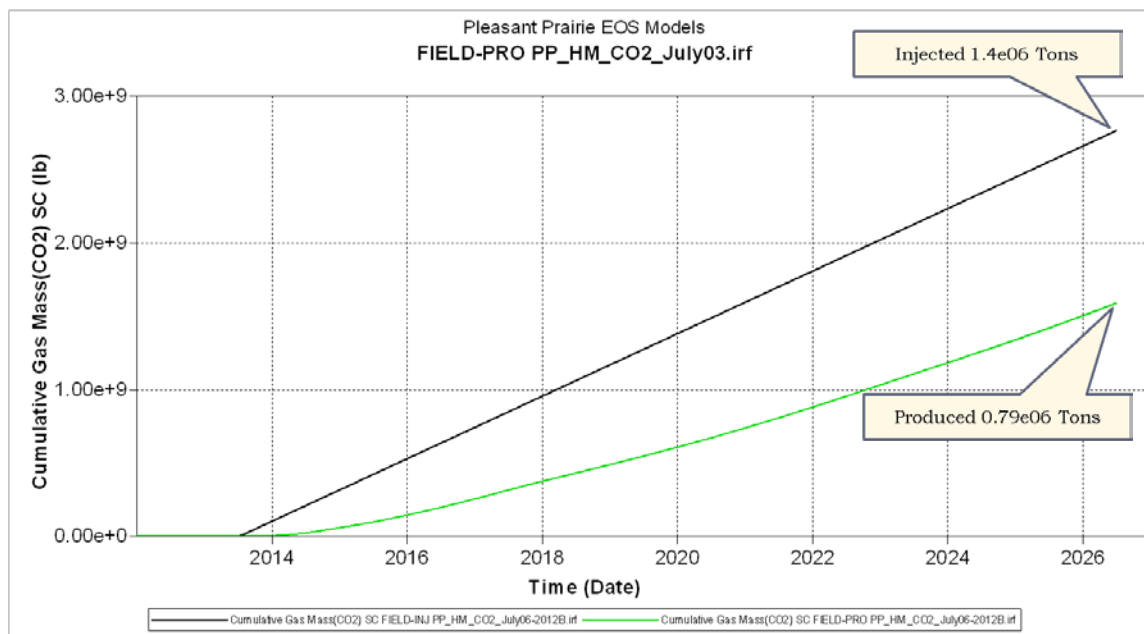


Figure 7.15 CO₂ cumulative volumes for the CO₂ injection case. The amount of CO₂ sequestered is the area between the lines.

7.5 Summary and discussion

Summary statistics are shown in Table 7.3. The forecasted volume of CO₂ sequestered through 2026 is 0.61 million tons with a total of 1.38 million tons injected and 0.77 million tons produced. Assuming this were a case where the field was being operated for economic gain through oil production, most of the 0.77 million tons would likely be captured, compressed and re-injected. Two metrics often used as a measure of efficiency in CO₂ EOR operations are gross utilization, the ratio of total CO₂ injected to oil produced; and net utilization, the ratio of CO₂ purchased to oil produced. In the case presented, if all oil produced after 2012 is included in the denominator, the gross and net utilization metrics are 11.2 and 5 mcf/bo, respectively, comparable to CO₂ floods in the West Texas Permian Basin.

Cumulative oil 2011 (mmbo)	4.48	
NFA cum. oil 2026 (mmbo)	4.64	
Cum. oil CO2 case (mmbo)	6.59	
Incremental oil CO2 (Cum.-NFA) (mmbo)	1.95	
Cumulative oil 2012-2026 (mmbo)	2.11	
		<i>mm tons</i>
CO2 injected (mmcf)	23.7	1.38
CO2 produced (mmcf)	13.2	0.77
CO2 sequestered (mmcf)	10.5	0.61
Gross utilization (mcf/bo)	11.2	
Net utilization (mcf/bo)	5.0	

Table 7.3 Summary statistics for CO2 injection forecasts. Abbreviations include NFA - No Further Action and Cum. - cumulative.

7.6 Recommendations for further analysis

The history match is not a unique solution. Several suitable matches were derived under different values for the uncertainty parameters. The CO2 sequestration volumes could be sensitive to the volumes in place and sensitivity analysis should be carried out using different models to evaluate this uncertainty.

The volume of CO2 that might be sequestered is sensitive to the injection and withdrawal assumptions. Further work is required to optimize the maximum volumes of CO2 that might be sequestered.

In most miscible and immiscible CO2 projects, there is a volume of oil that is not contacted by the injected fluid. This uncontacted volume is represented in a model using the SORM (residual oil to miscible) keyword. The magnitude of SORM is unknown until such time it can be approximated through history matching. Typical values in mature miscible CO2 projects might be in the 5% to 10% range. Further analysis is required to evaluate the effect of SORM on sequestered CO2 volumes.

8. Discussion and further work to consider

It is believed that the modeling and dynamic simulation results fairly represent the reservoir system, but due to uncertainly additional work could be warranted. The most significant looming uncertainty is the moveable oil volume. Considering that reservoir petrophysical relationships and fluid properties are well-grounded, the physical pore volume available to be produced (in communication with the well bores) is the single-most likely variable to need improvement (possible reduction). That is, if it is in need of improvement. The most obvious metric for suggesting the pore volume may need downward adjustment is the relatively low recovery factor (30.4% of OOIP) when compared to that of three other Chester waterflood units in the IVF system (31.1%, 39.7%, and a projected 41% RF). However, because a third of the Pleasant Prairie South flood patterns are less than optimal, the low RF could be due, at least in part, to the reservoir not being swept in those particular regions lowering the overall RF.

Dynamic flow modeling required a pore volume reduction to a volume-weighted average of 79% of static model pore volume for the best history match of primary and secondary production. This could be assumed to indicate that 21% of the reservoir is excess volume or at least not in communication with the wellbores. Gross volume reduction could be reasonably accomplished by locally reducing the valley volume (width and angle of the valley wall). Diminishing the efficiency with which the wellbores are in contact with the reservoir could be "reintroduced" by modifying the upscaling process. The method used in the current workflow was to upscale porosity in the reservoir from an average layer thickness of 2 feet to 10 feet without regard to vertical heterogeneity in the reservoir. This had a tendency to diminish any baffling and barrier effects of the thin (2 to 4-ft thick) limey conglomerate lithofacies which have low porosity and permeability. These relatively continuous beds, if preserved in the model might prevent stratigraphic intervals in local areas from being drained and swept efficiently. If this mechanism were to be proven, then recompletions, reconfiguring or drilling additional wells could be justified to tap poorly swept regions.

Neither of the above-recommended approaches could be investigated without substantial effort. However, those further investigations mentioned above or other possible improvements would not alter significantly the basic findings in this study: the modeling suggests that a relatively substantial volume of CO₂ can be injected and sequestered and a significant volume of oil recovered in the process. If more time is allocated to this particular study, perhaps it might be best spent on evaluating other CO₂ injection scenarios (increased rates) and patterns to optimize the economics.

9. Summary and conclusions

Based on this study it appears feasible to inject and sequester a relatively large volume of CO₂ into the Pleasant Prairie South Chester reservoir and recover a significant volume of oil recover oil during the process. This report documents characterize the geologic characterization, building a detailed static reservoir model, using dynamic models, both black oil and compositional simulators, to predict the results of CO₂ injection. Following are the highlights of the Pleasant Prairie South study:

1. The Chester sandstone reservoir was deposited in a tidally influence fluvial system in an estuarine setting in a deeply incised (150-ft) nearly linear 1000-ft wide valley as Chesterian seas overlapped the exposed Meramecian surface.
2. Pleasant Prairie South located in the northern portion of a nearly linear incised valley system stretching nearly 50 miles to the Oklahoma border and beyond. The Pleasant Prairie South reservoir appears to be similar in deposition and properties to the Chester IVF in the Eubank and Shuck fields to the south.
3. Although there is room for improvement in the static model and justification for further dynamic modeling, the current models are sufficient to demonstrate with confidence that substantial volumes of CO₂ can be injected and sequestered and a significant volume of oil recovered in the process.
4. Dynamic model calculations indicate that 5 MMCFD (290 tons/day) CO₂ injection over a 13 year period could result in a net 0.61 million tons CO₂ volume sequestered. A total of 1.38 million tons CO₂ would be injected and 0.77 tons would be produced along with the oil. Theoretically 0.61 million tons could be delivered to the field and injected and the produced tons recycled through the reservoir resulting in a total of 1.38 million tons injected overall.
5. Primary and secondary oil recovery to December 2011 was 4.5 MMBO. Without further action, and continuation of the water injection, an additional 160,000 barrels of oil might be recovered. EOR under the CO₂ injection scenario discussed, the model calculates an additional 1.95 million barrels could be recovered.
6. As the history is demonstrated under water injection, uncertainty remains with respect to how gas injection might perform. For example, the volume of potential oil recovered might be significantly less if residual oil to miscible CO₂ is greater than the zero value assumed in these model predictions.
7. Lessons learned and workflows established in the Pleasant Prairie South project will be applied in the other three field studies underway.

Acknowledgements

Material presented is based upon work supported by the U.S. Department of Energy (DOE) National Energy Technology Laboratory (NETL) under Grant Number DEFE0000002056. This project is managed and administered by the Kansas Geological Survey/KUCR, W. L. Watney and Jason RushPIs, and funded by DOE/NETL and cost-sharing partners

We wish to thank the companies that contributed data, technical support, and input: Anadarko Petroleum Corp., Berexco LLC, Cimarex Energy Company, Glori Oil Limited, Elm III, LLC, and Merit Energy Company; and the support of Sunflower Electric Power Corp., a Kansas-based electric utility. *And* Kansas Geological Survey, through the Kansas University Center for Research *and* the U.S. Department of Energy. Others contributing in technical support, but not listed as co-authors include Lynn Watney, KGS - project PI, John Doveton, KGS - petrophysics, Jason Rush, KGS - modeling support, Raymond Sorenson, consultant - data sleuthing and overall technical knowledge, David Newell, KGS - brine properties, Anthony Walton, Department of Geology, University of Kansas - sedimentology. Data and contract support was also provided by the KGS and funding and support for Senior's MS thesis work was provided by the Tertiary Oil Recovery Project, Department of Chemical and Petroleum Engineering, University of Kansas.

Disclaimer:

This report was prepared as an account of work sponsored by an agency of the United States Government. Neither the United States Government nor any agency thereof, nor any of their employees, makes any warranty, express or implied, or assumes any legal liability or responsibility for the accuracy, completeness, or usefulness of any information, apparatus, product, or process disclosed, or represents that its use would not infringe privately owned rights. Reference herein to any specific commercial product, process, or service by trade name, trademark, manufacturer, or otherwise does not necessarily constitute or imply its endorsement, recommendation, or favoring by the United States Government or any agency thereof. The views and opinions of authors expressed herein do not necessarily state or reflect those of the United States Government or any agency thereof.

References

- Abegg, F.E., 1994, Lithostratigraphy of the Shore Airport Formation (Chesterian), in southwestern Kansas: *in*, Baars, D.L., (compiler.); Revision of stratigraphic nomenclature in Kansas: Kansas Geological Survey, Bulletin, no. 230, p. 21-38.
- Bohling G. C., and Doveton, J. H., 2000, Kipling.xla: An Excel add-in for nonparametric regression and classification, Kansas Geological Survey: <http://www.kgs.ku.edu/software/Kipling/Kipling1.html> (accessed January 3, 2012).
- Bowen, D.W., and Weimer, P., 2003, Regional sequence stratigraphic setting and reservoir geology of Morrow incised-valley sandstones (lower Pennsylvanian), eastern Colorado and western Kansas: AAPG Bulletin, vol. 87, no. 5, p. 781-815.
- Cirilo, L. L., 2002, Transgressive estuarine fill of an incised paleovalley, Upper Mississippian Chesterian Series, Shuck field area, Seward County, Kansas: Unpublished .M.S. thesis, University of Houston, Houston, TX, 194 p.
- Dalrymple, R.W., Zaitlin, B.A., and Boyd, R., 1992, Estuarine facies models: Conceptual basis and stratigraphic implications: *Journal of Sedimentary Petrology*, v. 62, no. 6, p. 1130-1146.
- Dubois, M.K., S.W. White and T.R. Carr, 2002, Co-generation, ethanol production and CO₂ enhanced oil recovery: a model for environmentally and economically sound linked energy systems: (abs) American Association of Petroleum Geologists Annual Convention, v. 11, p. A46, *and* Kansas Geological Survey Kansas Geological Survey Open-file Report 2002-6. <http://www.kgs.ukans.edu/PRS/Poster/2002/2002-6/index.html>
- Dubois, M. K., Byrnes, A. P., Bohling, G. C., and Doveton, J. H., 2006, Multiscale geologic and petrophysical modeling of the giant Hugoton gas field (Permian), Kansas and Oklahoma, U.S.A., *in* Harris, P. M. and Weber, L. J., eds., Giant hydrocarbon reservoirs of the world: From rocks to reservoir characterization and modeling: AAPG Memoir 88/SEPM Special Publication, p. 307–353.
- Dubois, M.K., G.C. Bohling, and S. Chakrabarti, 2007, Comparison of four approaches to a rock facies classification problem: *Computers & Geosciences*, v 33, p. 599-617.

Gray, Thomas A., 2001, Petrophysical Analysis of North Eubank Chester Waterflood, proprietary report prepared for OXY USA, Inc., Houston, TX. by Petrophysical Solutions, Inc., Houston, TX.

Goebel, E. D., 1968, Mississippian rocks of western Kansas: AAPG Bulletin, vol. 52, no. 9, p.1732-1778.

Handford, C.R., and Francka, B.J., 1991, Mississippian carbonate-siliciclastic eolianites in southwestern Kansas, *in* Lamando, A. J., Harris, P. M., eds., Mixed Carbonate Siliciclastic Sequence: SEPM Core Workshop 15, p. 205-244.

Krystinik, L.F., and Blakeney, B.A., 1990, Sedimentology of the upper Morrow formation in eastern Colorado and western Colorado: *in*, Sonnenberg, S.A., Shannon, L.T., Rader, K., von Drehle, W.F., and Martin, G.W., (editors) Morrow sandstones of southeast Colorado and adjacent areas: Rocky Mountain Association of Geologists, p. 37-50.

Laubach, S. E., Reed, R. M., Olson, J. E., Lander, R. H., and Bonnell, L. M., 2004, Coevolution of crack-seal texture and fracture porosity in sedimentary rocks: cathodoluminescence observations of regional fractures: Journal of Structural Geology, v. 26, no. 5, p. 967-982.

Maher, J. C., and Collins, J. B., 1949, Pre-Pennsylvanian geology of southwestern Kansas, southeastern Colorado, and the Oklahoma Panhandle: U.S. Geol. Survey, Oil and Gas Inv., Prelim. Map 101, 4 sheets.

Merriam, D. F., 1963, The Geologic History of Kansas: Kansas Geological Survey, Bulletin 162, 307 pages.

Montgomery, S. L., and Morrison, E., 1999, South Eubank Field, Haskell County, Kansas: A case of field redevelopment using subsurface mapping and 3-D seismic data: AAPG Bulletin, v. 83, no. 3, p. 393-409.

Rascoe, B., Jr., and Adler, F. J., 1983, Permo-Carboniferous hydrocarbon accumulations, Mid-Continent, U.S.A.: AAPG Bulletin, v. 67, p. 979-1001.

Schlumberger Well Services, 1986, Resistivity of NaCl solutions" (Chart Gen-9), p. 5, *in* Schlumberger Well Services, 1986, Log Interpretation Charts, Houston Texas, 122 p.

Severy, C. L., 1975, Subsurface Stratigraphy of the Chesterian Series, Southwest Kansas: Unpublished M.S. thesis, University of Colorado, Boulder, CO, 61 p.

Shonfelt, J. P., 1988, Geologic heterogeneities of a Chesterian sandstone reservoir, Kinney-Lower Chester field, Stevens and Seward counties, Kansas, and their affect on hydrocarbon production: Unpublished M.S. thesis, Wichita State University, Wichita, KS, 206 p.

Smith L. B., and Read, J. F., 2000, rapid onset of late Paleozoic glaciation on Gondwana: Evidence from Upper Mississippian strata of the Midcontinent, U.S.A.: *Geology*, v. 28, p. 279-282.

Sorenson, R. P., Kelly, S. P., and Cantwell, D., 1999, Tar mat formation within the Hitch oil field, Seward County, Kansas: Transactions of the 1999 AAPG Midcontinent Section Meeting (Geoscience for the 21st Century), p. 156-165.

Technical Committee, Eubank North Unit, 2001, Eubank North Unit waterflood feasibility study, proprietary report prepared for participating operators.

Watney, W.L., Franseen, E.K., Byrnes, A.P., and Nissen, S.E., 2008, Contrasting styles and common controls on Middle Mississippian and Upper Pennsylvanian carbonate Platforms in the Northern Midcontinent, U.S.A.: in Lukasik, J., and Simo, A., editors, Controls on Carbonate Platform and Reef Development, SEPM Special Publication 89, Society of Sedimentary Geology, Tulsa, p. 125-145.